Durham E-Theses

Study of Thermally Activated Delayed Fluorescent Exciplexes and their Practical Applications in OLEDs

COLELLA, MARCO

How to cite:

COLELLA, MARCO (2020) *Study of Thermally Activated Delayed Fluorescent Exciplexes and their Practical Applications in OLEDs*, Durham theses, Durham University. Available at Durham E-Theses Online: http://etheses.dur.ac.uk/13504/

Use policy

Study of Thermally Activated Delayed Fluorescent Exciplexes and their Practical Applications in OLEDs

Marco Colella

Organic Electroactive Materials Research Group

Department of Physics

University of Durham

A Thesis submitted for the Degree of Doctor of Philosophy

August 2019

Abstract

Exciplexes are intermolecular charge transfer (CT) complexes in which one electron donating (D) and one electron accepting (A) molecule interact in the excited state. The new bimolecular CT excited state species is the exciplex, a shortening of EXCIted state comPLEX. Until recently exciplexes were avoided in OLEDs structures since they constituted an efficiency loss pathway since they commonly possess low photoluminescence quantum yield (PLQY).

Recently, the rise of thermally activated delayed fluorescence (TADF) applications for triplet harvesting in fluorescent OLEDs has resulted in renewed research interest in these bimolecular excited states. The TADF mechanism in fact, allows to upconvert triplet excited states (which are non-emissive in normal fluorescent emitters) into emissive singlet excited states thus boosting the efficiency of the emitter.

To be efficient, the TADF mechanism needs to have minimal overlap between the highest occupied molecular orbital (HOMO) and the lowest occupied molecular orbital (LUMO). Exciplexes intrinsically possess this characteristic since the CT excited state is formed between two different molecules making exciplexes the perfect candidates as TADF emitters. For this reason, TADF exciplexes are attracting more and more attention although always in the shadow of their more successful intramolecular counterpart (covalently linked D-A fragments in a single molecule) since they could be more easily tailored to maximise their efficiency and modify their properties.

The first part of this thesis demonstrates the surprising discovery that exciplex electronic energy and PLQY are not intrinsically fixed by the D/A couple forming the exciplex, and that these characteristics can be tuned and improved through solid state dilution. It is shown that the exciplex electronic energy can be controllably increased by varying average intermolecular distance between the D and A molecule within the exciplex blend by inserting a third inert molecule in the blend forming the film.

The change in the exciplex electronic energy and PLQY is rationalised by a general reduction of the coulombic binding energy with D-A separation. In contrast, the PLQY enhancement is not general and determined to be related to the degree of flexibility of the exciplex forming molecules.

The second part of this thesis showcases work that broadens the range of potential applications of TADF exciplex OLEDs, demonstrating their suitability as emitters for solution processed devices and how they can be used to confine the recombination zone of a standard phosphorescent OLED - leading to performance and stability improvements.

Table of Contents

List of Acronyms

A	Electron accepting unit/molecule
CB	Chlorobenzene
CCD	Charge coupled device
CF	Chloroform
CIE	Commision International D'Eclairage
CT	Charge transfer
D	Electron donating unit/molecule
DF	Delayed fluorescence
EBL	Electron blocking layer
EIL	Electron injection layer
EML	Emissive layer
EQE	External quantum efficiency
ETL	Electron transporting layer
HBL	Hole blocking layer
HIL	Hole injection layer
HOMO	Highest occupied molecular orbital
HTL	Hole transporting layer
ITO	Indium Tin oxide
LE	Locally excited
LiF	Lithium Fluoride
LUMO	Lowest unoccupied molecular orbital
Nd:YAG	Neodymium doped Yttrium Aluminium Garnet
OLED	Organic light emitting diode
PF	Prompt fluorescence
PH	Phosphorescence
PL	Photoluminescence
PLQY	Photoluminescence quantum yield
IC	Internal conversion
ISC	Intersystem crossing

rISC	Reverse intersystem crossing
RT	Room Temperature
RTP	Room temperature phosphorescence
SOC	Spin orbit coupling
TADF	Thermally activated delayed fluorescence
TF	Tooling factor
TTA	Triplet-triplet annihilation
VTE	Vacuum thermal evaporation

List of Publications

1. **<u>Marco Colella</u>,** Andrew Danos, Andrew P. Monkman. Identifying the Factors That Lead to PLQY Enhancement in Diluted TADF Exciplexes Based on Carbazole Donors. *J. Phys. Chem. C* **2019**, 123, 28, 17318-17324

2. Patrycja Stachelek, Jonathan S. Ward, Paloma L. dos Santos, Andrew Danos, **<u>Marco Colella</u>**, Nils Haase, Samuel J. Raynes, Andrei S. Batsanov, Martin R. Bryce , Andrew P. Monkman. Molecular Design Strategies for Color Tuning of Blue TADF Emitters, *ACS Appl Mat and Interfaces* **2019**, 11, 30, 27125-27133

3. **<u>Marco Colella</u>,** Andrew Danos, Andrew P. Monkman. Less Is More: Dilution Enhances Optical and Electrical Performance of a TADF Exciplex. *J. Phys. Chem. Lett.* **2019**, 793–798

4. Amruth,C; **<u>Marco Colella</u>**, Jonathan Griffin, James Kingsley, Nicholas Scarratt, Beata Luszczynska, Jacek Ulanski. Slot-Die Coating of Double Polymer Layers for the Fabrication of Organic Light Emitting Diodes. *Micromachines* **2019**,10, 53

5. **<u>Marco Colella</u>,** Piotr Pander, Daniel de Sa Pereira, Andrew P. Monkman. Interfacial TADF Exciplex as a Tool to Localize Excitons, Improve Efficiency, and Increase OLED Lifetime. *ACS Appl Mat and Interfaces* **2018,** 10, 40001-40007

6. Piotr Pander, Simon Gogoc, **<u>Marco Colella</u>**, Przemyslaw Data, Fernando Dias. Thermally-Activated Delayed Fluorescence in Polymer-Small Molecule Exciplex Blends for Solution-Processed Organic Light Emitting Diodes, *ACS Appl Mat and Interfaces* **2018,** 10, 34, 28796-28802

7. **<u>Marco Colella</u>,** Piotr Pander, Andrew P. Monkman. Solution processable small molecule based TADF exciplex OLEDs. *Organic Electronics,* **2018,** 62, 168-173

Declaration

All material contained in this thesis is original and is the result of my own work except where explicit reference is made to the work of others. This thesis has not been submitted in whole or part of a degree at this or any other university.

Study of Thermally Activated Delayed Fluorescent

Exciplexes and their practical applications in OLEDs

Marco Colella

Acknowledgements

First, I would like to acknowledge my supervisor, Prof. Andy Monkman to provide the support necessary for my success during the last three years but especially for supporting me every time I went to visit him with strange half bad ideas. My co-supervisor, Fernando Dias for always being ready to offer a comforting word when needed. I would also like to acknowledge the precious members of the OEM group with which I had the pleasure to work side to side, Daniel, Piotr, Patrycja, Heather and Marc. A special mention in this category goes to Andrew with whom I have shared some of the most enjoyable, fruitful and exciting moments of my short academic research career.

I spent the first part of my PhD in a beautiful company of which I enjoyed every moment. I want here to thank everyone for the support I received during those two beautiful years, James, Nick, Chris, Monika, Max, Jon, Tom, Omar, Hadi, Lidya, Hunan, Rosie and Ian.

This PhD has taken me away from my family and friends which have never stopped supporting me and making me feel like I never left. For this reason, I want to thank my dear friends Lorenzo (also known as er Fragola), Jacopo and Andrea.

I want to thank Sabrina, Roberto, Giorgia and Nicholas for making me feel part of their family for the last thirteen years.

I want to thank my brother Massimo and his fantastic wife Giusy for simply being part of who I am.

I could not forgive myself if do not properly thank my parents, Francesco and Elisabetta for always pushing me to become the better version of myself while always letting me be who I wanted be for this, I will never thank you enough and I hope I will be able to do the same with my children.

Finally, I need to thank my wife Veronica to have agreed to spend the rest of her life with me for supporting me and SOpporting me. I love you.

A mia moglie Veronica,
la mia compagna di avventure.

Chapter 1 :

Introduction

1.1 Motivation

Organic light emitting diode (OLED) technology has recently gained a significant share of the display market. OLED displays are now mass produced for mobile phones, tablets, TVs, and wearables already representing a market worth tens of billions.[1] Current academic and commercial research into OLEDs is stimulated by the demand for new materials to enable cheaper, more efficient and stable products.[2]

Current consumer OLED technologies are based upon phosphorescent emitters.[2,3] While these molecules are incredibly efficient with external quantum efficiency above 20% and power efficiency >100lm/W putting them in competition with the organic light emitting diodes (LEDs) which currently dominate the market, their critical weakness lies in photochemical instability of blue emitters. In fact, where the red and green phosphorescent emitters have achieved lifetimes well above the commercial requirement of 10,000 hrs while the blue emitters do not survive 1000 hrs which limits the lifetime of the screens fully produced with this technology.[4] To overcome this problem OLED displays produced nowadays use as blue emitter a normal fluorescent emitter which lowers the overall efficiency of the resulting device since no triplet harvesting mechanism is active.[5]

More recently, a new way to obtain high efficiency emitters has been found via the thermal activated delayed fluorescence (TADF) mechanism which promises to join the record efficiency of the phosphorescent emitters with the stability of the fluorescent ones.[6]

TADF emitters can be broadly separated into two sub classes: intramolecular and intermolecular. The latter of these two categories, TADF exciplexes have been largely overlooked as potential emitters compared to their intramolecular counterparts. This is because beyond the coarse control of initial choice of the donor (D) and acceptor (A) materials, it was

common belief that exciplexes could not be finely tuned or improved. In contrast, studies of slightly modified D-A intramolecular TADF materials have since proliferated.

This thesis aims to deepen the photophysical understanding of TADF exciplexes and improve their potential as emitters for future generations of OLED devices. The data presented in this thesis has been collected in Sheffield (Ossila Ltd, Kroto Innovation Centre, Sheffield) and Durham (OEM group, Physics department, Durham).

1.2 Thesis Organization

Chapter 2 presents the background theory necessary to analyse and understand the data and results contained in this thesis. It starts by introducing the concept of excited state multiplicity (singlet and triplet states), and the quantum mechanical origin of their energy difference. The concept of intersystem crossing and its role in phosphorescent and TADF emitters is then introduced. A Jabłonski diagram is then used to explain the three main triplet harvesting mechanisms relevant to OLEDs: triplet-triplet annihilation (TTA), TADF, and phosphorescence. Finally, the working principles of OLEDs and the processes that give rise to their stability issues are discussed.

Chapter 3 lists the materials discussed in this thesis and their application. The sample preparation methods for photophysical measurements is presented along with the spectroscopical techniques employed. The OLEDs fabrication and measurement methods are then explained.

Chapter 4 is the first of the experimental chapter and it presents the effects of solid state dilution on the TADF exciplex formed between 4,4'-(Diphenylsilanediyl) bis(N,N-diphenylaniline) (TSBPA) and 2,4,6-tris[3-(diphenylphosphinyl)phenyl]-1,3,5-triazine (PO-T2T). The results show how the exciplex emission blueshifts with increasing host vol% and that this is followed by an increment in its photoluminescence quantum yield (PLQY). This PLQY increment is then directly translated in OLED performance.

Chapter 5 shows how solid state dilution affects the TADF exciplexes formed by the three carbazole based donors, 1,3-Bis(carbazol-9-yl) benzene (mCP), 4,4'-Bis(carbazol-9-yl) biphenyl (CBP) and 4,4'-Bis(carbazol-9-yl)-2,2'-dimethylbiphenyl (CDBP). The study shows that the emission blueshift is common to all of them since is due to a weakened coulombic interaction between the donor and the acceptor at larger distances. In contrast, the PLQY enhancement is not general, and appears to require a certain degree of molecular flexibility to be observed.

Chapter 6 presents the optimisation study of a solution processable TADF exciplex formed between 9-[2,8]-9-carbazole-[dibenzothiophene-*S,S*-dioxide]-carbazole (DCz-DBTO2) and 4,4′-cyclohexylidenebis [*N,N*-bis(4methylphenyl) benzenamine] (TAPC). The study shows that the solvent system is of critical importance in order to guarantee the optimal film formation and donor-acceptor orientation within the film in order to maximise the efficiency. The best

result approaches the one obtained for the previously reported vacuum deposited OLEDs for the same system demonstrating the viability of TADF exciplexes as solution processable TADF emitters.

Chapter 7 shows how an interfacial exciplex at the interface between the emissive layer (EML) and the electron transporting layer (ETL) junction can improve considerably its performance and stability in a Phosphorescent OLED (PhOLED) device. In the chapter is shown how this is achieved by inducing an extremely effective localization of the recombination zone (within 5 nm) and by recycling via the TADF mechanism the piled up charges at the interface that are converted into exciplexes and then transferred by both Dexter and Forster energy transfer to the phosphorescent emitter.

Chapter 8 Summarises the findings presented from chapter 4 to 7 and speculating at further work based on these investigations.

1.3 <u>References</u>

(1)   OLED   market   https://www.marketsandmarkets.com/Market-Reports/oled-market-200.html?gclid=Cj0KCQiA9orxBRD0ARIsAK9JDxQfunmhpmum_SZXn1iekqn_TF YmFQxqU764r1lfMaTZtZ2-PpKneLIaAnf0EALw_wcB (accessed Jan 18, 2020).

(2)   U.S. Departmentof Energy. 2018 Solid-State Lighting R&D Opportunities. **2019**, No. January.

(3)   Yersin, H. *Highly Efficient OLEDs: Materials Based on Thermally Activated Delayed Fluorescence*; Wiley-VCH, 2018.

(4)   Song, W.; Lee, J. Y. Degradation Mechanism and Lifetime Improvement Strategy for Blue Phosphorescent Organic Light-Emitting Diodes. *Adv. Opt. Mater.* **2017**, *5* (9), 1600901. https://doi.org/10.1002/adom.201600901.

(5)   Lee, J.-H.; Chen, C.-H.; Lee, P.-H.; Lin, H.-Y.; Leung, M.; Chiu, T.-L.; Lin, C.-F. Blue Organic Light-Emitting Diodes: Current Status, Challenges, and Future Outlook. *J. Mater. Chem. C* **2019**, *7* (20), 5874–5888. https://doi.org/10.1039/C9TC00204A.

(6)   Dias, F. B.; Penfold, T. J.; Berberan-Santos, M. N.; Monkman, A. P. Photophysics of Thermally Activated Delayed Fluorescence in Organic Molecules. *Methods Appl. Fluoresc.* **2017**, *5*, 012001. https://doi.org/10.1142/9789813230194_0006.

Chapter 2:

Background Theory

This chapter introduces fundamental background theory and concepts necessary to analyse and understand the work presented in later chapters. The chapter starts by introducing the concept of molecular excited states and the origin of the singlet-triplet energy splitting. A brief overview of allowed and forbidden electronic transitions then follows, with schematic representation using a Jabłonski diagram. The three main triplet harvesting (TTA, TADF and phosphorescence) mechanisms relevant to OLEDs are then presented, with special attention given to TADF, which is the focus of this thesis. Finally, the working principles and the main stability issues of organic light emitting diodes are summarised.

2.1 <u>Fundamental Theory</u>

2.1.1 Excited states in Organic Semiconductors

When an organic molecule absorbs electromagnetic radiation and becomes excited, an electron is promoted from its highest occupied molecular orbital (HOMO) to the lowest unoccupied molecular orbital (LUMO) level.[1] The excited electron, now in the LUMO, leaves behind an hole (i.e. vacancy) in the HOMO. The negatively charged electron and positively charged hole can interact with each other forming a quasiparticle called an exciton.

The energy and multiplicity of an exciton is defined by the quantum state of the electron that comprise the state. Generally, an atomic electron state is fully defined by four quantum numbers: the principal quantum number (n) that defines the energy level of the electron, the angular momentum quantum number (l) that defines the shape of the orbital occupied by the electron, the magnetic quantum number (m_l) that describe the spatial orientation of the orbital and the spin quantum number (s) that describes the angular moment of the electron. Pauli's exclusion principle establishes that two electrons cannot have the same set of quantum numbers, which leads to the fact that only two electrons ($s = \pm 1/2$) can exist in any one orbital (n, l, m_l) and that they must have opposite spin. Electrons possess semi integer values of spin, either +1/2 or -1/2. Electrons with spin value of +1/2 are commonly represented with an arrow pointing upward ($\uparrow$ or α) while an arrow pointing downward ($\downarrow$ or β) is used for electrons with value of -1/2.

2.1.1.1 Singlet and Triplets

The spin state of a molecule is given by the sum of the spin of all electrons in all orbitals. However, electrons in doubly filled orbitals are paired with an opposite spin partner (one electron spin up and the other spin down) and so contribute zero to the total spin of the system. It is therefore sufficient to consider only the unpaired electrons to describe an excited state configuration which are themselves usually the highest energy electrons.

The total spin $\mathbf{S}$ of a singlet (or triplet) excited state of a molecule is $\mathbf{S} = 0$ (or $\mathbf{S} = 1$). This occurs when the electron in the LUMO and the remaining electron in the HOMO are antiparallel (or parallel). In such a two particle system there will be four resulting eigenstates due to the four possible values of the secondary spin quantum number $\mathbf{m_s}$ which describes the angular momentum of an electron. For a certain value of the total spin $\mathbf{S}$ there can be $2\mathbf{S} + 1$ values of $\mathbf{m_s}$ with values ranging from $-S$ to $+S$ in steps of one. Therefore, for S = 0; $m_s = 0$

and for S = 1; m_s = -1, 0, 1. As schematically shown in (Figure 2.1). the two electrons forming the singlet (S = 0; m_s = 0) are anti parallel and their precession around the axis is out of phase therefore cancelling each other and giving a total m_s=0 with an anti-symmetric spin wavefunction, shown in the figure, typical of the singlet state. In the case of the triplet state there are three isoenergetic states where the two interacting electrons are in phase in all three combinations giving symmetric spin wave functions (shown in the figure) typical of a triplet state (S = 1; m_s = -1, 0, 1).
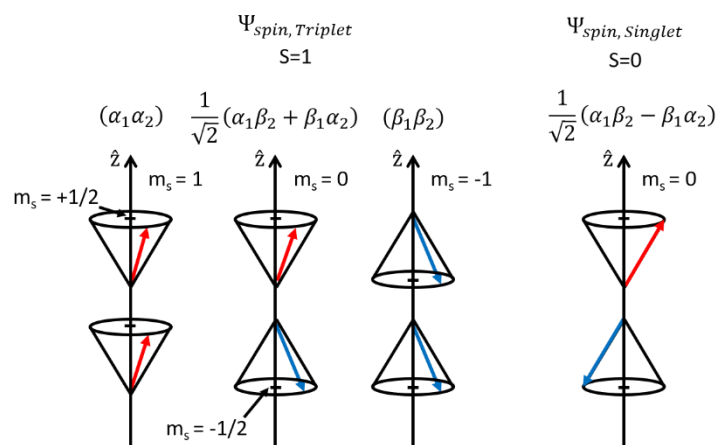
Figure 2.1 Spin Wavefunctions and cones of orientation of a two electron system, the index 1 and 2 refer respectively to electron 1 and 2. The red arrow indicates a spin-up electron with m_s = + 1/2 while the blue arrow represents a spin down electron with m_s = - 1/2. At the top of the figure is reported the total spin of a triplet (S = 1 and a singlet (S = 0). Below (left) are reported the three symmetric spin wavefunctions of the triplet and (right) the anti-symmetric singlet wave function. The two cases where m_s = 0 are distinguished by the phase of the precession of the two electrons forming the triplet where are in-phase and forming the singlet where are out of phase thus describing a symmetric spin state (triplet) and an anti-symmetric spin state (singlet).

In contrast, the ground state of an organic molecule is typically a singlet state, where the two electrons occupy the same orbital with antiparallel spin (Pauli's exclusion principle).

2.1.1.2 Origin of the singlet-triplet gap

For systems more complex than a hydrogen atom, the singlet and triplet state are not degenerate. In fact, their energy differs by twice the exchange energy (J) (Equation 2.1).[2] The exchange energy is the energy required to exchange the two electrons forming the singlet and the triplet state.

Equation 2.1

$$J = \iint \Phi(1)\Psi(2)\left(\frac{e^2}{r_1-r_2}\right)\Phi(2)\Psi(1)dr_1 dr_2$$

Where Ψ and Φ represent the HOMO and LUMO wavefunctions; r_1 and r_2 are the spatial coordinates of the electron labelled respectively 1 and 2; e is the elementary charge of the electron ($e = 1.6 \times 10^{-19}$ C).

To a first order approximation, the exchange interaction scales exponentially with the overlap of the respective electronic wavefunctions. This is particularly relevant for TADF emitters because the energy difference between the singlet and triplet state is given by $\Delta E_{ST}=2J$. This means that if the wavefunctions of the electron in the HOMO and the one in the LUMO overlap significantly, this results in a large exchange energy and thus a large ΔE_{ST} in the order of 0.7–1.0 eV is found for large overlap systems, which is not favourable for a TADF emitter where a ΔE_{ST} as close as possible to zero is desirable.[3]

In the case of Exciplexes Equation 2.1 represents an approximation since the HOMO and LUMO levels are located on two different molecules and the integral overlap of the wavefunctions will be effectively zero. On the other hand, this simplified picture highlights the intrinsic advantage that exciplexes have into fulfilling the energy level alignment requirements to emit efficiently via the TADF mechanism (illustrated in section 2.3.3).

2.1.1.3   Local and charge transfer excited states

This thesis focuses on systems that have a small ΔE_{ST} gap which promotes TADF (presented in section 2.3.3). To achieve this condition a small wavefunction overlap of the HOMO and LUMO orbital must be secured. A strategy commonly used to engineer this is to spatially separate HOMO and LUMO, for example by having them located on different fragments of a larger molecule, leading to materials that possess intra-molecular charge transfer (CT) states. Alternatively, this can be achieved between two different molecules (inter-molecular CT state), the latter case is also called an Exciplex. CT character identifies such excited states as having large separation between HOMO and LUMO. In contrast Locally Excited (LE) states involve the whole molecule and have large HOMO-LUMO overlaps.

The wavefunction of any state can be expressed as a combination of local and CT contribution.[4]

Equation 2.2

$$\psi = c_1\psi(M_1^- M_2^+) + c_2\psi(M_1^+ M_2^-) + c_3\psi(M_1^* M_2) + c_4\psi(M_1 M_2^*)$$

Where the subscripts 1 and 2 represent the indexes that distinguish the two molecules that are interacting; the superscripts + and - respectively represent a positively and negatively charged molecule while * represent the localisation of the excited electron onto one of the two

molecules forming the excited state. The first two terms of Equation 2.2 describe the contribution of the CT character to the total wave function while the last two terms describe its local character. The stronger the local character the stronger the oscillator strength due to the greater overlap with the ground state.[2,4] This means that, while LE states can more rapidly decay by radiative processes, their larger ΔE_{ST} values make them less capable of harvest triplets than CT states. At the same time CT excited state are less coupled to the ground state and so cannot emit as quickly, although they are ideal for triplet harvesting.

2.1.1.4 Intersystem Crossing and reverse Intersystem crossing

Intersystem crossing (ISC) and reverse intersystem crossing (rISC) are formally forbidden processes that allow an excited state to change its total spin which is usually a conserved quantity. For ISC and rISC to happen it is therefore necessary that the singlet and the triplet states mix so that the spin flip from one to the other becomes partially allowed.[2] In the zeroth-order approximation (Figure 2.2a) it is assumed that there is no intersystem crossing mechanism active thus if a molecule is initially in the singlet or triplet state this cannot change from one to the other. If mixing mechanisms are active the singlet and the triplet states will mix at the crossing point of their potential energy surfaces (i.e some critical nuclear coordinate where J vanishes).

Two of the main state mixing mechanisms exploited in materials used as emitters in OLED devices are spin orbit coupling (SOC) and vibronic coupling (VC). The magnitude of the first one grows with the fourth power of atomic number (Z) of the atoms constituting the molecule (SOC $\propto Z^4$). This is why efficient phosphorescent materials often contain heavy atoms such as Ir or Pt. The second one instead depends critically on the ΔE_{ST} gap which gives rise to rISC (i.e. TADF).
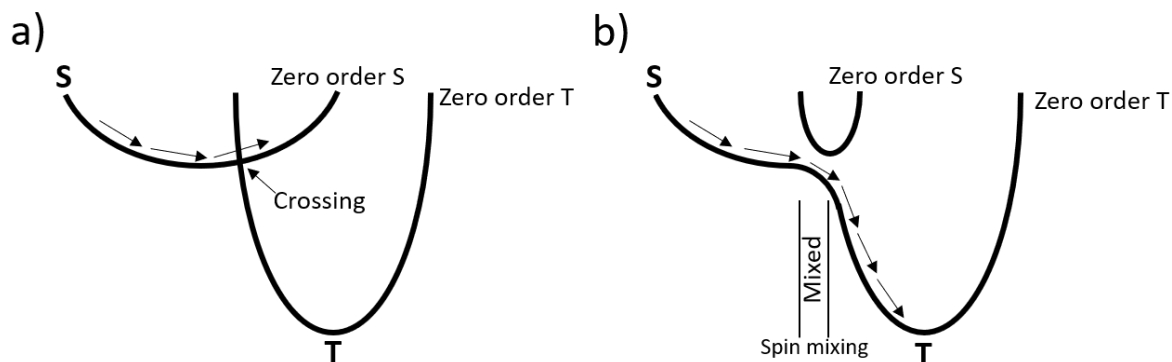
Figure 2.2 (a) Intersystem crossing is forbidden in the zero order approximation (b) it becomes partially allowed when a spin-mixing mechanism is available near the crossing point of the energy curves for the S and T states. Figure adapted from Turro[2]

2.2 <u>Jabłonski Diagram</u>

A Jabłoński diagram is a visual representation of molecular energy levels arranged with energy on the vertical axis. It is normally used to highlight relevant energy levels and the possible optical transitions in a molecule (or in the case of this thesis, an exciplex). For simplicity it is practice to separate states with different multiplicity in different horizontal regions.

A general Jabłoński diagram is shown in Figure 2.3. The thick lines represent the different electronic levels, while the thinner lines above them represent the excited vibrational states of the electronic levels. The dashed arrows represent non radiative processes while the solid arrows represent either absorption or emission transitions. The horizontal wavy arrows represent internal conversion (IC) processes where an excited state rapidly converts to an isoenergetic vibronic state on a lower electronic band. On a typical Jabłoński diagram it is possible to visualize transitions between states like absorption, fluorescence, delayed fluorescence, phosphorescence, vibrational relaxations as well as intersystem crossing (ISC) and reverse intersystem crossing (rISC). The diagram in Figure 2.3 also shows typical rates that are involved for the different optical processes. Absorption (k_{abs}) happens in the femtosecond regime, while emission from the prompt fluorescence (k_{PF}) occurs in the nanosecond timescale. Depending on the photophysical properties of the system studied, an equilibrium between the singlet and triplet populations may be established by the ISC and rISC. If the rISC is efficient in the order of microseconds and it can give rise to delayed fluorescence (k_{DF}) through TADF.

Conversely, phosphorescent emission (k_{PH}) from the lowest triplet to the ground state can be commonly observed in the millisecond region. This latter process is much slower than k_{PF} because it is spin forbidden but can take place if SOC is present and all non-radiative processes heavily suppressed. This criterion is commonly achieved by cooling the sample to liquid nitrogen temperature (or even below) while the first is entirely material dependent. Very efficient SOC can also boost k_{PH} in the microsecond region.
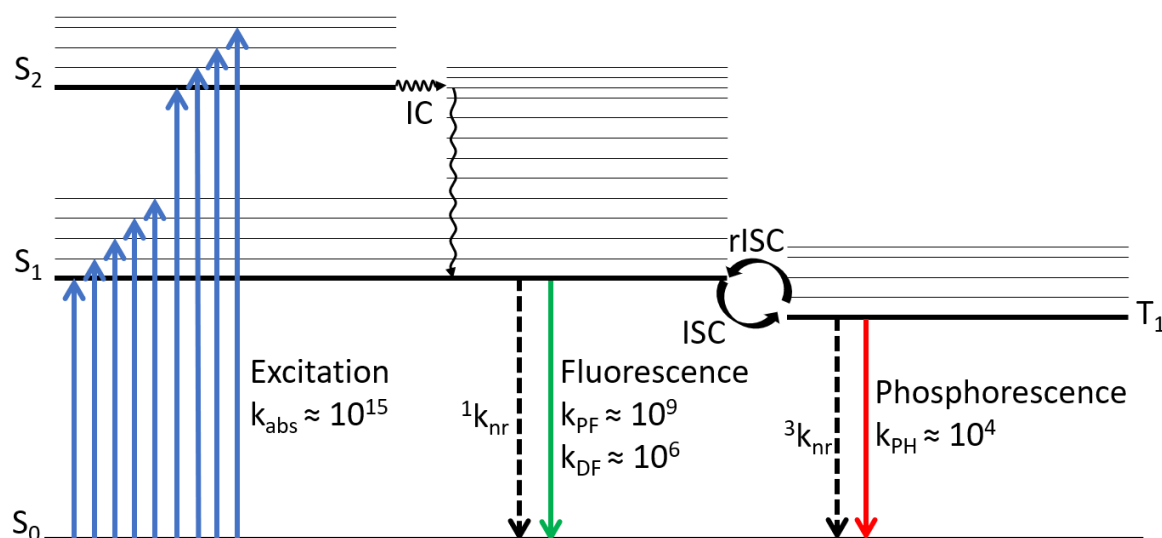
Figure 2.3 Jabłonski diagram with thick lines to represent the electronic states while the thinner lines represent the vibrational states. S_0 is the ground state, S_1 and T_1 are the first singlet and triplet excited states respectively. The dashed arrows represent non radiative processes while the solid arrows represent either absorbed or emitted radiation. k_{abs}, k_{PF}, k_{DF} and k_{PH} are respectively the transition rates of absorption, prompt fluorescence, delayed fluorescence and phosphorescence.[5]

2.3 Triplet Harvesting Mechanisms

While triplet states are generally not optically accessible, they are formed three times more often than singlet states under electrical excitation. This is because optical selection rules prevent the photoexcited electron to spin flip from the singlet ground state which it originates from.[2,6] This constraint does not apply when the excitons are formed electrically since the electrons are injected into the organic film where they are free to interact according to the spin statistic presented in section 2.1.1.1. As such, finding ways to convert non emissive triplets into emissive singlets is important for OLED applications.

Three mechanisms have been investigated to harvest triplet for light production; phosphorescence, triplet-triplet annihilation (TTA) and thermally activated delayed fluorescence (TADF). The photophysical mechanisms of each are schematically shown in

Figure 2.4 which shows simplistically the main key concepts behind the three triplet harvesting mechanisms that are being discussed, more details about the physics and the energy levels involved are given in the following dedicated sections.

a) Phosphorescence　　b)　　TTA　　c)　　TADF

$k_{ISC} \approx 10^{12}$ s^{-1}　　TTA　　$k_{rISC} \approx 10^{6}$ s^{-1}

S_1　　　　　　S_1　　　　　　S_1　　　T_1

　　　T_1　　　　　2xT_1　　　$k_{ISC} \approx 10^{7}$ s^{-1}

$k_{PH} \approx 10^{6}$ s^{-1}　　$k_F \approx 10^{9}$ s^{-1}　　$k_F \approx 10^{9}$ s^{-1}

S_0　　　　　　S_0　　　　　　S_0
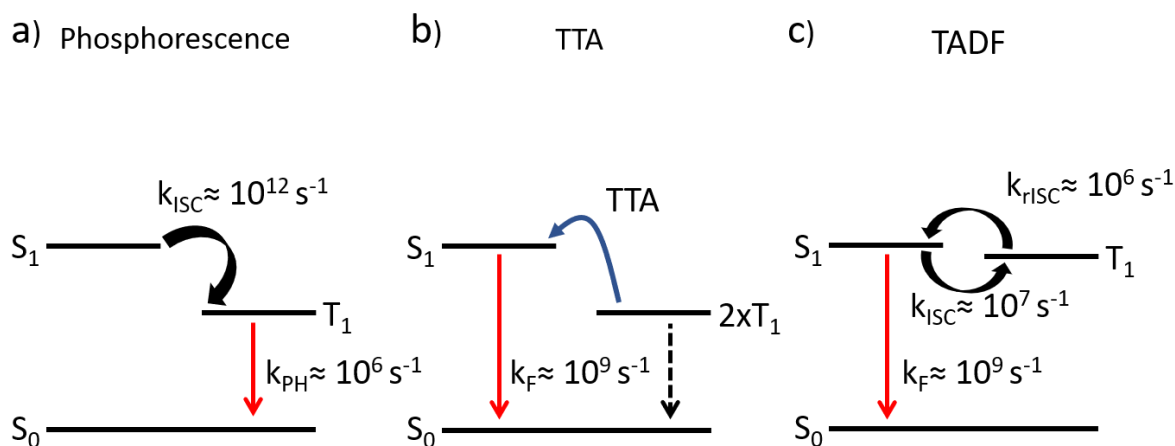
Figure 2.4 Schematic representation of the three triplet harvesting mechanisms used to maximise the efficiency of the OLED devices, (a) Phosphorescence (b) TTA and (c) TADF. The black arrows in (a) and (c) represent the the ISC-rISC processes. In (a) the ISC process is ultrafast in the picosecond or faster timescale and the process bottleneck is represented by the lifetime of the triplets.[7,8] In (b) the arrow is different (blue) because the nature of triplet harvesting is collisional and the rate depends on carrier density, and so comparing to intrinsic ISC or rISC rates is not valid, nonetheless the upconverted states will emit in the nanosecond timescale typical of fluorescent processes.[9,10] In (c) rISC and ISC are typically comparable with the latter usually an order of magnitude faster. The difference in the equilibrium is given by the fact that the upconverted singlets will emit at a rate two order of magnitudes faster than ISC thus making the triplet harvesting mechanism effective.[11,12]

2.3.1 Phosphorescence

The first triplet harvesting mechanism to be efficiently exploited was phosphorescence (Figure 2.4a) where singlet states converted into triplets trough ISC and directly generated triplet states can emit efficiently thanks to effective SOC maximised by the presence of heavy metals in the molecular structure of the emitter (eg Ir, Pt). The magnitude of the SOC is proportional to Z^4 (as previously mentioned) and hence more effective with heavy atoms.[13] This SOC makes the spin flip necessary for direct emission out of T_1 weakly allowed and competitive with other non-radiative decay rates that make phosphorescence undetectable in most materials at room temperature. It has been demonstrated that for Ir and Pt complexes the PLQY can reach values close to 100% at room temperature which has made them ideal candidates as emitters in OLEDs.[13]

2.3.2 TTA

TTA (Figure 2.4b) is a bi-excitonic collisional process where two excited triplets form an encounter complex, promoting (ideally) one triplet to the singlet excited state while the other relaxes to the ground state. This process is allowed as long as $2E_{T1} > E_{S1}$.

The encounter complex of two triplets can create 9 different states with three different characters, a singlet, a triplet or a quintet depending of the total resulting spin of the two interacting triplets forming the encounter complex. The most useful resulting state (for OLED application) is the singlet since it can produce an excited singlet state according to Equation 2.3 which can decay radiatively originating delayed fluorescence (DF).

Equation 2.3

$$2T_1 \rightarrow S_0 + S_1$$
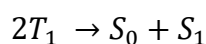
Conversely to the singlet encounter complex, the triplet and the quintet cannot produce and excited singlet state thus effectively acting as quenching mechanisms to singlet complexes.

Even considering the ideal situation where level alignment minimises the loss mechanisms ($2E_{T1} < E_{Tn}$ with $n > 1$ and $2E_{T1} \neq S_1$ to avoid singlet fission) the limitation of the TTA process is that as a 2:1 triplet to singlet process only 50% of the triplets produced can be recycled into singlets. Therefore, the theoretical maximum efficiency achievable by an ideal TTA emitter in an OLED is the 25% singlets excitons (directly generated) plus half of the triplet excitons, all of which form efficient TTA pairs, resulting in 25%+0.5*75%=62.5%.[14]

In practice TTA only becomes efficient at high density of triplets and is considered a loss mechanism for OLED devices based on phosphorescence and TADF emitters which can harvest the entire triplet population (and not only half) leading a maximum efficiency of 100%.

To identify that the DF observed from a system arises from TTA, the measurement of the power dependence of the DF intensity is of fundamental importance to distinguish it from the other triplet harvesting mechanisms (eg TADF).

2.3.3 TADF

The current model for the TADF mechanism presented here is based on the work of Penfold et al[15], Marian et al[16] and from Monkman group[17–19]. If phosphorescence and non-radiative decay of the triplet state is slow and the energy gap between the singlet and triplet states is small enough (normally <0.2 eV), then rISC back to the singlet state can occur efficiently. Initial

studies assumed that TADF occurred between the [1]CT and [3]CT states, however El Sayed's rule instead demands that there must be a change in orbital type in order to have a non-negligible k_{ISC}. In other words, ISC between two states of the same orbital character is strictly forbidden.[20] Later Monkman and co-workers [18,19] showed that the states involved in TADF could be independently tuned by the environment, and therefore must be of different character.

This result led to the insight that a local excited triplet state ([3]LE) must be mediating the rISC process. Dias et al.[19] showed that different molecules with very similar energy gaps (ΔE_{ST}) exhibit large variations in k_{rISC}. They show that by sterically hindering the motion of Donor (D) and Acceptor (A) groups, the emission could be switched from TADF to room temperature phosphorescence (RTP).[21] This result demonstrated experimentally the fundamental role of vibronic coupling in the TADF process, as steric restriction of the vibrational motion removed the coupling mechanism between the [3]CT and the [3]LE necessary to achieve high k_{rISC}. Concurrently Etherington et al.[22] showed by experimentally tuning the CT in and out resonance with the [3]LE states the rISC could be tuned and it was maximum when the CT was in resonance with the [3]LE. Later Gibson et al[23] would later show by simulation that the two main processes of the TADF mechanisms are reverse Internal Conversion (rIC) (Equation 2.4) which establishes an equilibrium between the [3]LE and [3]CT depending of the size of the vibronic coupling and rISC mediated by the energy gap to convert [3]LE into [1]CT. Equation 2.5 shows how the coupling between [3]CT and [1]CT is always mediated by the [3]LE (Figure 2.5).

Equation 2.4

$$k_{IC} = \frac{2\pi}{\hbar} \left| \langle \Psi_{3_{CT}} | \widehat{H}_{vib} | \Psi_{3_{LE}} \rangle \right|^2 \delta\left(E_{3_{CT}} - E_{3_{LE}}\right)$$

Equation 2.5

$$k_{rISC} = \frac{2\pi}{\hbar} \left| \frac{\langle \Psi_{1_{CT}} | \widehat{H}_{SOC} | \Psi_{3_{LE}} \rangle \langle \Psi_{3_{LE}} | \widehat{H}_{vib} | \Psi_{3_{CT}} \rangle}{E_{3_{CT}} - E_{3_{LE}}} \right|^2 \delta\left(E_{1_{CT}} - E_{3_{LE}}\right)$$

Where k_{IC} and k_{rISC} are the internal conversion and reverse intersystem crossing rates; $\hbar$ is the Planck's constant $\Psi_{3_{LE}}$, $\Psi_{1_{CT}}$, $\Psi_{3_{CT}}$ are respectively the locally excited triplet, the charge transfer singlet and the charge transfer triplet wavefunctions; $\widehat{H}_{vib}$, $\widehat{H}_{SOC}$ are the vibronic and the spin orbit coupling Hamiltonians; $E_{3_{LE}}$, $E_{1_{CT}}$ and $E_{3_{CT}}$ are the electronic energy levels of the locally excited triplet, the charge transfer singlet and the charge transfer triplet; $\delta\left(E_{3_{CT}} - E_{3_{LE}}\right)$ and $\delta\left(E_{1_{CT}} - E_{3_{LE}}\right)$ are Kronecker deltas of the two equations. The Kronecker

delta function is equal to 1 if the energy levels inside the round brackets are equal is otherwise zero for any other case.

This assumes that the electronic energy must be resonant for IC and rISC processes to be efficient we nonetheless know from the literature that this condition is not as stringent as it is represented in Equation 2.4 and 2.5 and that there are numerous examples of molecules and exciplexes that emit efficiently via TADF with a $\Delta E_{ST} \neq 0$ althoug still very small in the order of tens of meV.[19,23,24]
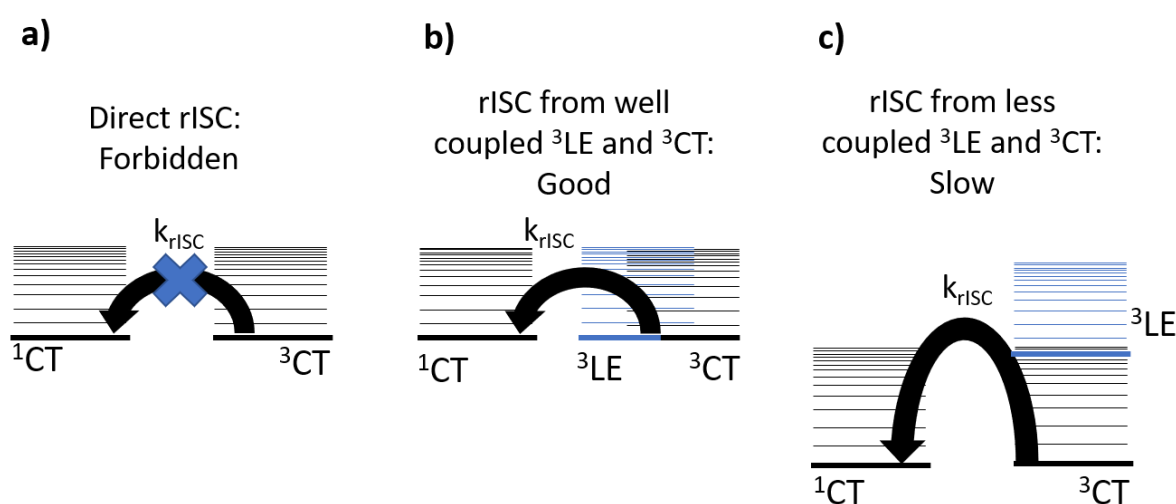
Figure 2.5 Schematic representation of the rISC pathways with different ^{3}LE-^{3}CT alignments. Figure adapted from Gibson et al.[23]

The size of the rISC rate is also strongly dependent by the ΔE_{ST} gap (Equation 2.6 empirically and Equation 2.5 theoretically).

Equation 2.6

$$k_{rISC} \propto e^{-\Delta E_{ST}/k_B T}$$

While all of the above work was performed on molecular TADF materials with intra-molecular CT states, similar findings concerning the TADF mechanism in exciplexes were also reported by Monkman et al. [25] While this work also highlight the fundamental role of the ΔE_{ST} gap, little can be said about the role of vibronic coupling since this cannot be controlled as it has been in the D-A molecules.

2.3.4 Exciplexes

An exciplex is an **exci**ted com**plex** that is bound in the excited state while does not interact in the ground state. It requires an electron donating (donor or D) and an electron accepting

(acceptor or A) molecule to form. It can be formed by photoexciting either the donor or the acceptor which will be locally excited with the state localised on excited molecule. This LE state separated at the D-A interface forming a CT exciplex. The exciplex formation when one of the two components is photoexcited (D^* or A^*) happens through electron transfer (ET) (schematically shown in Figure 2.7a). The wavefunction of the exciplex (DA)* can be then written similarly to Equation 2.2 with M_1 and M_2 being the acceptor (A) and the donor (D).

Equation 2.7

$$\psi([DA]^*) \approx c_1\psi(D^*A) + c_2\psi(DA^*) + c_3\psi(D^+A^-)$$

With $|c_3|^2$ representing the fraction of CT states in the exciplex wavefunction.

Not all D-A couples will form an exciplex, it has been showed in the literature that a driving force for the electron transfer has to be present for it to form in the first place. This driving force has been identified in the difference between the LUMO and HOMO levels of the D and A components. The minimum requirement for exciplex formation can be summarised as $E_{LUMO}^A - E_{LUMO}^D > 0$ and $E_{HOMO}^A - E_{HOMO}^D > 0$, if these conditions are not met, ET in not energetically favourable as schematically shown in Figure 2.6.[26]
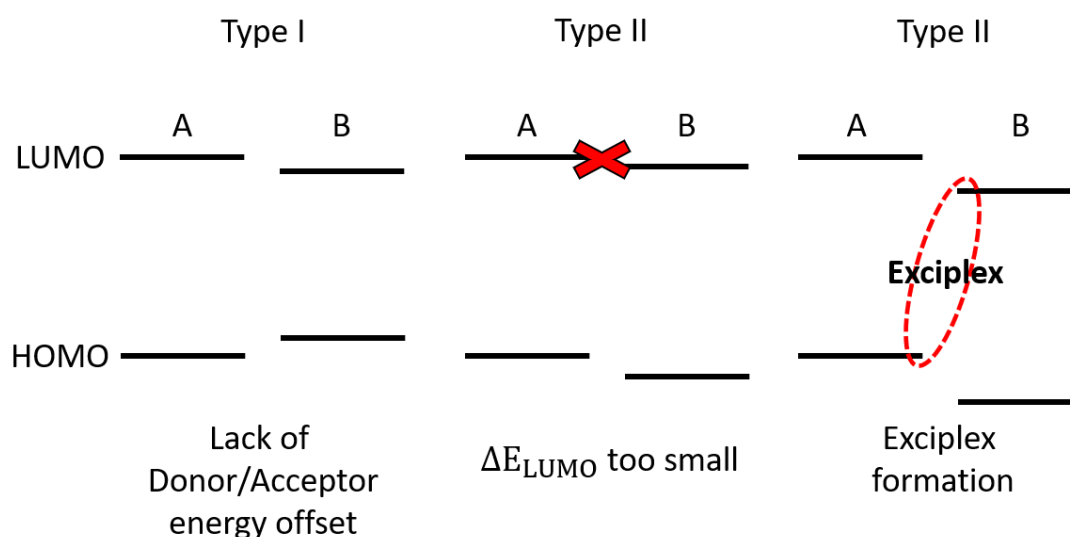
Figure 2.6 From left to right: The materials do not form a D-A couple, charge transfer is not possible and energy transfer from A to B occurs instead, this kind organic heterojunction is referred to as Type I. Donor (A) and acceptor (B) have very similar LUMO energies so the ET will be inefficient; donor (A) and acceptor (B) with suitable energy levels to promote efficient ET thus exciplex formation can take place efficiently. The organic heterojunctions shown in the middle and right part of the figure are referred to as Type II.

The exciplex emission happens at the D-A interface and its maximum theoretical energy is, in first approximation, the difference between the $E_{LUMO}^A - E_{HOMO}^D$ (Figure 2.7b). An important contribution to total energy of the exciplex is given by the Coulomb attraction energy $E_C(r) =$

$\frac{e^2}{4\pi r \varepsilon_0 \varepsilon}$ between the D-A couple.[4,27] The exciplex energy can be then written in first approximation as:

Equation 2.8

$$E_{Exciplex} = E_{LUMO}^{A} - E_{HOMO}^{D} - E_{C}(r)$$

It is clear from Equation 2.8 that, the more physically separated the D-A couple is, the more blueshifted its emission will be due to the reduction of the $E_C(r)$ term. Furthermore, Attar et al[27] proved that it is possible to induce blueshift in interfacial exciplexes were a preferential orientation of the D-A exciplex dipoles can be induced proving that pulling the D-A couples apart by using external electric field assuming that the HOMO and LUMO levels of D and A do not change under the effect of the electric field.
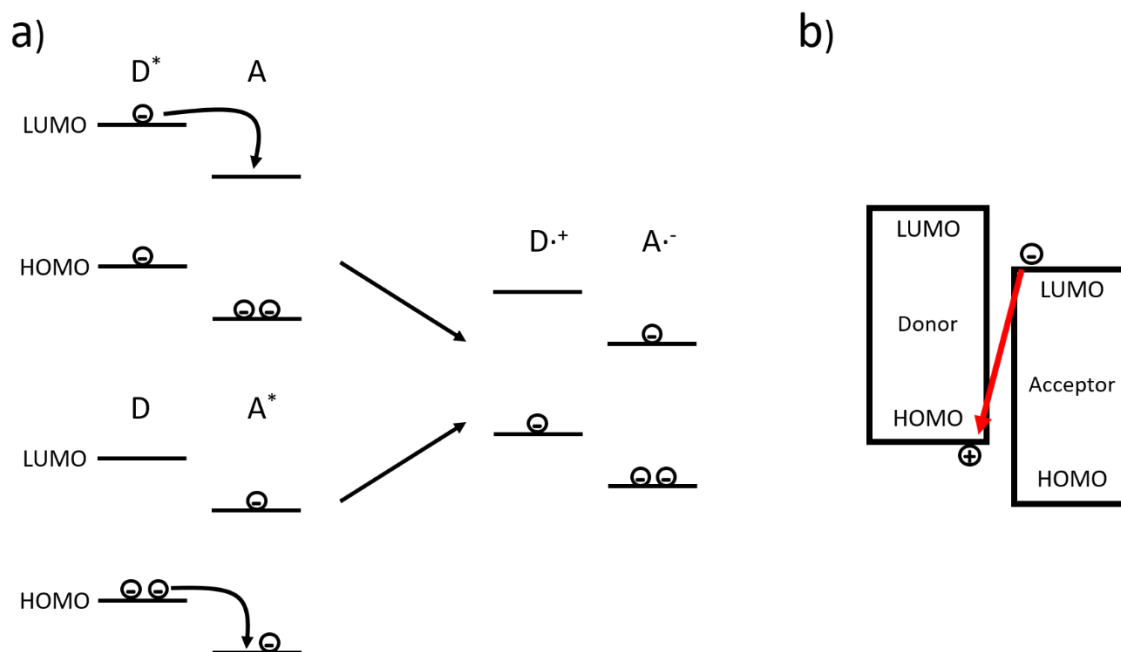
Figure 2.7 (a) Schematic representation of exciplex formation through electron transfer in the case of donor excitation or acceptor excitation, Figure adapted from Turro et al[28]. (b) Schematic representation of exciplex emission where only the $E_{LUMO}^{A} - E_{HOMO}^{D}$ contribution is being represented.

2.4 OLEDs

2.4.1 Working principle

An OLED is an optoelectronic device in which electroluminescence (EL) is used to produce light from an electrical input. This property was firstly observed in organic materials by André

Bernanose and co-workers in the early 1950s,[29] and in 1987 Tang and Van Slyke published the first efficient multilayer OLED.[30]

Figure 2.8b is shows a generic structure of an OLED, while Figure 2.8a shows a schematic representation of the correspondent energy level alignment of the different layer materials. Electrons are injected from the cathode, which is made of a low work function metal. In order to be injected from the cathode into the electron transport layer (ETL) the electrons need to overcome the electron injection barrier (ΔE_e); the energy difference between the work function of the cathode (ϕ_C) and electron affinity (EA) of the ETL. Holes, are injected from the anode, commonly formed by high work function transparent metal oxides such as the indium tin oxide (ITO), the transparency is required to allow the EL to emerge from the OLED. Similarly, holes have to overcome an hole injection barrier (ΔE_h), defined as the energy difference between the work function of the anode (ϕ_A) and the ionization potential of the hole transport layer (HTL). The purpose of the ETL and HTL is to reduce the injection barriers and facilitate the transport of the carriers to the emissive layer (EML). Once the carriers are injected in the device they can then interact in the EML, ideally forming an exciton that decays radiatively. All the other processes are considered energy loss pathways
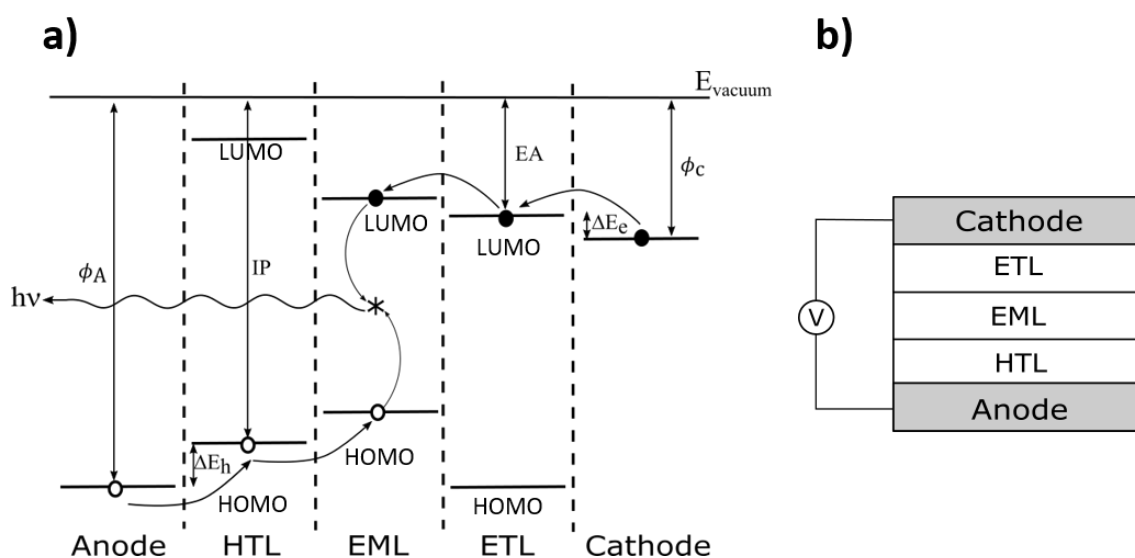
Figure 2.8 (a) Schematic representation of the energy level alignment of an OLED structure. (b) General structure of a multilayer OLED.

2.4.1.1 Exciplex OLEDs

Interfacial exciplexes were for long avoided in OLEDs structures since they represented a design flaw in the OLED stack and an efficiency loss pathway.[31,32] On the other hand,

exciplexes offer the possibility to working structures with only two organic materials since an exciplex is essentially composed by an hole transporting and a electron transporting material. This offers the possibility of building structures of the kind HTL|EML(Exciplex)|ETL (Figure 2.9) where the exciplex in this case it would be a mixture of the HTL and the ETL. This simplified yet effective structure characteristic offers a great practical advantage when industrial upscaling is taken into account.
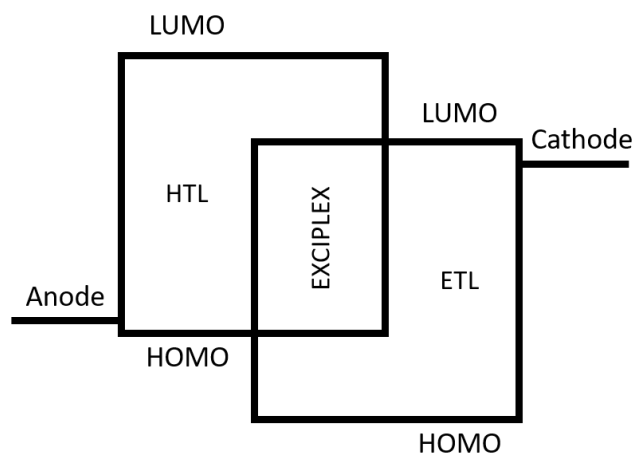
Figure 2.9 Schematic representation of an OLED structure where only two exciplex forming materials are employed. The HTL and ETL act respectively as donor and acceptor materials in the EML (EXCIPLEX) blend.

Even before exciplexes were investigated as promising candidates for the EML, they were widely used as hosts due to the great exciton confinement capability that they offer while being able to exploit energy transfer to higher PLQY emitters (eg PHOLEDs or laser dyes).[33–36] Their natural exciton confinement capabilities derive from the driving force necessary to form the exciplex in the first place. The HOMO-HOMO and LUMO-LUMO offset necessary to stabilise the exciplex couples is also what prevents the charges injected into the device from leaking through the remaining layers of the OLED stack thus remaining confined in the EML for the radiative processes.

The interest in exciplexes as emitters increased greatly after Goushi et al[37] demonstrated that it was possible to harvest triplets via TADF in the same way it was recently demonstrated small molecules.[25,26,38,39] Strategies to achieve efficient TADF in exciplex OLEDs were then further investigated. Dos Santos et al[25] highlighted the importance of the proximity of the LE triplet levels of the D-A couple to the exciplex energy to minimise the ΔE_{ST} thus maximise the rISC. Kim et al[40] demonstrated that cooling down an exciplex OLED is a possible way to boost its efficiency by reducing the non-radiative emission pathways. Later the same group reported a study showing that the relative orientation of the D-A couple would affect its photophysics.[41]

2.4.2 Stability

The failure mechanisms of OLED devices can be classified as either intrinsic or extrinsic. Intrinsic deterioration involves problems in the stability of the organic thin films, interfaces between anodes and organic layers, excited state stability, movement of ionic impurities, diffusion of transparent electrode metals into the active layers, cation instability, large energy barriers for charge carriers, positive charge accumulation, and width of recombination zones.[13] Extrinsic deterioration involves all the failure mechanisms unrelated to the materials and device structure. For Example, environmental factors such as atmospheric oxygen and moisture dramatically affect the lifetime of OLED devices. Environmental exposure of organic materials leads to the formation of non-emissive dark spots within the device area.[42] It is possible nonetheless to avoid the extrinsic degradation if the devices are properly encapsulated and therefore isolated from the environment.

Generally, intrinsic degradation processes lead to a progressive and spatially uniform loss of luminance efficiency over time during operation.[43] Initial studies focused on the thermal stability of the thin films, the formation of traps and luminescence quenchers, the interfacial degradation between adjacent layers and the anode instability. The concern was that the principal cause of the short operational lifetime was due the low glass transition temperatures (Tg) of the materials and especially of the HTL which would suffer the thermal stress as the device operates at high current. Adachi et al. then demonstrated that low T_g hole transport layers can also exhibit long lifetimes and vice versa.[44] The trap formation in the bulk has two effects, first the traps lead to the formation of non-radiative recombination centres, secondly, they are responsible for the decrease of the carrier mobility and hence the increasing of the operating voltage.[43,45] These effects add up over time and eventually significantly degrade the device performance. Understanding and avoiding these problems is therefore important for commercial applications.

2.5 <u>References</u>

(1)   Lakowicz, J. R. *Principles of Fluorescence Spectroscopy*; 1999. https://doi.org/10.1007/978-0-387-46312-4.

(2)   Turro, N. J.; Ramamurthy, V.; Ramamurthy, V.; Scaiano, J. C. *Principles of Molecular Photochemistry: An Introduction*; University science books, 2009.

(3)   Köhler, A.; Bässler, H. *Electronic Processes in Organic Semiconductors: An Introduction*; John Wiley & Sons, 2015.

(4)   Gordon, M.; Ware, W. R. *The Exciplex*; Academic Press, 1975.

(5)   Yersin, H. *Highly Efficient OLEDs: Materials Based on Thermally Activated Delayed Fluorescence*; Wiley-VCH, 2018.

(6)   Köhler, A.; Bässler, H. Triplet States in Organic Semiconductors. *Mater. Sci. Eng. R* **2009**, *66*, 71–109. https://doi.org/10.1016/j.mser.2009.09.001.

(7)   Scattergood, P. A.; Ranieri, A. M.; Charalambou, L.; Comia, A.; Ross, D. A. W.; Rice, C. R.; Hardman, S. J. O.; Heully, J.-L.; Dixon, I. M.; Massi, M.; et al. Unravelling the Mechanism of Excited-State Interligand Energy Transfer and the Engineering of Dual Emission in [Ir(C∧N)2(N∧N)]+ Complexes. *Inorg. Chem.* **2020**. https://doi.org/10.1021/acs.inorgchem.9b03003.

(8)   Hedley, G. J.; Ruseckas, A.; Samuel, I. D. W. Ultrafast Intersystem Crossing in a Red Phosphorescent Iridium Complex. *J. Phys. Chem. A* **2009**, *113* (1), 2–4. https://doi.org/10.1021/jp808944n.

(9)   Cheng, Y. Y.; Fückel, B.; Khoury, T.; Clady, R. G. C. R.; Tayebjee, M. J. Y.; Ekins-Daukes, N. J.; Crossley, M. J.; Schmidt, T. W. Kinetic Analysis of Photochemical Upconversion by Triplet−Triplet Annihilation: Beyond Any Spin Statistical Limit. *J. Phys. Chem. Lett.* **2010**, *1* (12), 1795–1799. https://doi.org/10.1021/jz100566u.

(10)   Jankus, V.; Snedden, E. W.; Bright, D. W.; Whittle, V. L.; Williams, J. A. G.; Monkman, A. Energy Upconversion via Triplet Fusion in Super Yellow PPV Films Doped with Palladium Tetraphenyltetrabenzoporphyrin: A Comprehensive Investigation of Exciton Dynamics. *Adv. Funct. Mater.* **2013**, *23* (3), 384–393. https://doi.org/10.1002/adfm.201201284.

(11)   dos Santos, P. L.; Ward, J. S.; Congrave, D. G.; Batsanov, A. S.; Eng, J.; Stacey, J. E.; Penfold, T. J.; Monkman, A. P.; Bryce, M. R. Triazatruxene: A Rigid Central Donor Unit for a D–A3 Thermally Activated Delayed Fluorescence Material Exhibiting Sub-Microsecond Reverse Intersystem Crossing and Unity Quantum Yield via Multiple Singlet–Triplet State Pairs. *Adv. Sci.* **2018**, *5* (6), 1700989. https://doi.org/10.1002/advs.201700989.

(12)   Haase, N.; Danos, A.; Pflumm, C.; Morherr, A.; Stachelek, P.; Mekic, A.; Brütting, W.; Monkman, A. P. Kinetic Modeling of Transient Photoluminescence from Thermally Activated Delayed Fluorescence. *J. Phys. Chem. C* **2018**, *122* (51), 29173–29179. https://doi.org/10.1021/acs.jpcc.8b11020.

(13)   Buckley, A. *Organic Light-Emitting Diodes (OLEDs): Materials, Devices and Applications*; Elsevier, 2013.

(14)   Monkman, A. P. Singlet Generation from Triplet Excitons in Fluorescent Organic Light-Emitting Diodes. *ISRN Mater. Sci.* **2012**, 670130.

(15)   Penfold, T. J.; Dias, F. B.; Monkman, A. P. The Theory of Thermally Activated Delayed Fluorescence for Organic Light Emitting Diodes. *Chem. Commun.* **2018**, *54* (32), 3926–3935. https://doi.org/10.1039/C7CC09612G.

(16)   Marian, C. M. Spin–Orbit Coupling and Intersystem Crossing in Molecules. *Wiley Interdiscip. Rev. Comput. Mol. Sci.* **2012**, *2* (2), 187–203. https://doi.org/10.1002/wcms.83.

(17)   Dias, F. B.; Penfold, T. J.; Berberan-Santos, M. N.; Monkman, A. P. Photophysics of Thermally Activated Delayed Fluorescence in Organic Molecules. *Methods Appl. Fluoresc.* **2017**, *5*, 012001. https://doi.org/10.1142/9789813230194_0006.

(18)   Santos, P. L.; Ward, J. S.; Data, P.; Batsanov, A. S.; Bryce, M. R.; Dias, F. B.; Monkman, A. P. Engineering the Singlet–Triplet Energy Splitting in a TADF Molecule. *J. Mater. Chem. C* **2016**, *4* (17), 3815–3824. https://doi.org/10.1039/C5TC03849A.

(19)   Dias, F. B.; Bourdakos, K. N.; Jankus, V.; Moss, K. C.; Kamtekar, K. T.; Bhalla, V.; Santos, J.; Bryce, M. R.; Monkman, A. P. Triplet Harvesting with 100% Efficiency by Way of Thermally Activated Delayed Fluorescence in Charge Transfer OLED Emitters. *Adv. Mater.* **2013**, *25* (27), 3707–3714. https://doi.org/10.1002/adma.201300753.

(20)   El-Sayed, M. A. Triplet State. Its Radiative and Nonradiative Properties. *Acc. Chem. Res.* **1968**, *1* (1), 8–16. https://doi.org/10.1021/ar50001a002.

(21)   Ward, J. S.; Nobuyasu, R. S.; Batsanov, A. S.; Data, P.; Monkman, A. P.; Dias, F. B.; Bryce, M. R. The Interplay of Thermally Activated Delayed Fluorescence (TADF) and Room Temperature Organic Phosphorescence in Sterically-Constrained Donor–Acceptor Charge-Transfer Molecules. *Chem. Commun.* **2016**, *52* (12), 2612–2615. https://doi.org/10.1039/C5CC09645F.

(22)   Etherington, M. K.; Gibson, J.; Higginbotham, H. F.; Penfold, T. J.; Monkman, A. P. Revealing the Spin–Vibronic Coupling Mechanism of Thermally Activated Delayed Fluorescence. *Nat. Commun.* **2016**, *7*, 13680.

(23)   Gibson, J.; Monkman, A. P.; Penfold, T. J. The Importance of Vibronic Coupling for Efficient Reverse Intersystem Crossing in Thermally Activated Delayed Fluorescence Molecules. *ChemPhysChem* **2016**, *17* (19), 2956–2961. https://doi.org/10.1002/cphc.201600662.

(24)   Dias, F. B.; Santos, J.; Graves, D. R.; Data, P.; Nobuyasu, R. S.; Fox, M. A.; Batsanov, A. S.; Palmeira, T.; Berberan-Santos, M. N.; Bryce, M. R.; et al. The Role of Local Triplet Excited States and D-A Relative Orientation in Thermally Activated Delayed Fluorescence: Photophysics and Devices. *Adv. Sci. (Weinheim, Baden-Wurttemberg, Ger.* **2016**, *3* (12), 1600080. https://doi.org/10.1002/advs.201600080.

(25)   dos Santos, P. L.; Dias, F. B.; Monkman, A. P. Investigation of the Mechanisms Giving Rise to TADF in Exciplex States. *J. Phys. Chem. C* **2016**, *120* (32), 18259–18267. https://doi.org/10.1021/acs.jpcc.6b05198.

(26)   Jankus, V.; Data, P.; Graves, D.; McGuinness, C.; Santos, J.; Bryce, M. R.; Dias, F. B.; Monkman, A. P. Highly Efficient TADF OLEDs: How the Emitter–Host Interaction Controls Both the Excited State Species and Electrical Properties of the Devices to Achieve Near 100% Triplet Harvesting and High Efficiency. *Adv. Funct. Mater.* **2014**, *24* (39), 6178–6186. https://doi.org/10.1002/adfm.201400948.

(27)   Al Attar, H. A.; Monkman, A. P. Electric Field Induce Blue Shift and Intensity Enhancement in 2D Exciplex Organic Light Emitting Diodes; Controlling Electron-Hole Separation. *Adv. Mater.* **2016**, *28*, 8014–8020. https://doi.org/10.1002/adma.201600965.

(28)   Kavarnos, G. J.; Turro, N. J. Photosensitization by Reversible Electron Transfer: Theories, Experimental Evidence, and Examples. *Chem. Rev.* **1986**, *86* (2), 401–449. https://doi.org/10.1021/cr00072a005.

(29)   Bernanose, A.; Vouaux, P. Organic Electroluminescence Type of Emission. *J. Chim. Phys* **1953**, *50*, 261.

(30)   Tang, C. W.; Van Slyke, S. A. Characterization and Optimization of High Brightness Organic Light Emitting Diodes (OLEDs). *Appl Phys Lett* **1987**, *51*, 913–915.

(31)   Tamoto, N.; Adachi, C.; Nagai, K. Electroluminescence of 1,3,4-Oxadiazole and Triphenylamine-Containing Molecules as an Emitter in Organic Multilayer Light Emitting Diodes. *Chem. Mater.* **1997**, *9* (5), 1077–1085.

(32)   dos Santos, P. L.; Ward, J. S.; Bryce, M. R.; Monkman, A. P. Using Guest–Host Interactions To Optimize the Efficiency of TADF OLEDs. *J. Phys. Chem. Lett.* **2016**, *7* (17), 3341–3346. https://doi.org/10.1021/acs.jpclett.6b01542.

(33)   Sarma, M.; Wong, K.-T. Exciplex: An Intermolecular Charge-Transfer Approach for TADF. *ACS Appl. Mater. Interfaces* **2018**, *10* (23), 19279–19304. https://doi.org/10.1021/acsami.7b18318.

(34)   Jankus, V.; Abdullah, K.; Griffiths, G. C.; Al-Attar, H.; Zheng, Y.; Bryce, M. R.; Monkman, A. P. The Role of Exciplex States in Phosphorescent OLEDs with Poly(Vinylcarbazole) (PVK) Host. *Org. Electron.* **2015**, *20*, 97–102. https://doi.org/https://doi.org/10.1016/j.orgel.2015.02.002.

(35)   Data, P.; Kurowska, A.; Pluczyk, S.; Zassowski, P.; Pander, P.; Jedrysiak, R.; Czwartosz, M.; Otulakowski, L.; Suwinski, J.; Lapkowski, M.; et al. Exciplex Enhancement as a Tool to Increase OLED Device Efficiency. *J. Phys. Chem. C* **2016**, *120* (4), 2070–2078. https://doi.org/10.1021/acs.jpcc.5b11263.

(36)   Wu, Z.; Yu, L.; Zhao, F.; Qiao, X.; Chen, J.; Ni, F.; Yang, C.; Ahamad, T.; Alshehri, S. M.; Ma, D. Precise Exciton Allocation for Highly Efficient White Organic Light-Emitting Diodes with Low Efficiency Roll-Off Based on Blue Thermally Activated Delayed Fluorescent Exciplex Emission. *Adv. Opt. Mater.* **2017**, *5* (20), 1700415. https://doi.org/10.1002/adom.201700415.

(37)   Goushi, K.; Yoshida, K.; Sato, K.; Adachi, C. Organic Light-Emitting Diodes

Employing Efficient Reverse Intersystem Crossing for Triplet-to-Singlet State Conversion. *Nat. Photonics* **2012**, *6*, 253.

(38) Graves, D.; Jankus, V.; Dias, F. B.; Monkman, A. Photophysical Investigation of the Thermally Activated Delayed Emission from Films of M-MTDATA:PBD Exciplex. *Adv. Funct. Mater.* **2014**, *24* (16), 2343–2351. https://doi.org/10.1002/adfm.201303389.

(39) Hung, W.-Y.; Fang, G.-C.; Lin, S.-W.; Cheng, S.-H.; Wong, K.-T.; Kuo, T.-Y.; Chou, P.-T. The First Tandem, All-Exciplex-Based WOLED. *Sci. Rep.* **2014**, *4*, 5161.

(40) Kim, K.-H.; Yoo, S.-J.; Kim, J.-J. Boosting Triplet Harvest by Reducing Nonradiative Transition of Exciplex toward Fluorescent Organic Light-Emitting Diodes with 100% Internal Quantum Efficiency. *Chem. Mater.* **2016**, *28*, 1936–1941. https://doi.org/10.1021/acs.chemmater.6b00478.

(41) Moon, C.-K.; Huh, J.-S.; Kim, J.-M.; Kim, J.-J. Electronic Structure and Emission Process of Excited Charge Transfer States in Solids. *Chem. Mater.* **2018**, *30* (16), 5648–5654. https://doi.org/10.1021/acs.chemmater.8b02011.

(42) Burrows, P. E.; Bulovic, V.; Forrest, S. R.; Sapochak, L. S.; McCarty, D. M.; Thompson, M. E. Reliability and Degradation of Organic Light Emitting Devices. *Appl. Phys. Lett.* **1994**, *65* (23), 2922–2924. https://doi.org/10.1063/1.112532.

(43) So, F.; Kondakov, D. Degradation Mechanisms in Small-molecule and Polymer Organic Light-emitting Diodes. *Adv. Mater.* **2010**, *22* (34), 3762–3777.

(44) Adachi, C.; Nagai, K.; Tamoto, N. Molecular Design of Hole Transport Materials for Obtaining High Durability in Organic Electroluminescent Diodes. *Appl. Phys. Lett.* **1995**, *66* (20), 2679–2681.

(45) Song, W.; Lee, J. Y. Degradation Mechanism and Lifetime Improvement Strategy for Blue Phosphorescent Organic Light-Emitting Diodes. *Adv. Opt. Mater.* **2017**, *5* (9), 1600901. https://doi.org/10.1002/adom.201600901.

Chapter 3:

Materials and Experimental Methods

This chapter details the main experimental methods employed to acquire the data discussed in the subsequent chapters. First, the set of organic materials studied are presented, then sample preparation methods and characterization techniques for the exciplex blends are outlined. Finally, the production and testing methods for OLED devices are presented.

3.1 Organic Materials Studied

In this thesis several donor-acceptor exciplex systems are examined. Almost all the molecules used were commercially available and used as received from Ossila, Sigma Aldrich and Lumtec. The only molecule used that is not commercially available was synthesised at the University of Strathclyde (D-A-D molecule "2d" in Chapter 6). Table 3.1-Table 3.5 summarise the chemical structures of all compounds utilised. All the materials used for OLED production were purified via vacuum sublimation under a temperature gradient or acquired pre-sublimed from the aforementioned suppliers. PEDOT:PSS was acquired from Ossila and filtered with a 0.45μm syringe filter to eliminate aggregates.

Table 3.1 Chemical structures of exciplex forming donors (D) used in this thesis including, chemical names, acronyms and chapters in which they feature.

Exciplex Donors					
Chemical Structure	**Chemical Name**	**HOMO/LUMO (eV)**	**E$_{gap}$ (eV)**	**Acronym**	**Chapter**
	4,4'-(Diphenylsilanediyl) bis(N,N-diphenylaniline)	5.9/2.3	3.6	TSBPA	4
	4,4'-Bis(carbazol-9-yl)-2,2'-dimethylbiphenyl	5.8/2.4	3.4	CDBP	5
	4,4'-Bis(carbazol-9-yl) biphenyl	5.8/2.3	3.5	CBP	5
	1,3-Bis(carbazol-9-yl) benzene	6.1/2.3	3.8	mCP	5
	4,4′-cyclohexylidenebis [*N,N*-bis(4methylphenyl) benzenamine]	5.5/2.0	3.5	TAPC	6
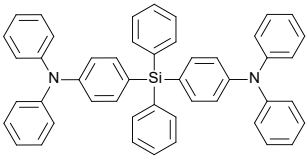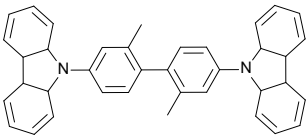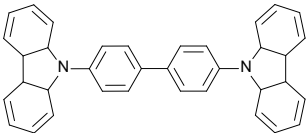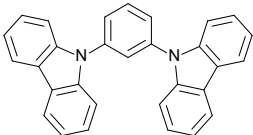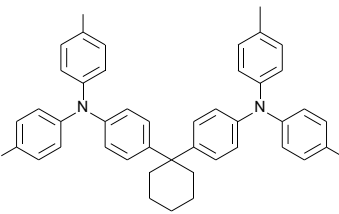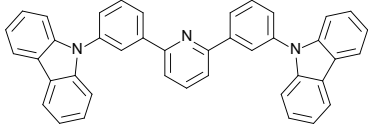
Chemical Structure	Chemical Name	HOMO/LUMO (eV)	E_gap (eV)	Acronym	Chapter
	2,6-bis[3-(9H-carbazol-yl)phenyl] pyridine	6.1/2.6	3.5	26DCzPPy	7

Table 3.2 Chemical structures of exciplex forming acceptors (A) used in this thesis including, chemical names, acronyms and chapters in which they feature

Exciplex Acceptors					
Chemical Structure	**Chemical Name**	**HOMO/LUMO (eV)**	**E$_{gap}$ (eV)**	**Acronym**	**Chapter**
	2,4,6-tris [3-(diphenylphosphinyl) phenyl] -1,3,5-triazine	7.1/3.2	3.9	PO-T2T	4,5,7
	9-[2,8]-9-carbazole-[dibenzothiophene-*S,S*-dioxide]-carbazole	6.1/3.1	3.0	2d DCz-DBTO2	6
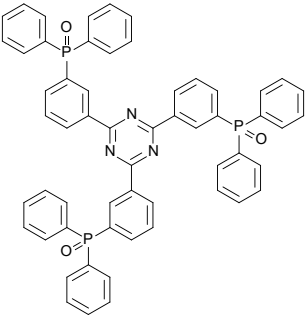
Table 3.3 Chemical structures of hosts used in this thesis including, chemical names, acronyms and chapters in which they feature

Hosts					
Chemical Structure	**Chemical Name**	**HOMO/LUMO (eV)**	**E$_{gap}$ (eV)**	**Acronym**	**Chapter**
	1,3-Bis(triphenylsilyl) benzene	7.1/2.8	4.3	UGH-3	4,5
	Bis[2-(diphenylphosphino) phenyl] ether oxide	6.5/2.0	4.5	DPEPO	4
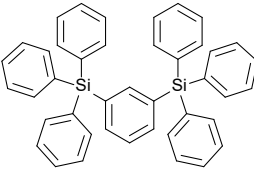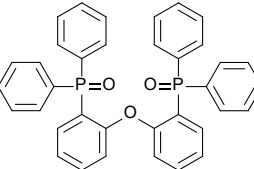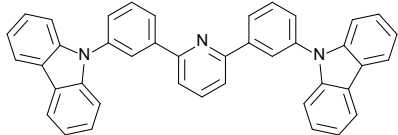
	2,6-bis[3-(9H-carbazol-yl)phenyl] pyridine	6.1/2.6	3.5	26DCzPPy	7

Table 3.4 Chemical structures of the hole transporting materials used in the OLEDs produced in this thesis including, chemical names, acronyms and chapter in which they feature
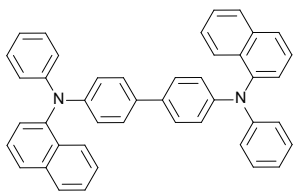
Hole Transporting Materials					
Chemical Structure	**Chemical Name**	**HOMO/LUMO (eV)**	**E$_{gap}$ (eV)**	**Acronym**	**Chapter**
	N,N′-Bis (naphthalen-1-yl)-N,N′ bis(phenyl)benzidine	5.5/2.4	3.1	NPB	4,5,7
	4,4'-(Diphenylsilanediyl) bis(N,N-diphenylaniline)	5.9/2.3	3.6	TSBPA	4
	4,4'-Bis(carbazol-9-yl)-2,2'-dimethylbiphenyl	5.8/2.4	3.4	CDBP	5
	4,4'-Bis(carbazol-9-yl) biphenyl	5.8/2.3	3.4	CBP	5
	1,3-Bis(carbazol-9-yl) benzene	6.1/2.3	3.8	mCP	5
	poly(3,4-ethylenedioxythiophene) polystyrene sulfonate	5.2 (Work Function)	n/a	PEDOT:PSS	6
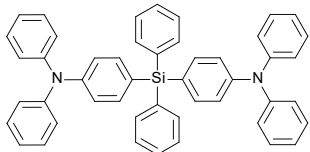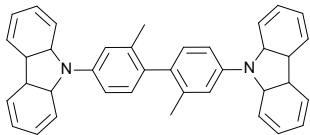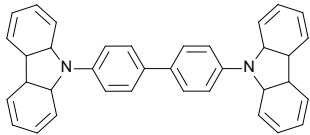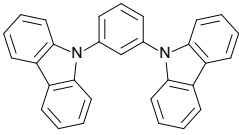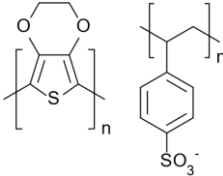
Table 3.5 Chemical structures of the electron transporting materials used in the OLEDs produced in this thesis including, chemical names, acronyms and chapter in which they feature
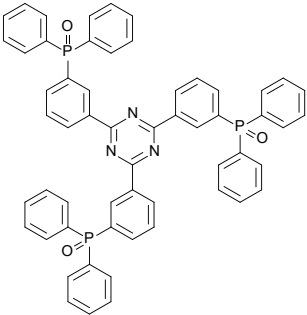
Electron Transporting Materials					
Chemical Structure	**Chemical Name**	**HOMO/LUMO (eV)**	**E$_{gap}$ (eV)**	**Acronym**	**Chapter**
	2,4,6-tris [3-(diphenylphosphinyl) phenyl] -1,3,5-triazine	7.1/3.2	3.9	PO-T2T	4,5,7
	2,2',2"-(1,3,5-Benzinetriyl)-tris(1-phenyl-1-H-benzimidazole)	6.2/2.7	3.5	TPBi	6,7
	2,9-Dimethyl-4,7-diphenyl-1,10-phenanthroline	6.4/3.0	3.4	BCP	7
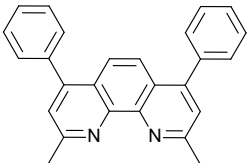
Table 3.6 Chemical structures of the Iridium complex used in the OLEDs produced in this thesis including, chemical names, acronyms and chapter in which they feature

Phosphorescent Red Dopant					
Chemical Structure	**Chemical Name**	**HOMO/LUMO (eV)**	**E$_{gap}$ (eV)**	**Acronym**	**Chapter**
	bis(2-(3,5-dimethylphenyl) quinoline-C2,N')(acetylacetonato)iridium(III)	5.3/3.3	2.0	Ir(dmpq)2acac	7

3.2 Sample Preparation

Photophysical characterization of exciplex blends was performed exclusively on solid state samples since it represents the closest condition to those in the OLED devices. The solid state samples were prepared either via drop casting or thermal evaporation on sapphire or quartz substrates. For drop casting, molecules were dissolved in toluene or chloroform at typical concentrations of 10 mg/ml, donor and acceptor solutions mixed in a 1:1 volume ratio, and then deposited on the substrate atop a pre-heated 50°C hotplate and left until completely dry in air. Lower concentrations were used if the solubility of a particular molecule was found to be below 10 mg/ml. This method affords rapid and simple access to thick films (desirable to increase absorption and emission signal) using small amounts of material but offers very little control on the microstructure of the deposited films. It is nonetheless a valuable tool to screen if a D-A blend forms an exciplex. Conversely, when a high degree of repeatability of the films deposited is required and, to minimise the segregation of the hetero molecules co-deposited and improve the heterogeneity of the dispersion in the exciplex-host blend, vacuum thermal evaporation (VTE) is the best option for film deposition. This technique is indeed well known to enable the production of reproducable films with minimum to none formation of aggregates, which are very likely to be found in films deposited via drop casting. The smoothness of the VTE deposited films is also important for the measurement of photoluminescence quantum yields of the blends, where scatter from surface roughness can influence the measurement. The downside of VTE is that material consumption is far greater.

3.3 Film Thickness Measurement

When preparing OLED devices it is critically important to be able to accurately measure the thickness of deposited films. In this thesis two techniques have been used to measure this parameter, ellipsometry and profilometry. In chapter 4, 5 and 7 a J.A Woollam VASE ellipsometer based in the physics department of Durham university has been used to measure film thickness for the calibration of the tooling factors of the vacuum deposited materials (see section 3.6.1). In chapter 6 a J.A Woollam VASE ellipsometer and a Dektak profilometer - both based at the Kroto Innovation centre in Sheffield - were used to measure the thicknesses of films deposited from solution and VTE.

3.3.1 Ellipsometry

Spectroscopic ellipsometry is a non-destructive optical technique based on the change in polarization of light as it is reflected obliquely from a thin film. Ellipsometry uses a model based approach to determine thin film properties such as the film thickness. The measurements were performed in the wavelength range of transparency of the films (typically 500-1100 nm) and the collected data were numerically fitted to estimate the film thickness. Films for this measurement were deposited on silicon oxide (SiOx) substrates of known SiOx thickness. The reason for using this substrate is twofold: firstly the highly reflective SiOx surface provides an optimal reflectance signal for the measurement, secondly the SiOx is a standard material in ellipsometry and it is very reliably fitted in the modelling software. This means that the sample model needs only to fit the organic film thickness to match the simulated and actual data.

3.3.2 Profilometry

In this technique a diamond stylus descends vertically into contact with a sample and is then dragged horizontally across the sample. The profilometer then measures small variations in vertical stylus displacement as a function of position. A small part of the deposited film is scratched away and the trace of the profilometer is taken across the valley formed by the scratch. The height difference between the scratched part of the sample and the untouched part of the film corresponds to the thickness of the sample. Profilometry is a direct technique with no modelling required, which is a significant advantage over ellipsometry (although the latter offers a more precise measurement when the sample is modelled correctly). In chapter 6 both techniques were used to measure the thickness of the spin coated films in order to cross validate the measurements.

3.4 <u>Steady-State Spectroscopy</u>

3.4.1 Optical Absorption

The absorption spectrum measures the ratio of absorbed to incident photons at a given wavelength (λ), which is proportional to the probability of a transition from the ground state to an excited state differing by the energy of the absorbed photon. The intensity of the light (wavelength λ) that passes through the sample (I) of known thickness (x) and concentration (c) is given by the Beer-Lambert law[1] (Equation 3.1).

Equation 3.1

$$I\left(\lambda\right) = I_0 e^{-\varepsilon(\lambda)xc}$$

Where I_0 is the intensity of the incident light and ε is the molar extinction coefficient which strongly depends of the incident wavelength.

Absorbance spectra were collected using a Shimadzu UV3600 double beam spectrometer in ambient conditions. All absorption spectra were collected from VTE deposited films using a blank substrate as reference. The instrument uses monochromated broad band light sources (deuterium lamp for the UV and tungsten for the Vis/NIR regions). The intensities of the transmitted light are collected with a PMT for the UV-Vis region and InGaAs detector for the Vis-NIR. The absorption spectrum is measured in terms of optical density (OD) which is defined in Equation 3.2.

Equation 3.2

$$OD = \log\frac{I_0}{I}$$

3.4.2 Photoluminescence

Photoluminescence (PL) spectra were recorded by measuring the intensity of emitted radiation as a function of the emission wavelength under continuous excitation with a selected wavelength. The PL spectrum is collected perpendicularly to the excitation in order to minimise reflected or scattered light from the excitation beam reaching the detector. The PL spectra were collected using either a Jobin Yvon Horiba Fluoromax 3 or Fluorolog spectrometers, both equipped with Xe arc lamp, an excitation monochromator, a reference photodiode, an emission monochromator and a PMT detector. The slits widths on both monochromators can be controlled to increase the resolution of the spectrum collected (at cost to signal intensity) and narrow the selected excitation wavelength (at cost of the total excitation power). The reference photodiode is used to normalise the intensity of the excitation beam in order to correct for the different output of the Xe lamp at different wavelengths and for output fluctuations over time. Finally, to take into account for the non-uniform sensitivity of the PMT to different wavelengths a (correction provided by the manufacturer) is applied automatically.

3.4.3 Photoluminescence Quantum Yield

The Photoluminescence quantum yield or PLQY of a material is defined as the number of photons emitted as a fraction of the number of photons absorbed (Equation 3.3).

$$PLQY = \frac{\text{\# Photons Emitted}}{\text{\# Photons Absorbed}}$$

This property of a fluorophore is of fundamental importance for understanding molecular behaviour and interactions of materials to be applied as emitters in OLEDs.

The PLQY measurements presented in chapter 4 were collected using a fibre coupled Thorlabs UV LED 340 nm as excitation source and an Ocean Optics HR2000+ spectrometer as detector connected to a 4" integrating sphere (Labsphere). The PLQY values measured on this system were calculated according to literature taking in account the direct and indirect interaction of the sample with the excitation beam.[2] The measurements presented in chapter 5 were acquired using a calibrated integrating sphere (Horiba Quanta-φ) coupled to a Horiba Fluorlog-3 spectrofluorometer (330 nm excitation) with calculations performed on included Fluoracle software. For all measurements the sphere was flushed with a stream of dry nitrogen gas for 30 minutes before measurement, unless otherwise specified.

3.5 Time Resolved Spectroscopy

3.5.1 Time-Gated Acquisition – CCD

Time resolved photoluminescence spectroscopy provides insight on the kinetics, energy levels (local or CT) and even the nature of the emissive process (eg TADF or TTA) of a given system. It is indeed possible to identify the dominant states giving rise to the prompt and delayed emission and their relative ratio. The setup (Figure 3.1a) uses a 10 Hz pulsed laser that hits the sample mounted in a cryostat oriented at 45°. The sample emission is then collimated and focused using two lenses onto a dual grating spectrograph that passes a variable spectral window to an intensified charge coupled device (iCCD) (Stanford Computer Optics 4Picos) triggerable with a 200 ps time resolution. The excitation source used was either the 3rd harmonic output of a Nd:YAG laser (355 nm output, FWHM of 150 ps) or a N_2 laser (337 nm output, FWHM of 3 ns). The shorter pulsed Nd:YAG was used to collect the PL decays since it allowed better temporal resolution in the prompt region of the decay, while the N_2 laser allowed a finer control of the excitation power and therefore was preferred for the acquisition of the laser fluences.
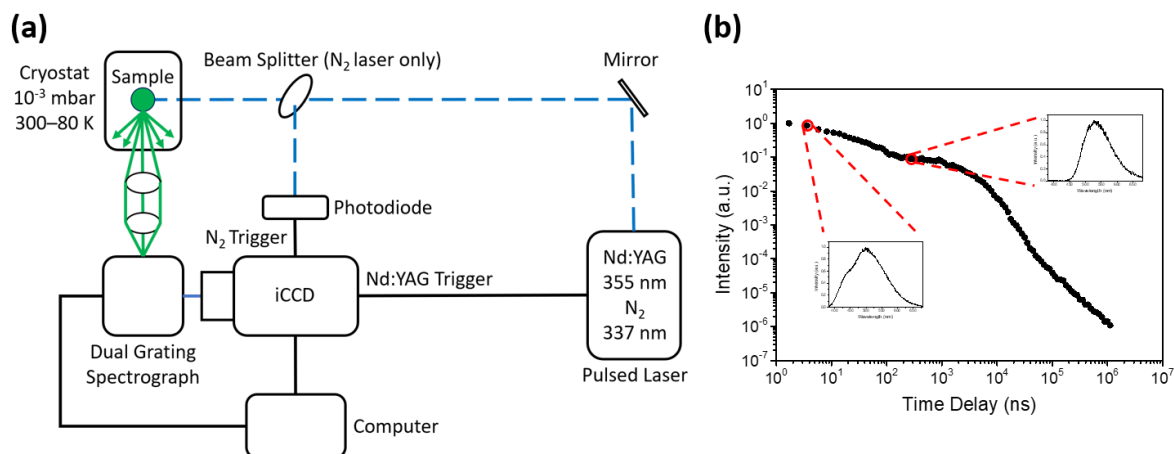
Figure 3.1 (a) Time gated PL spectrum acquisition system. The Nd:YAG uses an electronic signal to trigger the iCCD camera while the N_2 laser beam triggers the iCCD through a fast photodiode. (b) The intensity of the spectra collected with the iCCD at each delay time is integrated and normalised over the specific integration time. The integrated time normalised spectra (inset figure b) are then plotted against the delay time to reconstruct the PL decay.

To synchronise the laser pulses with the camera shutter, the iCCD has to be precisely triggered. The Nd:YAG laser is equipped with an electronic trigger that occurs before the laser pulse emerges and communicates directly with the camera. After the camera receives the trigger signal a fixed minimum delay time takes into account the time for the laser pulse to reach the sample in the cryostat which is mostly due to the internal optical processes inside laser itself such has the flashlamp/Q_{switch} timing. This fixed delay time has been measured at 975.5 ns, which appended to the FWHM of the Nd:YAG laser (150 ps) constitutes the zero time of the decays. This value has to be subtracted from the delay time of each spectrum as a constant the data analysis. The N_2 laser uses a fast photodiode as optical trigger but is used exclusively for laser fluence measurements where the delay time is much longer (> several µs) than the zero time of the system so no delay constant is introduced in the data processing of the spectra acquired with this laser. All measurements performed in this setup where carried out under vacuum (10^{-3} mbar) when at room temperature (≈ 290 K) or under stream of dry nitrogen when at 80 K.

3.5.1.1 Data Analysis

The spectra acquired with the system described in Figure 3.1a, are normalized over the spectral integration time, then plotted against the delay time to reconstruct the PL decay (Figure 3.1b). Information about the kinetics and the energy of the states involved in the emissive process can then be extracted from the decays and spectra. As many as three emission regions can often be observed in a PL decay (Figure 3.2a), the prompt fluorescence (PF), delayed fluorescence (DF) and phosphorescence (PH). These regions are not fixed and can occur at varying delay time,

especially when the temperature is changed from room temperature (RT) to 80K. At RT the phosphorescence usually cannot be observed, but sometimes even at low temperature it is not trivial to identify the emission from the local triplet (as later shown in chapter 5). Figure 3.2b shows how the ΔE_{ST} gap is determined from the difference between the onset of the steady state spectrum measured with the fluorimeter (giving ^1CT) and the phosphorescence acquired with iCCD system at low temperature and long delay time (giving ^3LE). The two onset values are converted in energy using the relation $E = h\nu/\lambda$ and their difference gives ΔE_{ST} gap.
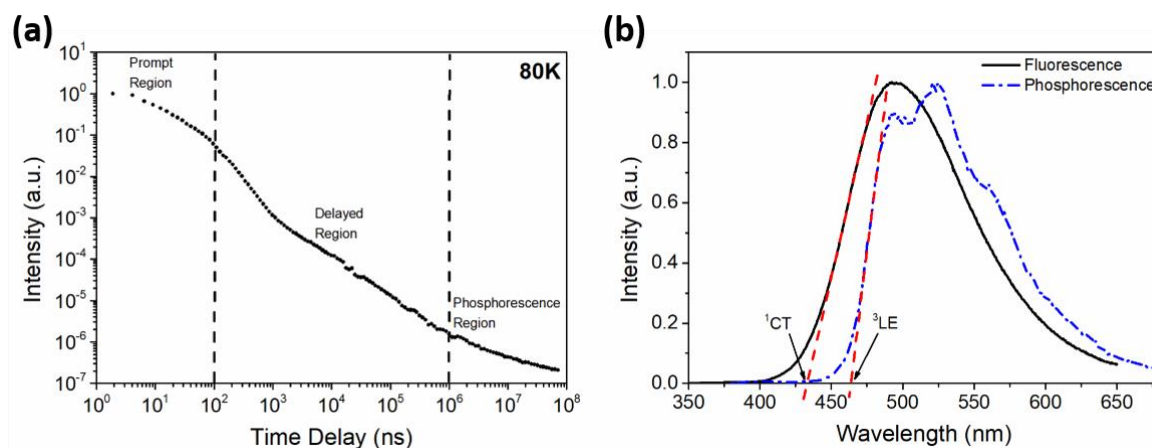
Figure 3.2 (a) PL decay measured at 80K where the prompt region, the delayed region and the phosphorescence region are highlighted (b) Identification of the ^1CT and ^3LE energy for an exciplex blend. The ^1CT is measured from the spectra acquired from the steady state measurement.

To quantify the kinetics of the emissive processes, the different regions of decays were fitted with a sum of exponential decay functions (Equation 3.4).

Equation 3.4

$$y(t) = \sum_{i=1}^{n} A_i e^{-t/\tau_i}$$

Where τ_i are the decay time constants or lifetimes of the species emitting in the region of the decay that is being fitted and A_i is a fit parameter. Both DF and PF can be fitted as aforementioned using different A_i and τ_i. An important parameter that can be derived from the decay is the ratio between the integrated intensity for the delayed region and the prompt region which indicates the contribution of the triplet harvesting process to the overall emission. This is the ratio of the DF and PF yield, Φ_{DF} and Φ_{PF} respectively. From this ratio and the lifetime of the DF region (τ_{DF}) is possible to calculate the rISC rate (k_{rISC}) according to Dias et al.[3]

Equation 3.5

$$k_{rISC} = \frac{1}{\tau_{DF}}(1 + \Phi_{DF}/\Phi_{PF})$$

3.6 <u>Organic Light Emitting Diodes (OLEDs)</u>

3.6.1 Fabrication

3.6.1.1 ITO cleaning

Regardless of the deposition process utilized, ITO substrates were cleaned in sonication baths of acetone and then isopropyl alcohol (IPA) for 15 minutes each. Afterward the substrates were dried with nitrogen (Sheffield, Chapter 6) or air (Durham, Chapter 4, 5 and 7) before being treated with UV ozone (Sheffield, Chapter 6) or oxygen plasma (Durham, Chapter 4, 5 and 7) for 10 minutes. Afterward the ITO substrates were ready for deposition (spin coating or VTE). Different ITO substrates were used across this thesis, in chapters 6 and 7 substrates purchased form Ossila (20 Ω/sq) were used with a pixel size of 4.5 mm^2. In chapter 4 and 5 VisionTek Systems ITO substrates were used with pixel sizes of 4, 8 and 16 mm^2.

3.6.1.2 Solution Processing

Spin coating is a versatile technique that allows deposition of thin films from solution in thicknesses ranging from μm to nm.[4] The technique uses centripetal force (generated by rotating the substrate at constant speed between few hundreds and few thousands rpm) to coat evenly the surface of a spinning substrate. Figure 3.3 shows how centripetal force pulls the liquid coating into an even covering. During deposition the solvent then evaporates to leave an even layer of the desired material. What makes spin coating so versatile is that it makes easily accessible a wide range of thicknesses. In fact, just three parameters can be changed to obtain the desired thickness (t): the rotation speed (ω), the concentration of the cast solution (C), and the viscosity of the solution (v), as shown in Equation 3.6.

Equation 3.6

$$t \propto \frac{vC}{\sqrt{\omega}}$$
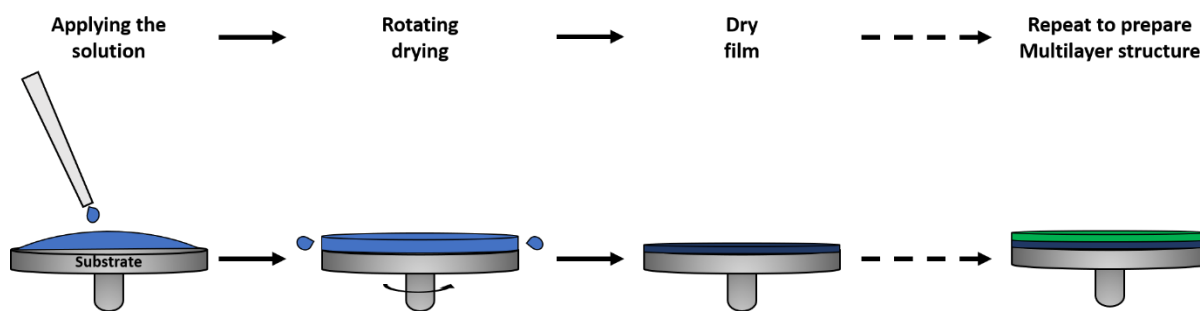
Figure 3.3 Schematic representation of the spin coating process. From left to right, solution dispensing, solvent evaporation due to the rotation, film drying, repeat if necessary to build multiple layers.

The first layer deposited in Chapter 6 is PEDOT:PSS Al 4083 (Ossila). Prior to deposition the PEDOT:PSS solution was filtered with a 0.45 µm PVDF filter. A 40 nm layer was then spun using 5000 rpm for 45 seconds. The films were then placed on a hot plate at 150°C for at least 10 minutes to evaporate all the remaining solvent and cooled down before depositing the next layer.

The emissive layer (EML) was then cast from chlorobenzene (CB), chloroform (CF) or a 5:95 vol% CB:CF solvent blend. All solutions were filtered using 0.1 µm PTFE filter and no thermal anneal was performed for the EML. The films deposited for the thickness study from CB were cast at spin speeds between 500 and 5000 rpm from a 20 mg/ml solution. For the thickness study from CF solvent the spin speed was kept constant at 6000 rpm and the concentration varied from 23.3-10 mg/ml in order to obtain the desired range of thicknesses. The spin speed for the films deposited from CF had to be kept constant and high because of the difficulty in obtaining good quality films when using this solvent for spin coating. The CB:CF solutions were prepared at 20 mg/ml concentration and spun at 6000 rpm. The different ratios were achieved by preparing solutions of the two components of the EML at the same concentration and then mixing these in the required volume ratios. The thicknesses of the films were measured using both ellipsometry and profilometry to ensure the validity of the measurements.

3.6.1.3   Vacuum Deposition

Thermal vacuum evaporation (VTE) is a technique used to deposit thin films from a wide range of materials with allows high level of control over the deposited thickness. The principle is to heat the material under high vacuum to produce vapour pressure. Under high vacuum conditions even a relatively low vapour pressure is sufficient to generate a cloud of gas inside the chamber that is free to travel through the chamber and deposit evenly onto the substrate itself, rotating at 10 rpm to ensure an even coverage. A schematic representation of a thermal evaporator is presented in Figure 3.4. In this scheme two different types of sources are shown,

one on the bottom of the chamber for metals and salts (LiF and Al in this thesis), and the others on the side of the chamber for organic materials (also called low temperature evaporation or LTE sources).

In this thesis three different evaporators were used: Lesker Spectros II systems at Sheffield (Chapter 6) and Durham (Chapter 7) that differed only in the number of LTE sources mounted in the chamber (2 in Sheffield and 6 in Durham), and a Lesker Super Spectros at Durham with 12 LTE sources. An important practical difference between the two Spectros II systems was that the one in Sheffield did not allow co-evaporation of multiple organic materials, while the one in Durham allowed routine 2 component co-evaporation. The Super Spectros on the other hand allowed simple co-evaporation of up to 6 materials at once (even though impractical for OLED production) necessary for the study presented in Chapter 4 and 5 were three materials needed to be co-evaporated. The Spectros II in Durham also differs slightly from the scheme presented in Figure 3.4, since it was equipped with a turbomolecular pump rather than a cryogenic pump.
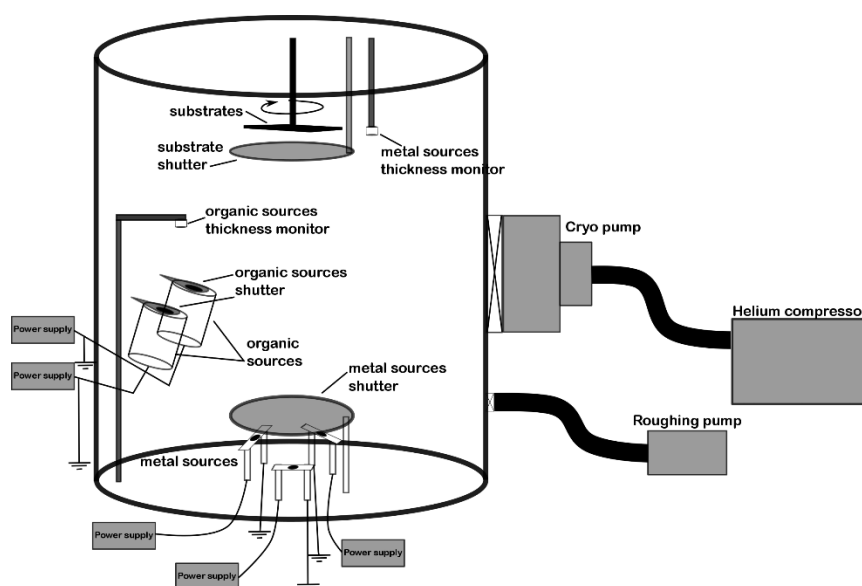
Figure 3.4 Schematic representation of a thermal evaporator with both organic and metal sources.

When fabricating OLEDs via VTE it is critically important to first correctly calibrate the thickness monitors. This operation is performed through the calculation of the tooling factor (TF). The TF is a correction factor that takes into account the relative orientation of the evaporation source with the thickness monitor itself as well as the geometry of the chamber (distance to thickness monitor-substrates). The TF is material dependant, and a calibration evaporation with a guessed TF must be initially performed in order to correct the TF (using Equation 3.7) by comparison the real thickness of the evaporated film determined by an

independent measurement. The thicknesses of the evaporated films for TF calibration were measured with J.A Woollam VASE ellipsometers.

Equation 3.7

$$TF_{material} = TF_{guessed} \frac{t_{measured}}{t_{QCM}}$$

After deposition all the substrates were encapsulated under inert atmosphere. In chapters 4, 5 and 7 encapsulation used a UV-curable epoxy (DELO Katiobond) along the outer edges of the active area with a glass cover slip in chapter 6 encapsulation was performed using a glass coverslip sealed by applying a drop of a low viscosity UV curable epoxy (Ossila) to cover the entire active area of the device with a glass coverslip.

3.6.2 Performance Testing

OLED devices were characterised by measuring the I-V-L characteristic, from which the performance metrics were calculated. I is the measured current, V the voltage and L is the Brightness or Luminance, defined as the intensity of light emitted from a surface per unit area in a given direction. As well as total luminance, the spectrum of the electroluminescence (EL) was also measured to allow the output photon flux to be determined. In this thesis two different OLED measurement setup have been used. The first, based in Durham (Figure 3.5a), is equipped with an Agilent Source Measure Unit (6632B) for electrical characterization of the devices and a calibrated fibre coupled Ocean Optics USB4000 spectrometer and a 10" integrating sphere (Labsphere) for optical measurements. The second setup based in Sheffield (Figure 3.5b) used an Ossila X100 source measure unit for the I-V acquisition and a Konica Minolta LS-110 for optical detection. The EL spectra of the OLED devices measured on the latter was acquired separately using a Stellarnet BLUE-Wave vis-25 spectrometer.
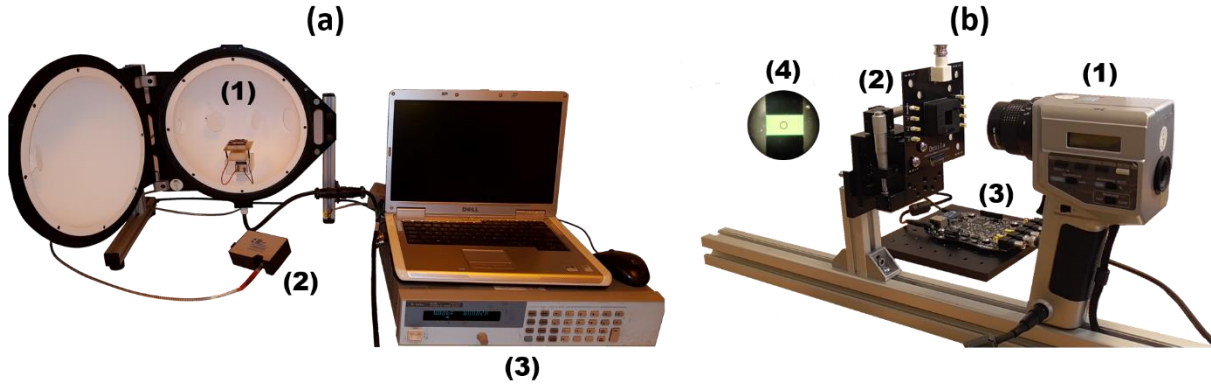
Figure 3.5 (a) Picture of the OLED testing system used in Chapters 4, 5 and 7 (Durham), where 1 is the 10" integrating sphere with OLED mounting, 2 is the USB spectrometer and 3 is the source measure unit. (b) Picture of the OLED testing system used in Chapter 6 (Sheffield), where 1 is the luminance meter, 2 oled mounting with x-y stage, 3 is the source measure unit and 4 shows a pixel in focus through the luminance meter.

The fundamental difference between the two setups is that the luminance meter assumes that the emission profile of the OLED device is Lambertian in order to proceed with the calculations necessary to determine the performance figures of merit. The integrating sphere does not work under this assumption but must be calibrated with a source of known intensity. This Lamberian assumption is generally good, but the use of an integrating sphere is always preferable.

The key reference metric for OLED devices is the external quantum efficiency (EQE), which describes the ratio between the number of photons (n_{ph}) that escape the surface of the OLED, and the number of electrons injected into it (n_e). The different setups use different derivations to obtain the number of photons.

The setup in Figure 3.5a measures the total radiant flux (W) emitted from the device in Watts by integrating the calibrated EL spectrum measured with the spectrometer. This quantity is then converted into number of photons by dividing by the energy of the photon at a given wavelength ($E_{ph} = hc/\lambda$) where λ is the wavelength, h is the Planck constant and c is the speed of light, integrating according to Equation 3.8.

Equation 3.8

$$n_{ph} = \int \frac{W(\lambda) \cdot \lambda}{h \cdot c} \, d\lambda$$

Conversely, the LS110 (Figure 3.5b) measures the total Luminance (L_{tot}) of the devices in cd/m^2. To calculate the number of photons from this measurement it is necessary to calculate the spectral distribution of the total luminance (ie, the EL spectrum) acquired separately with the spectrometer using Equation 3.9.

Equation 3.9

$$L(\lambda) = L_{tot} \cdot I(\lambda)$$

Where I(λ) is the area normalised EL spectrum. Assuming that the distribution of the light from the surface of the OLED is Lambertian (ie isotropic) the distribution of the Luminous flux (Lum) measured in lumens (lm) is equal to:

Equation 3.10

$$Lum(\lambda) = L(\lambda) \cdot \pi \cdot A$$

Where A is the device area. The Luminous flux can also be described in terms of the radiant flux:

Equation 3.11

$$Lum(\lambda) = W(\lambda) \cdot V(\lambda) \cdot 683$$

Where V(λ) is the luminosity function of the human eye and 683 lm/W is a conversion factor. Combining the last two equations, the radiant flux can be expressed as a function of the luminance:

Equation 3.12

$$W(\lambda) = \frac{L(\lambda) \cdot \pi \cdot A}{V(\lambda) \cdot 683}$$

Substituting this expression into Equation 3.8 it is possible to calculate the total number of photons using the Luminance meter:

Equation 3.13

$$n_{ph} = \int \frac{L(\lambda) \cdot \pi \cdot A \cdot \lambda}{683 \cdot V(\lambda) \cdot h \cdot c} \, d\lambda$$

In both setups n_e is calculated by dividing the measured current I by the elementary charge e.

Equation 3.14

$$n_e = \frac{I}{e}$$

The EQE is then finally calculated as the ratio of n_{ph} and n_e.

Equation 3.15

$$EQE = \frac{n_{ph}}{n_e}$$

The EQE can also be described using the PLQY of the emitter, the fraction of excited states that can emit radiatively (γ), the charge balance in the device (χ) and the outcoupling factor (η_{out}), as shown in Equation 3.16.

Equation 3.16

$$EQE = PLQY \cdot \chi \cdot \gamma \cdot \eta_{out}$$

This equation is used to estimate the maximum theoretical EQE achievable for an emitter after its PLQY has been measured. Commonly γ is assumed to be 100% for TADF and phosphorescent emitters since both classes of materials allow harvesting of all the produced excited states for emission. χ can also be assumed to be unitary when the excitons are well confined within the EML. Finally, η_{out} describes the fraction of photons produced in the device that escape the substrate surface and, (if the device surface is not specially engineered nor the emitters aligned), it is assumed to be between 0.25 and 0.3 due to total internal reflection and internal losses at the cathode and depending by the degree of anisotropy of the emitter.[5–7]

Other performance metrics used to describe OLED devices are the current efficiency (CE) and the power efficiency (PE, also know as luminous efficacy). The first of these is defined by the ratio between the Luminance (L_{tot}) and the current density (J) flowing into the device (Equation 3.17) and is measured in cd/A.

Equation 3.17

$$CE = \frac{L_{tot}}{J}$$

The second describes the ratio between the luminous flux (optical power weighted by the luminosity function) emitted by the device and the electrical power, calculated as the product of the voltage (V) applied to the device and the measured current (I) that flows through it, necessary to produce it (Equation 3.18), and is measured in lumens/Watt.

Equation 3.18

$$PE = \frac{Lum}{I \cdot V}$$

3.6.3 Lifetime Testing

The main issue in lifetime testing of OLED devices is to make the extrinsic deterioration mechanisms negligible, so that only the intrinsic ones related to material used will be active. In order to do this, a proper encapsulation has to be performed at the end of the OLED preparation to protect it from the degradation due to moisture and oxygen that can attack reactive organic layers or metals.[8]

For these lifetime measurements the encapsulation has been performed using a metallic coverslip on top the active area of the device. The coverslip then has a cavity where a getter is included, to avoid it contacting directly with the OLED stack (Figure 3.6). The function of the getter is to absorb any moisture and oxygen that can permeate the sealant over time, thus excluding lifetime shortening effects on the tested devices.
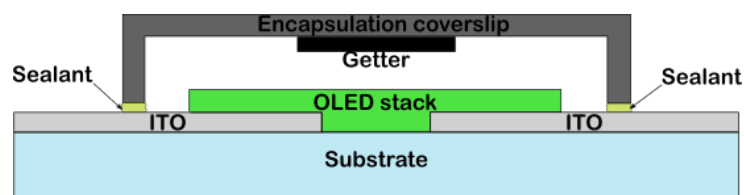
Figure 3.6 Scheme of an encapsulated OLED device for lifetime testing.

The parameter commonly used to test the stability of the OLEDs is the luminance of the devices. By tracking the luminance decay over time it is possible to define the operational lifetime of the devices as the time required for the luminance to drop to a target percentage of the initial value (L_0). Commonly this target value is 90% and this parameter is called LT90 although other targets are possible (eg LT50).

Lifetime characterization of the devices was carried out after performance test to determine the L-J characteristics. Using this information, it is possible to select the necessary current (I_0) to start the lifetime test at the desired L_0. The current (I_0) is then kept constant increasing the voltage, and the decay of the luminance from its initial value (L_0) is recorded over time with a photodetector. The measurements have been performed using an Ossila OLED Lifetime system which uses a Si photodiode to measure the relative luminance decay and an Ossila X100 source measure unit to drive the OLED at constant current and measure the variation of the current in the photodiode.

3.7 <u>References</u>

1. Lakowicz, J. R. *Principles of Fluorescence Spectroscopy*. (1999). doi:10.1007/978-0-387-46312-4

2. Pålsson, L.-O. & Monkman, A. P. Measurements of Solid-State Photoluminescence Quantum Yields of Films Using a Fluorimeter. *Adv. Mater.* 757–758 (2002).

3. Dias, F. B., Penfold, T. J., Berberan-Santos, M. N. & Monkman, A. P. Photophysics of Thermally Activated Delayed Fluorescence in Organic Molecules. *Methods Appl. Fluoresc.* **5**, 012001 (2017).

4. Schubert, D. W. & Dunkel, T. Spin coating from a molecular point of view: its concentration regimes, influence of molar mass and distribution. *Mater. Res. Innov.* **7**, 314–321 (2003).

5. Gather, M. C. & Reineke, S. Recent advances in light outcoupling from white organic light-emitting diodes. *J. Photonics Energy* **5**, 1–20 (2015).

6. Sun, Y. & Forrest, S. R. Enhanced light out-coupling of organic light-emitting devices using embedded low-index grids. *Nat. Photonics* **2**, 483 (2008).

7. Kim, J.-S., Ho, P. K. H., Greenham, N. C. & Friend, R. H. Electroluminescence emission pattern of organic light-emitting diodes: Implications for device efficiency calculations. *J. Appl. Phys.* **88**, 1073–1081 (2000).

8. Burrows, P. E. *et al.* Reliability and degradation of organic light emitting devices. *Appl. Phys. Lett.* **65**, 2922–2924 (1994).

Chapter 4:

Influence of Solid State Dilution on the Photophysical Performance of a TADF Exciplex

This chapter shows for the first time how diluting an exciplex in the solid state surprisingly can improve its performance. Using the TSBPA donor and PO-T2T acceptor to form an exciplex it was possible to blueshift the emission, increase the PLQY from 58% to 80%, and increase the device EQE from 14.8% to 19.2% by simply diluting the exciplex with an inert high triplet energy host material – here either UGH-3 or DPEPO. These effects are explained in terms of an increasing donor-acceptor distance and associated charge separation, while different behaviours observed in the different hosts are attributed to different energy barriers to electron transfer through the host. This then highlights the importance of the chosen host on photophysical experiments. The inappropriate choice of host may hinder the exciplex formation by not offering a suitable LUMO level to assist long distance electron transfer through thermodynamically favourable hopping

The photophysical measurements were carried by Marco Colella together with Andrew Danos. All authors contributed to the data interpretation and the preparation of the manuscript.

4.1 <u>Introduction</u>

Efficient TADF has been observed in both intermolecular and intramolecular CT systems[1,2]. At present, reports investigating new structures, colour tuning methods, and strategies for improving device performance of TADF molecules greatly outnumber similar reports for exciplexes[3–7]. Furthermore, when taking into considerations polymeric structures where substituents exhibiting TADF in intra-molecular (intra-substituent in this case) CT states have been more successful than polymers where the structure was studied to obtain the CT state between two different substituents (inter-substituent).[8–10]

Nonetheless, existing studies show the potential of TADF exciplexes as high performance emitters or triplet harvesting host for fluorescent/phosphorescent emitters [2,11–15].While the donor (D) and acceptor (A) spacing is rigidly set by the chemical structures of molecular TADF materials, D-A spacing in exciplexes has only gained limited attention as a design parameter until recently.

Adachi *et al*. recently reported that inserting a spacer layer between an interfacial exciplex blueshifts its emission rather than preventing entirely its formation[13]. Similar colour shifts have also been reported by Monkman and Al'Attar for interfacial exciplexes through the effect of applied electric field[15]. Graves *et al* initially described how sample inhomogeneity caused dispersion of the singlet-triplet energy gap (ΔE_{ST}) in exciplex films, resulting in non-exponential decay kinetics and time dependent emission spectra [14]. Kim *et al*. have meanwhile used computational methods to show how critical the D-A distance and orientation is to the singlet and triplet energies in an exciplex blend, which ultimately control the effective ΔE_{ST} and rate of reverse intersystem crossing (rISC)[12]. Kim *et al*. have also recently reported the surprising result that a TADF exciplex OLED shows improved performance at low temperatures[11]. Although low temperatures decrease the rISC rate, this is outcompeted by a simultaneous increase in exciplex photoluminescence quantum yield (PLQY) - as non-radiative singlet decay channels are also suppressed at low temperatures.

In this chapter a similarly surprising yet highly practical approach is developed to improve the performance of a recently reported TADF exciplex blend [16], with donor and acceptor structures shown in Figure 4.1a. Using a fixed 1:1 ratio of 4,4'-(Diphenylsilanediyl)bis(N,N-diphenylaniline) (TSBPA) donor and 2,4,6-tris[3-(diphenylphosphinyl)phenyl]-1,3,5-triazine (PO-T2T) as acceptor, it is possible to blueshift emission (summarized in Figure 4.1b), increase

PLQY (from 58% to 80%) and increase device external quantum efficiency (EQE) from 14.8% to 19.2% by simply diluting the exciplex with an inert host material – either 1,3-Bis(triphenylsilyl)benzene (UGH-3) or Bis[2-(diphenylphosphino)phenyl]ether oxide (DPEPO). These hosts were selected because they are both optically and UV transparent (essential for photophysical measurements), have high triplet energies (crucial for device performance), while also allowing comparison of the effects of different host polarities and HOMO/LUMO levels. They are also demonstrated to not form any exciplex themselves with TSBPA or PO-T2T in contrast to the subsequent report of the same effect[17].
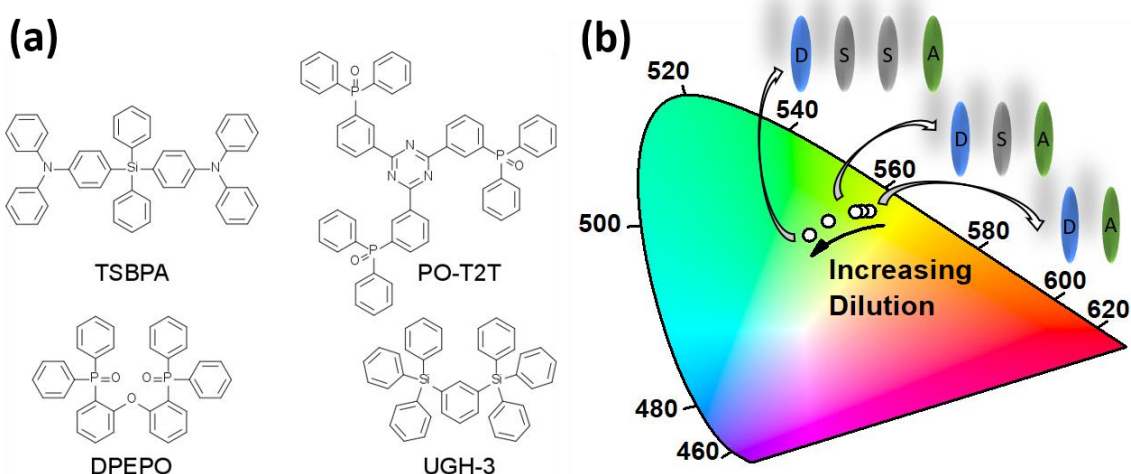
Figure 4.1 (a) Molecular structures of exciplex forming molecules TSBPA and PO-T2T and the hosts molecules, UGH-3 and DPEPO. (b) 1931 CIE chromaticity diagram schematically showing the blueshift of the exciplex emission with increasing dilution from the neat exciplex to 90% vol% UGH-3.

4.2   Results and Discussion

4.2.1 Photophysical characterization

To investigate the effect of the solid state dilution the photophysical properties of 100 nm thick vacuum deposited films were first investigated. In Figure 4.2 it is shown that the absorption spectrum of the neat exciplex (i.e. not diluted) it is the sum of the absorption spectra of the donor and acceptor that form the exciplex. Furthermore, no direct exciplex CT absorption

band[18] is observed for the exciplex blend as expected. The exciplex formation is indeed an excited state interaction and the molecules do not interact in the ground state.
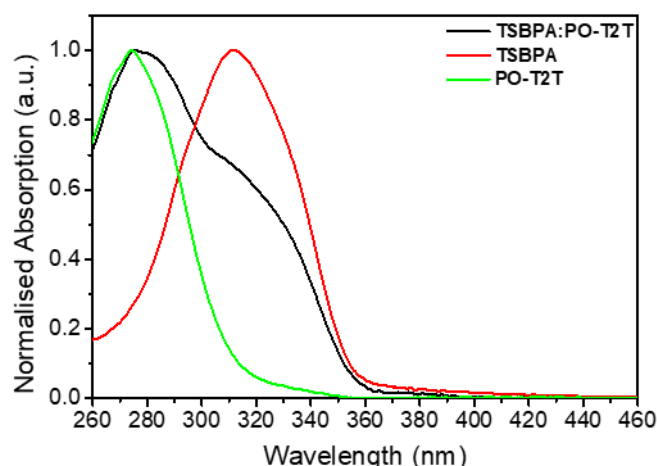
Figure 4.2 Normalised absorption spectra of evaporated neat TSBPA, neat PO-T2T and TSBPA:PO-T2T films.

In Figure 4.3a and Figure 4.3b show the evolution of the absorption spectra with increasing amount of host. At all dilutions it is clear that no ground state interaction is present and that the spectra are composed by just the sum of the three components of the evaporated films. It should be noted that UGH-3 and DPEPO do not show any absorption at 340 nm and 355 nm, which are the excitation wavelengths used for the following PLQY and TRPL.
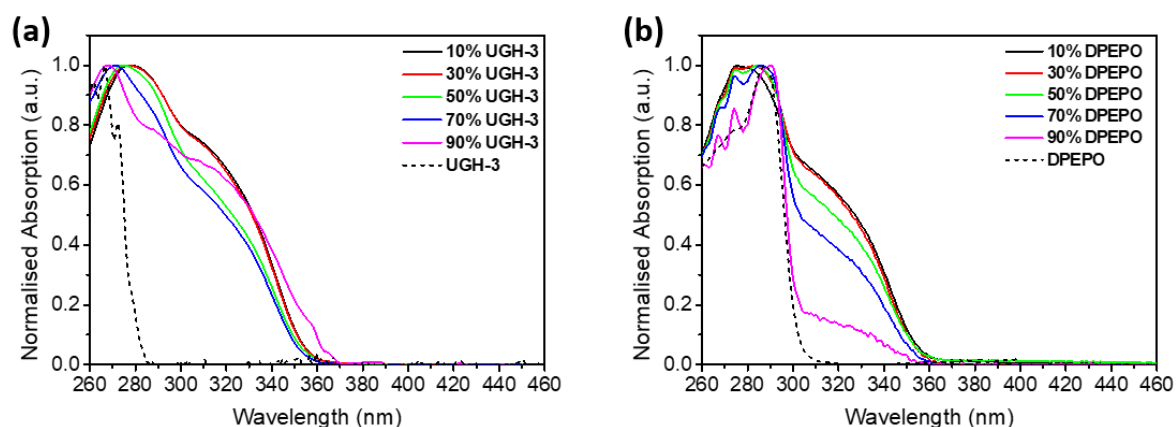
Figure 4.3 Absorption spectra of evaporated TSBPA:PO-T2T exciplex films with increasing vol% of (a) UGH-3 and (b) DPEPO.

From the steady state PL a substantial blueshift of the exciplex emission is observed in both hosts (Figure 4.4), with onset energies given in Table 4.1. The onset of the neat exciplex (without any dilution) is observed at 2.67 eV and increases with dilution in both hosts up to

2.85 eV in 90 vol% UGH-3, and 2.80 in 90 vol% DPEPO. In both 90% host films (i.e. exciplex highly diluted) TSBPA emission becomes clearly visible at wavelengths below 425 nm, indicating that the exciplex formation is being hindered, however it is extremely surprising that the exciplex is still so dominant even diluted at 90 vol% host.
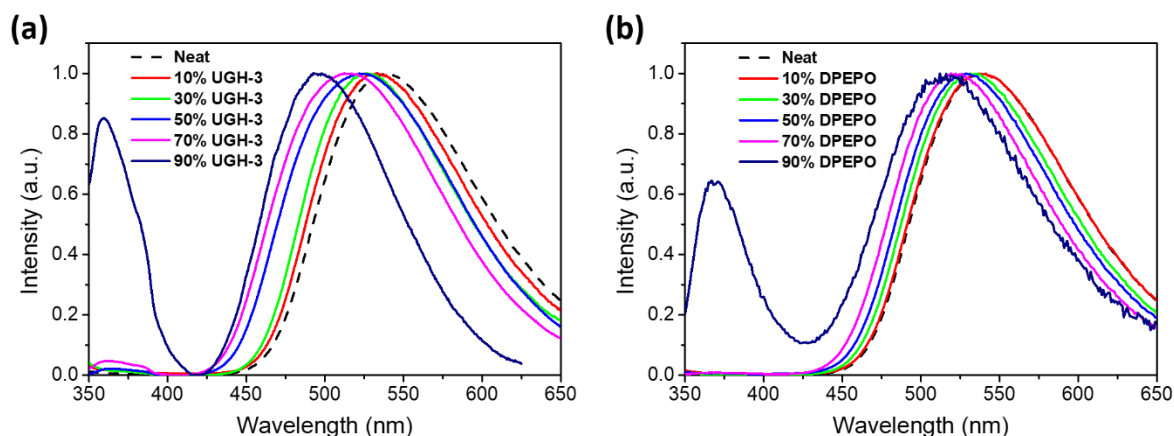
Figure 4.4 Steady state PL spectra of vacuum deposited TSBPA/PO-T2T (1:1 ratio) films in (a) UGH-3 and (b) DPEPO. Legend percentages are vol% of the host material, with 'Neat' equivalent to 0% host

Table 4.1 Exciplex photophysical properties at different dilutions in UGH-3 or DPEPO

Dilution	vol%	Average D-A distance (Å)	τ_{DF} (µs)	PL onset (eV)	PL FWHM (eV)	PLQY air/N$_2$
Neat exciplex	0	6.0	2.4 ± 0.1	2.67	0.51	0.45 / **0.58**
UGH-3	10	6.3	2.2 ± 0.1	2.68	0.52	0.50 / **0.63**
UGH-3	30	6.8	2.8 ± 0.1	2.70	0.51	0.51 / **0.65**
UGH-3	50	7.6	3.1 ± 0.1	2.79	0.58	0.67 / **0.80**
UGH-3	70	9.0	3.1 ± 0.2	2.83	0.58	0.49 / **0.70**
UGH-3	90	13	-	2.85	0.48	0.35 / **0.35**
DPEPO	10	6.3	2.4 ± 0.1	2.67	-	0.52 / **0.68**
DPEPO	30	6.8	2.5 ± 0.1	2.67	-	0.34 / **0.45**
DPEPO	50	7.6	2.3 ± 0.1	2.70	-	0.23 / **0.28**

| DPEPO | 70 | 9.0 | 2.9 ± 0.1 | 2.73 | - | 0.28 / **0.38** |
| DPEPO | 90 | 13 | 2.8 ± 0.1 | 2.80 | - | 0.06 / **0.07** |

The blueshift of the exciplex emission onset (hv_{max}) is assigned to the increase in the average D-A separation distance as the host vol% increases. Increasing the average D-A distance and therefore the separation, *r*, of electron and hole in the CT state causes the coulombic potential energy, $E_C(r)$, to rise (towards zero) as per Equation 4.1.

Equation 4.1

$$E_C(r) = \frac{e^2}{4\pi r \varepsilon_0 \varepsilon}$$

Equation 4.2

$$hv_{max} \approx I_D - A_A - E_C$$

where e is the electron charge, ε_0 and ε are respectively the permittivity of the vacuum and of the medium. I_D and A_A are the ionization potential of the donor and the electronic affinity of the acceptor. The electric field term (E_C) in Equation 4.1 has the effect of broadening the CT emission band as the field increases[15].

The average distances between nearest neighbor D-A pairs has also been estimated in Table 4.1. using the molecular masses and volume fractions of the films and assuming a uniform cubic lattice, uniform orientation distribution, and density of 1.1 g/mL (approximated from tetraphenylsilane) for all materials[19,20]. The total energy of the CT state thus increases with separation (Equation 4.2) resulting in higher energy exciplex and emission, in accordance with the findings of Al'Attar [12] and calculations reported by Kim et al.[12] This observation is also consistent with previously mentioned recent work of Adachi *et al.*[13]

The difference in the magnitudes of the observed blueshift between the two hosts is rationalized by their different polarities. Rich in polar O-C and O=P bonds, DPEPO is indeed known to be a very polar host[21], while UGH-3 is largely aromatic and non-polar[21]. Increased host polarity allows the exciplex CT state to relax further before emission (by shielding the coulomb term through increased ε), resulting in a consistently smaller overall blueshift for DPEPO films than for UGH-3. The sensitivity of the exciplex emission to polarity even at high dilutions suggest that the exciplex maintains CT character even at the largest D-A distances examined here.

To better understand how the presence of a host affects the kinetics of charge separation, exciplex formation, and emission, time-resolved PL decays of these films were measured, (Figure 4.5-Figure **4.7**). The prompt region was not fitted because of the multiexponential kinetics arising from the competition between the emission from the TSBPA donor, TSBPA excimer (see Figure 4.8 for better reference of the TSBPA excimer position) and the exciplex. The delayed region (the second cascade region of the log-log intensity time plots) is dominated by the exciplex emission and were fitted with mono-exponential decay functions. The fitted lifetimes (τ_{DF}) are included in Table 4.1.

Figure 4.5a shows the time resolved photoluminescence decay measured for the neat exciplex film. The competition between the three different PF emission processes can be seen in the broad spectrum collected at 1.9 ns delay time (Figure 4.5b). The most intense peak at 500 nm is assigned to the prompt emission of the exciplex while the shoulder at 440 nm it is assigned to the TSBPA excimer. Already at 19.6 ns delay time the emission is dominated by the exciplex centered at 520 nm. The emission continuously redshifts up to 22.4 µs where it is centered at 550 nm, after which no further redshift is observed. The dependence of the DF intensity with excitation dose shows a gradient close to 1 (Figure 4.5c). which eliminates TTA as a possible competing DF mechanism.
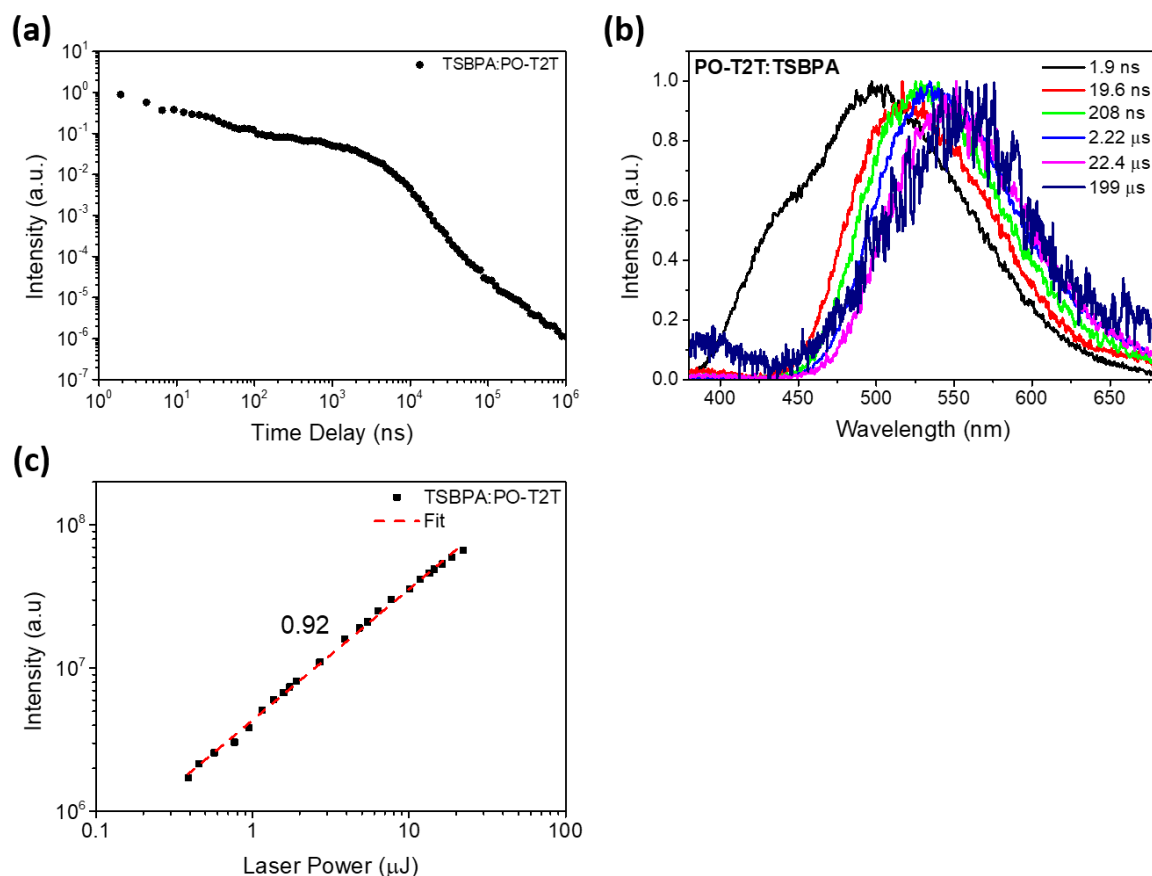
Figure 4.5 (a) Room temperature photoluminescence decays of evaporated TSBPA:PO-T2T exciplex film. (b) Photoluminescence spectra of TSBPA:PO-T2T 1:1 ratio evaporated film at different delay times. (c) Linear fit of the log of the integrated intensity vs log of the laser power of TSBPA:PO-T2T 1:1 ratio evaporated film.

Figure 4.6 and Figure 4.7 show the time resolved PL decays and spectra acquired for films diluted in UGH-3 and DPEPO. A general small increase in τ_{DF} was observed with increasing dilution for both hosts, with values given in Table 4.1. The increase in delayed lifetime can be indicative of a decrease in non-radiative decay from the exciplex triplet state, although this explanation cannot be asserted from lifetimes alone. In contrast to the spectra measured at 1.9 ns delay for the neat exciplex film at similar delay times in the films diluted with 10 and 30 vol% UGH-3 (Figure 4.6b and Figure 4.6c) no donor emission is observed. On the other hand, the prompt region of the decays maintains the same multiexponential behaviour. This may indicate that the kinetics of the exciplex excited state formation does not change at low level of dilution but that the exciplex formation now is more favourable. The same behavior is observed for the films diluted with 10-30-50 vol% of DPEPO (Figures 4.7b, 4.7c and 4.7d). For further dilutions in both hosts emission from TSBPA starts to be observable again in the early spectra (1.7-1.9 ns delay). The signal from TSBPA increases in intensity with increasing amount of host, indicating that the D-A interaction is being weakened and that there is an

increasing fraction of excited donors that cannot form the exciplex state efficiently anymore. For 90 vol% UGH-3 the DF signal is very weak (Figure 4.6f) indicating that almost no exciplex is being formed. For the 90 vol% DPEPO the DF emission is still clearly visible. The PF is dominated by donor emission at 1.7 ns delay time that quickly disappears at 21.3 ns delay. The increasing contribution of donor emission in the decays makes the prompt region lose some of its multiexponential characteristic, evolving smoothly toward the pure TSBPA decay when no PO-T2T is present in the blend (Figure 4.8). The different behavior observed for the two films diluted with 90 vol% UGH-3 and DPEPO is assigned to the tendency of UGH-3 to crystallize at low dopant concentration which might have hindered the exciplex formation.

As a general trend, in all the exciplex blends it is observed that the delayed CT emission blueshifts with increasing delay time up to 22.4 µs. It is interesting that the magnitude of the CT blueshift observed for the more diluted films is smaller than the one observed for the more diluted blends. This indicates that, in the more diluted films there is a narrower distribution of D-A distances and D-A geometries[12].
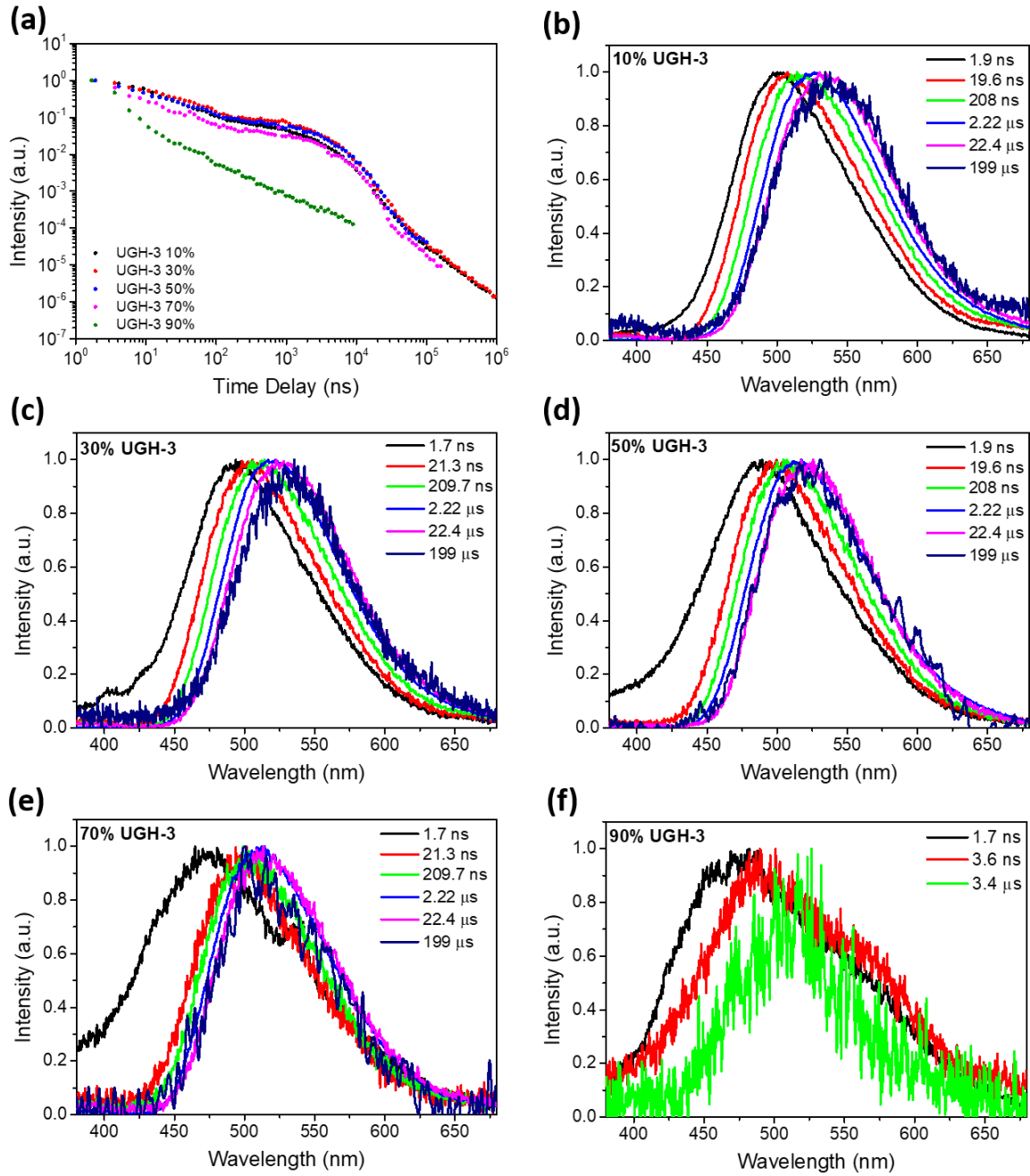
Figure 4.6 (a) Room temperature photoluminescence decays of evaporated TSBPA:PO-T2T exciplex films with increasing vol% of UGH-3. (b-f) Photoluminescence spectra of TSBPA:PO-T2T 1:1 ratio diluted in 10-90 vol% UGH-3 evaporated film at different delay times.
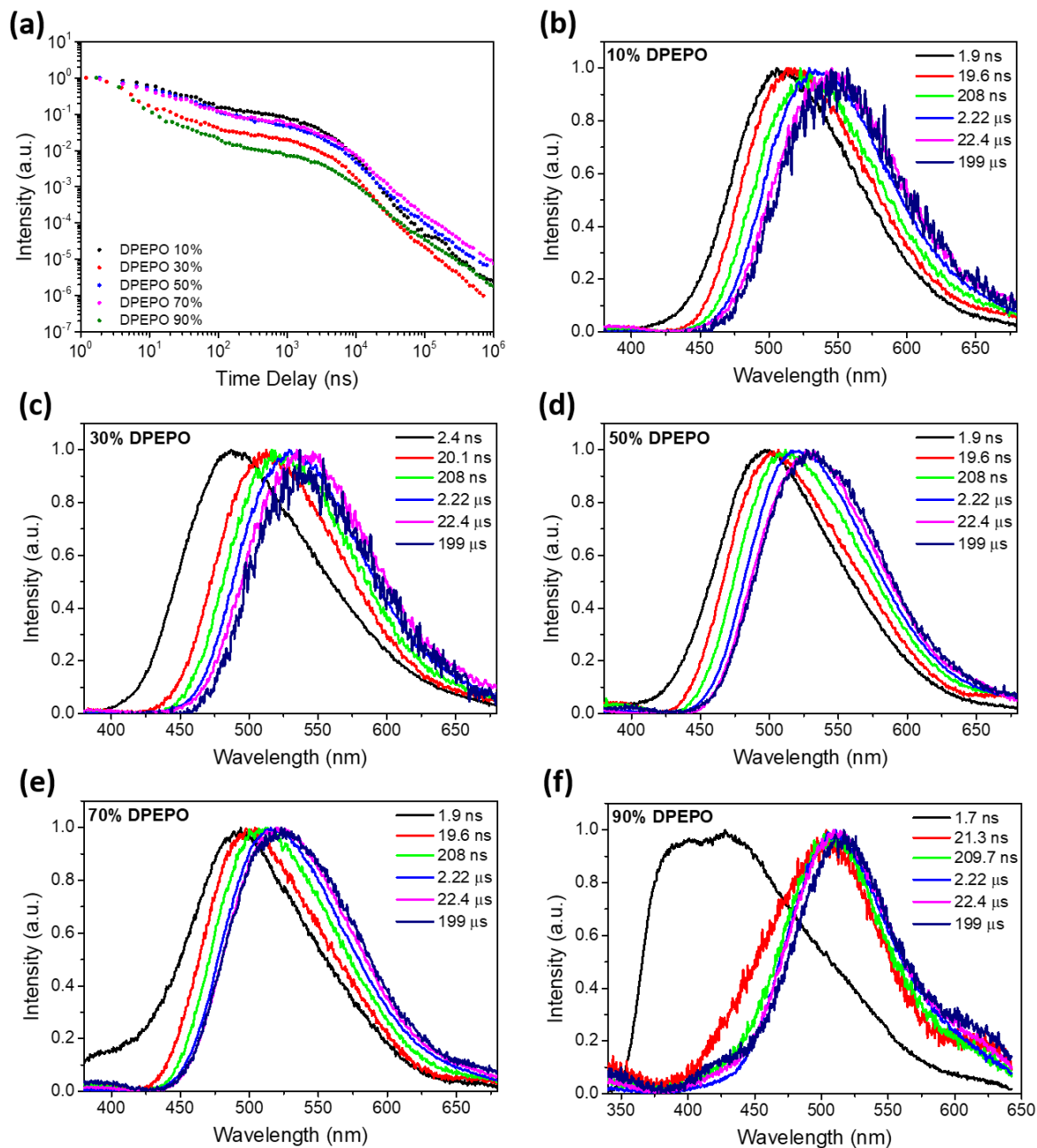
Figure 4.7 (a) Room temperature photoluminescence decays of evaporated TSBPA:PO-T2T exciplex films with increasing vol% of DPEPO. (b-f) Photoluminescence spectra of TSBPA:PO-T2T 1:1 ratio diluted in 10-90 vol% DPEPO evaporated film at different delay times.

To be sure that the excited donor was not interacting with the chosen hosts films, of TSBPA vol% in DPEPO or UGH-3 (without PO-T2T) were fabricated. The spectra at 1.2 ns in both hosts is dominated by the TSBPA emission at 375-380 nm with a second peak from the prompt TSBPA excimer emission centered at 460 nm. At 3.9 ns the most intense peak in both films is from the excimer. At 9.7 ns only the excimer emission is visible and centered at 480 nm. At 40.9 ns a slightly blueshifted emission is still present although the spectra are slightly distorted

because of the low signal to noise ratio at this delay time. As shown in Figure 4.8a, in both decays no strong DF nor exciplex formation is observed. These results confirms that in absence of PO-T2T, TSBPA does not interact with the chosen hosts.
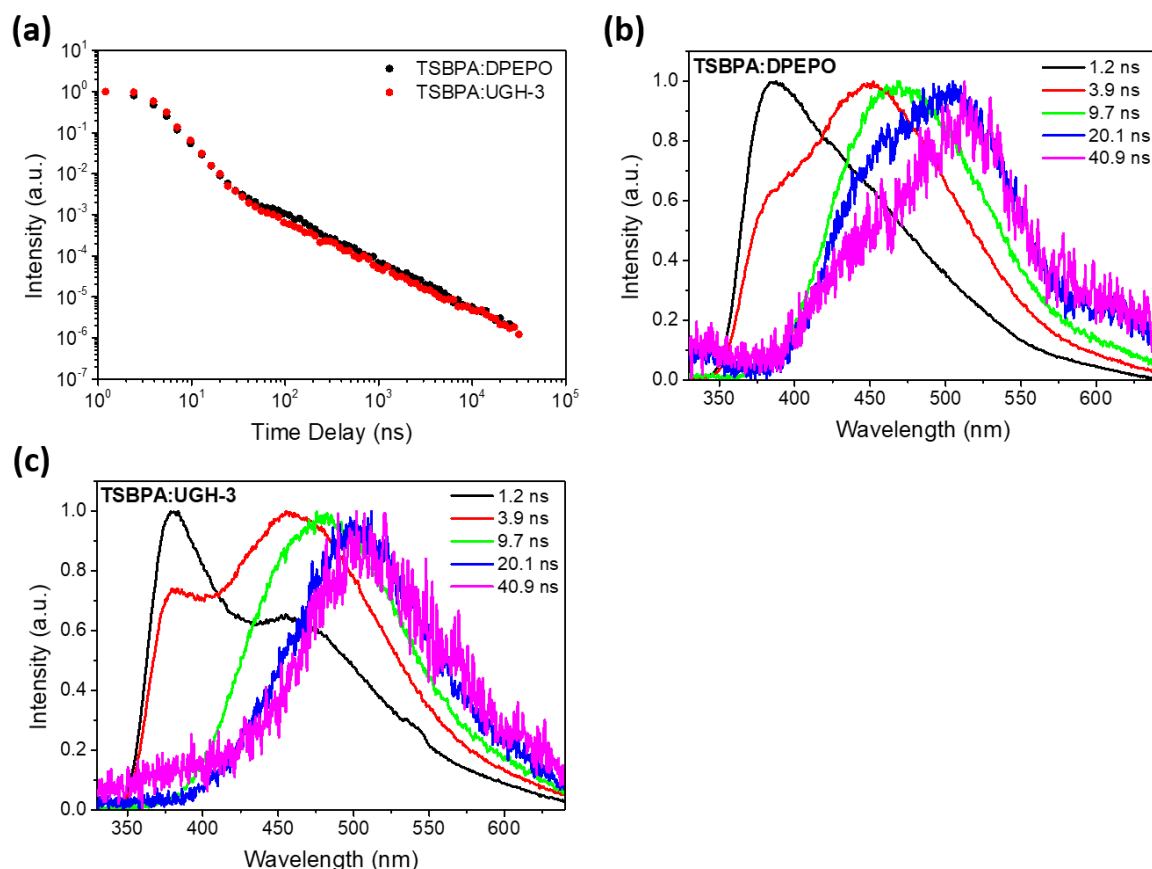
Figure 4.8 (a) Room temperature photoluminescence decays of evaporated TSBPA:DPEPO and TSBPA:UGH-3 exciplex films. Photoluminescence spectra of (b) TSBPA:DPEPO and (c) TSBPA:UGH-3 1:1 ratio evaporated films at different delay times.

The dependence of the delayed emission intensity upon excitation power was also checked for each diluted sample (Figure 4.9 and Figure **4.10**) in order to confirm the DF is arising from the TADF mechanism rather than from TTA. All the films show a close to 1 gradient of the log-log plot of the emission intensity against the excitation power, therefore indicating a single exciton process, i.e TADF, excluding TTA. This demonstrates that the overall DF mechanism does not change with dilution.
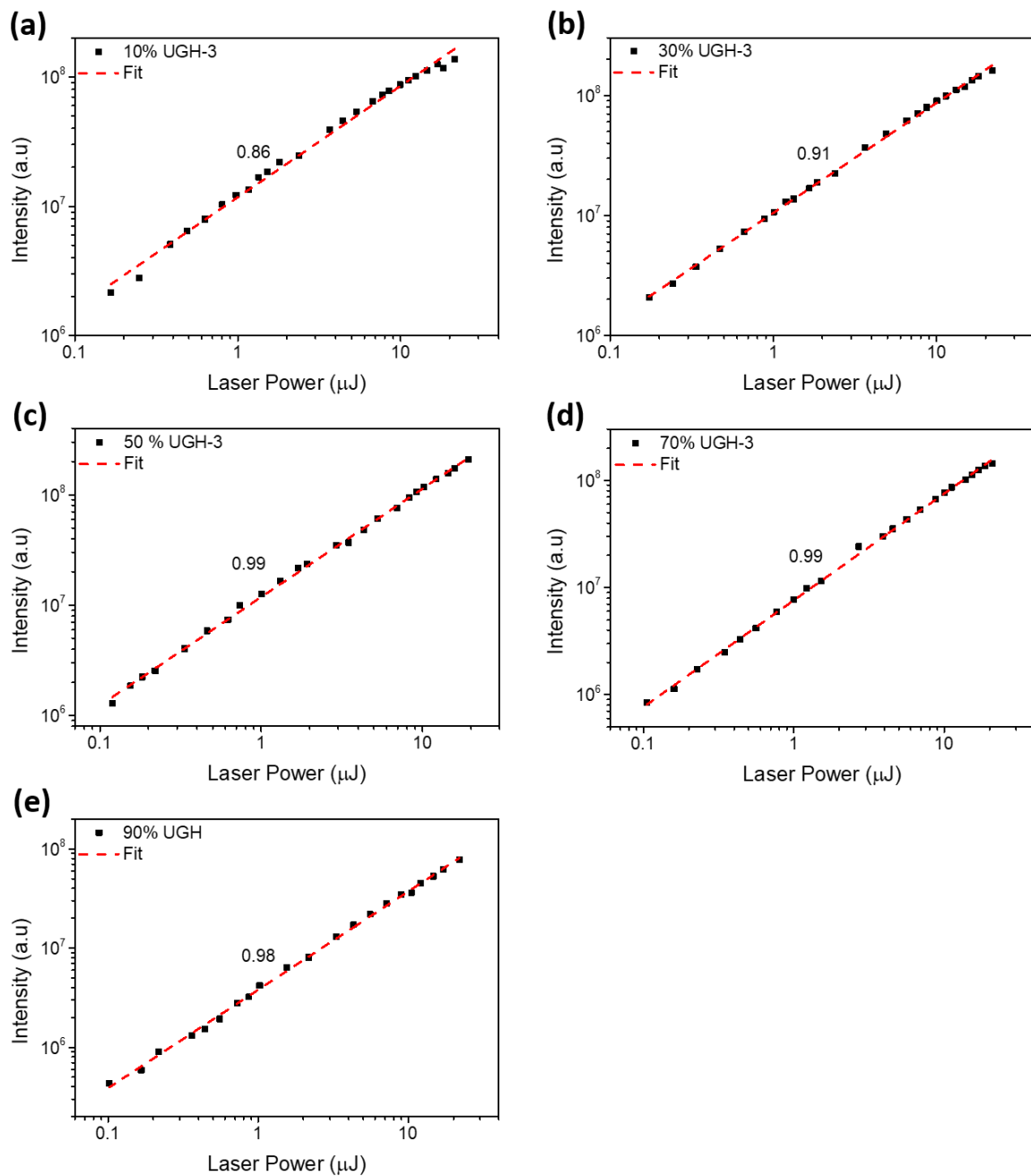
Figure 4.9 (a-e) Linear fit of the log of the integrated intensity vs log of the laser power of TSBPA:PO-T2T 1:1 ratio evaporated film diluted in 10-90 vol% UGH-3.
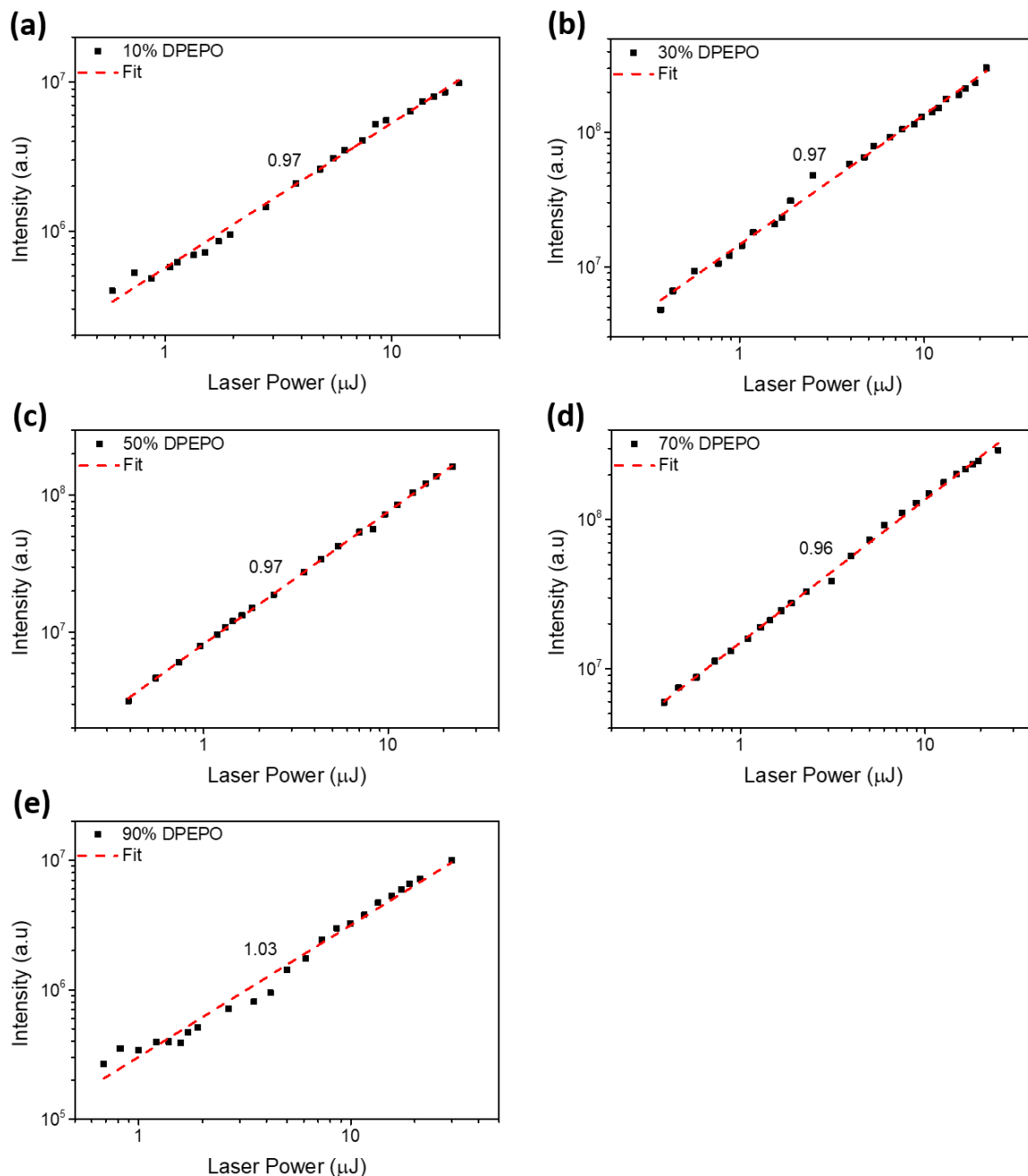
Figure 4.10 (a-e) Linear fit of the log of the integrated intensity vs log of the laser power of TSBPA:PO-T2T 1:1 ratio evaporated film diluted in 10-90 vol% DPEPO.

To better understand the cause of the observed increase in τ_{DF} the absolute PLQYs of the films were measured, with values reported in Figure 4.11 and Table 4.1. For all films the PLQY was found to increase with removal of atmospheric oxygen, confirming that triplet harvesting is occurring. For the UGH-3 diluted films the PLQY increased from 58% for the neat exciplex to a maximum of 80% when diluted with 50 vol% UGH-3. The PLQYs then decreased when the exciplex was further diluted. This decrease could be due to the fact that at very high dilution (and corresponding large D-A distances) the probability of exciplex formation begins to

decrease so that eventually most of excitons remaining localized on the donor and therefore decay through low efficiency pathways. The maximum PLQY achievable is the given by the balance between the increasing exciplex PLQY and the dilution percentage that still provides close to zero donor emission This is supported by the growth of the 340 nm TSBPA donor emission band at high dilutions in Figure 4.4, as well as the fact that at 90% dilution the PLQYs in air and vacuum converge, indicating negligible contribution to emission from TADF. This is also seen in the time resolved spectra, where a higher ratio of overall prompt (containing both exciplex and donor contributions) to delayed emission (exciplex only) is seen in higher dilution time-resolved PL traces (Figure 4.6 and Figure **4.7**,). This changing ratio of prompt to delayed emission manifests as an apparent lower level of DF when decays are normalized to initial time points.

4.2.2 Electron transfer
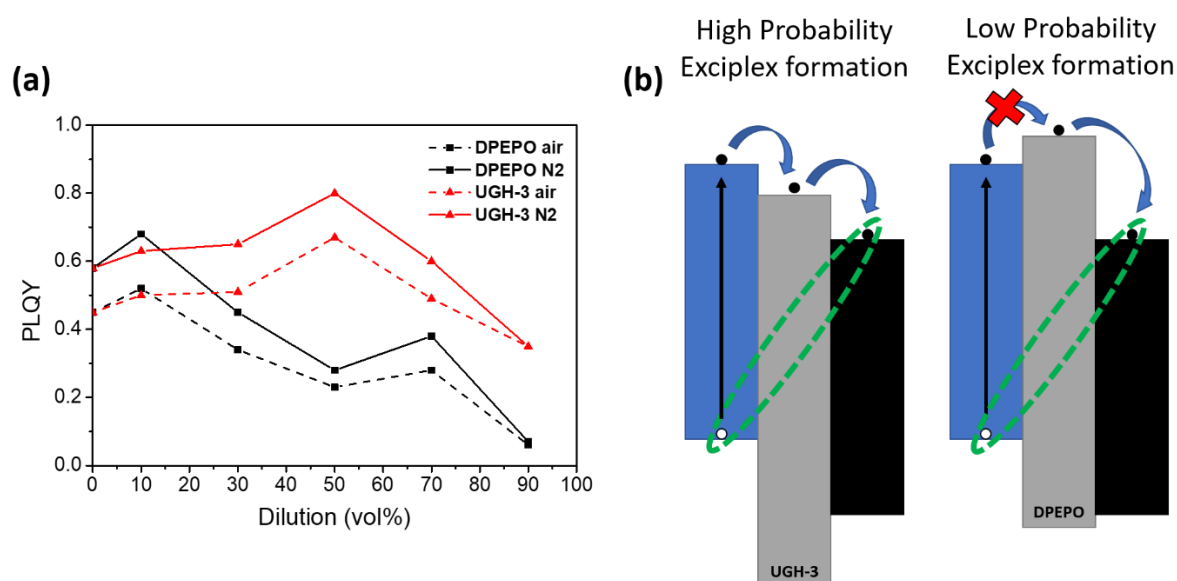
Figure 4.11 (a) PLQY values (error of ± 5 % is assumed) of vacuum deposited films in air and nitrogen atmosphere with the different dilution in UGH-3 and DPEPO (the dashed and full lines are present only to guide the eye). (b) Schematic representation of the D (blue), A (black), and host (grey) HOMO and LUMO levels relevant to electron transport (blue arrows) and exciplex formation (green oval).

Combined, the tandem increases in τ_{DF} and PLQY with dilution strongly suggest that some concentration quenching pathways are reduced for exciplexes with larger D-A distances but this increment is then outcompeted by other low efficiency emission pathways (eg donor emission) leading to a PLQY reduction upon further dilution. This observation may also indicate that PLQY is enhanced through reduction in the degree of charge separation in the excited state, for example avoiding non radiative radical ion pair formation.[22,23] Despite the fact that the PL emission onsets blueshift on dilution closer to the TSBPA and PO-T2T triplet

energies (2.90 and 2.97 eV respectively)[16]it can be ruled out the possibility that the increase in PLQY arises from a distance associated minimisation of ΔE_{ST} (and improvement of triplet harvesting), as this would accelerate rISC leading instead to a shorter τ_{DF} [7].

Surprisingly, the trend in PLQY shown for UGH-3 diluted exciplex is not reproduced for those diluted in DPEPO. Instead the PLQY has an initial increase up to 68% for the 10 vol% (similar to that measured for the sample diluted with 10 vol% UGH-3) but only decreases on further dilution. The difference in optical behaviour for different hosts demonstrates that the CT state formation in the diluted films must be mediated by the host, as a tunnelling or purely through-space mechanism would be independent of the choice of host. Furthermore, from the estimated D-A separations it is clearly seen that ET occurs strongly at separations greater than 0.6 nm, which again indicates that the host is acting as a mediator between the LUMO orbitals of TSBPA (-2.3 eV[18]) and PO-T2T (-3.2 eV[19]). As pictured in Figure 4.11b, the differences in the LUMO levels of the hosts then readily explains why UGH-3 spacer (LUMO -2.8 eV[17]) still allows exciplex formation and high PLQY at larger distances, whereas DPEPO (LUMO -2.0 eV[3]) does not[27,28]. Furthermore, comparing the FWHM for the CT emission band as a function of UGH-3 dilution (Table 4.1) an increment is observed as the dilution increases, until 90% UGH-3 were it instead narrows. This might imply that only certain orientations of D and A facilitate hopping ET through the intermediate host molecule. The broadened spectra results from a distribution of emitting CT states having different conformations and ET routes[29] and at 90% dilution only the highly blueshifted and narrowed exciplexes can form. This then gives an indication of a possible way to produce narrow emission bands from exciplex systems. It should be again stressed that in all photophysical measurements only the donor is excited, so that electron transfer (ET) through the host is required for exciplex formation in the diluted films. This is not the case for electrical excitation where the CT state is formed directly from free charges, as discussed in the context of OLEDs below.

The distance dependence of ET was estimated by plotting the ratio of residual donor emission to exciplex emission from the spectra in Figure 4.4 (normalizing for changes in exciplex PLQY on dilution). For UGH-3 an exponential increase in donor emission with average D-A spacing is observed (Figure 4.12), from which a distance decay constant $\beta_f = 1.1$ Å^{-1} is estimated, indicating efficient hopping ET with similar distance dependence found in other organic systems.[28] For DPEPO, the mechanism for long range ET cannot proceed exothermically and is not yet understood, but based on the PLQY roll off is not as efficient as in UGH-3.
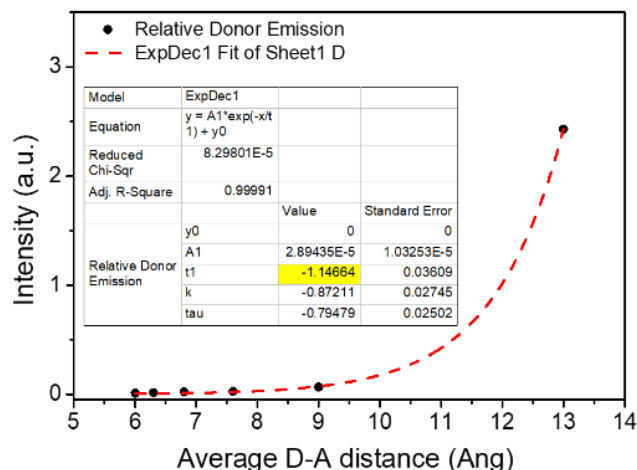
Figure 4.12 Distance dependence of residual donor emission (from Figure 4.4, UGH-3 series) corrected for differing exciplex PLQYs.

4.2.3 Device Performance

To assess the practical application of the dilution enhanced exciplex, OLEDs with different host vol% DPEPO and UGH-3 were produced. The structure used was NPB (40 nm)|TSBPA (10 nm)|TSBPA:PO-T2T 1:1 in X vol% Host (30 nm)|PO-T2T (50 nm)|LiF (1 nm)|Al (100 nm), where X was varied from zero to 70 vol%. In both device series the maximum EQE (shown in Figure 4.13a and Figure **4.13**c) increases with dilution up to 50 vol%, matching the trend seen for UGH-3 film PLQYs in Figure 4.11a. The maximum device brightness decreases with increasing dilution, as this reduces the total amount of exciplex D and A in the fixed thickness EML. The EL spectra of both UGH-3 (Figure 4.13b) and DPEPO (Figure 4.13d) OLEDs blueshift with dilution, consistent with the trend observed in the steady state PL spectra (Figure 4.4), although the EL spectra are each slightly redshifted with respect to their PL counterparts. This redshift of EL compared to PL is commonly seen in TADF systems, and is likely due to the differences between direct charge carrier combination to form the CT state in devices, compared to photoexcitation and ET to form the CT state in photophysics[20].
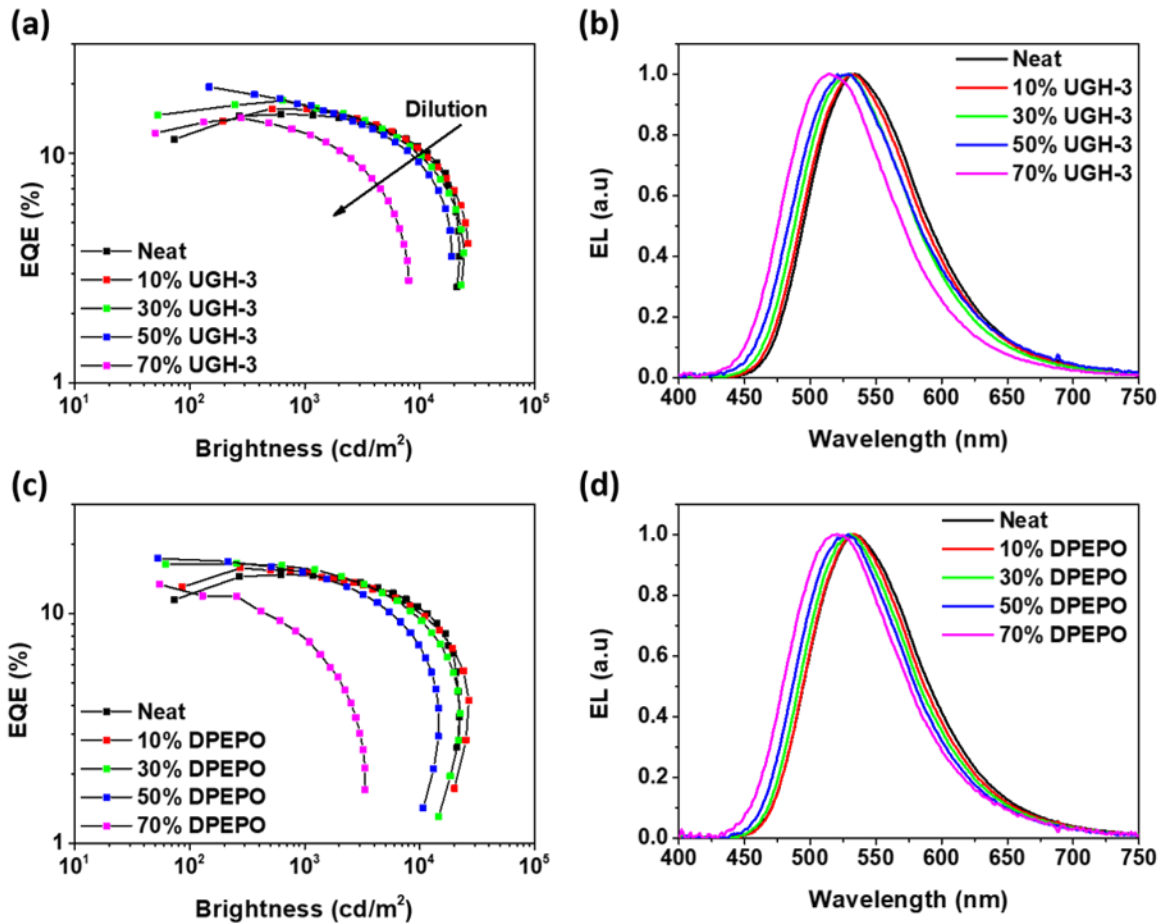
Figure 4.13 EQE vs brightness and EL spectra of OLEDs with different dilution vol% respectively in UGH-3 (a and b) and DPEPO (c and d)

In Figure 4.14a compares the values of maximum measured EQE for the devices produced with estimates based on the PLQYs using EQE $= \eta_{out} \cdot PLQY \cdot \gamma \cdot \eta_{fr}$, where η_{out} is the outcoupling factor (assumed here to be 0.25), the PLQY values taken from Table 4.1 are those from the UGH-3 samples, γ is the charge balance factor (assumed to be 1) and η_{fr} is the fraction of excited states that can radiatively decay, which is 1 for TADF exciplexes that can harvest both singlets and triplets. UGH-3 PLQYs are used here, having identified that DPEPO blocks ET and exciplex formation after optically excitation. In contrast, in electrically driven devices there is no need for ET through the diluting host material, as shown schematically in Figure 4.14b. As such the same early decrease in DPEPO device EQEs was not observed conversely to the aforementioned for PLQY values.
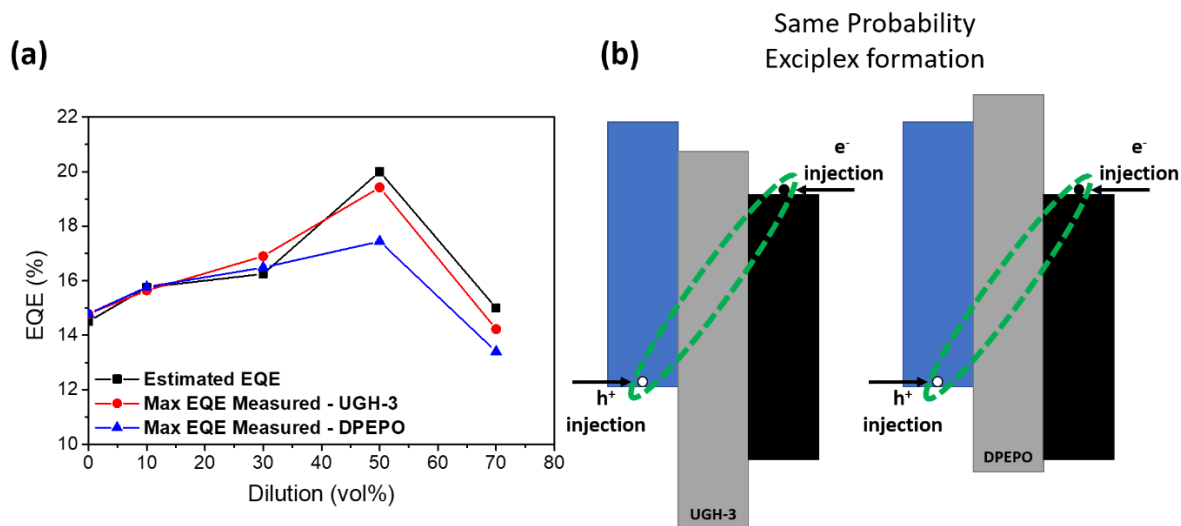
Figure 4.14 (a) Comparison between the measured Max EQE values of OLED devices with different dilutions in UGH-3 and DPEPO, along with estimated EQE values calculated from UGH-3 nitrogen PLQYs. (b) Schematic representation of the exciplex formation mechanism under electrical excitation in OLED devices.

Indeed, the estimated EQE values in Figure 4.14a are in very good agreement with the measured maximum EQE values for both UGH-3 and DPEPO based devices for dilution up to 30 vol%. At 50 vol% dilution the UGH-3 device still shows a very good agreement with an estimated EQE of 20% and a measured one of 19.2% (the highest measured EQE in this study, and a 30% enhancement of the neat exciplex), while the DPEPO device qualitatively follow the estimated trend but quantitatively underperform. At higher dilutions the maximum EQE decreases, again in line to what was observed for PLQYs, and again thought to be due to extreme D-A distances inhibiting exciplex formation.

It is not trivial to explain the discrepancy between the estimated EQEs and those measured in hosts at 50 vol% and above. This might be caused by the different polarities and dielectric constants of DPEPO and UGH-3, large values of which would electrostatically screen the donor and acceptor, reducing their coupling and the probability of exciplex formation. If this is the case, significant care must be taken to choose appropriate hosts for future studies in exciplex dilution. Similar to the requirements for molecular TADF hosts, these hosts will need to balance both polarity and electrical transport properties to achieve the best devices. Alternatively, it could be that the discrepancy is a simple problem a charge balance in these specific devices, and that further optimization of the organic stack could increase efficiency closer to the estimated values. Nonetheless both device series and the estimates show the same qualitative trend.

4.3   Conclusion

In conclusion this chapter reports the unprecedented result that diluting the exciplex formed by TSBPA and PO-T2T greatly improves its photophysical properties and its behaviour as the emitting layer in OLED devices. The dilution was performed using two different hosts with different polarities. Rather than immediately preventing exciplex formation as expected, it is observed that dilution blueshifts the emission of the exciplex due to the reduction of the electrostatic interaction between D and A over greater distances. The exciplex maintains a strong CT character despite the increased D-A separation. The films diluted in DPEPO were systematically slightly redshifted compared to those in UGH-3 due to the effect of polarity on CT state relaxation. In addition to the blueshifted emission, an increase in the PLQY of the exciplex passing from 58% to 80% it is observed before further dilution begins to hinder exciplex formation. The increase in PLQY is directly transferable into OLEDs, where the maximum EQE increases from 14.8% for the neat exciplex to 19.2% for the device diluted with 50 vol% of UGH-3, in good agreement with the estimated EQE values.

These effects are attributed to simple increases in D-A distance and reduction in concentration quenching. An in-depth study over the effect that the dilution induces into the morphology of the deposited films it is also needed to better understand the photophysical phenomena.

On the other hand, in the absence of a more complex explanation of the dilution enhancement, it is likely that these effects will be general to other exciplex blends and inert host materials. Optimisation of exciplex dilution – previously assumed to only inhibit exciplex formation – will therefore likely allow exciplex based TADF devices to rapidly match and exceed the performance of leading molecular TADF materials.

4.4 <u>References</u>

(1)   Uoyama, H.; Goushi, K.; Shizu, K.; Nomura, H.; Adachi, C. Highly Efficient Organic Light-Emitting Diodes from Delayed Fluorescence. *Nature* **2012**, *492* (7428), 234–238. https://doi.org/10.1038/nature11687.

(2)   dos Santos, P. L.; Dias, F. B.; Monkman, A. P. Investigation of the Mechanisms Giving Rise to TADF in Exciplex States. *J. Phys. Chem. C* **2016**, *120* (32), 18259–18267. https://doi.org/10.1021/acs.jpcc.6b05198.

(3)   dos Santos, P. L.; Ward, J. S.; Bryce, M. R.; Monkman, A. P. Using Guest–Host Interactions To Optimize the Efficiency of TADF OLEDs. *J. Phys. Chem. Lett.* **2016**, *7* (17), 3341–3346. https://doi.org/10.1021/acs.jpclett.6b01542.

(4)   dos Santos, P. L.; Ward, J. S.; Batsanov, A. S.; Bryce, M. R.; Monkman, A. P. Optical and Polarity Control of Donor − Acceptor Conformation and Their Charge-Transfer States in Thermally Activated Delayed- Fluorescence Molecules. *J. Phys. Chem. C* **2017**, *121*, 16462–16469. https://doi.org/10.1021/acs.jpcc.7b03672.

(5)   Higginbotham, H. F.; Yi, C.; Monkman, A. P.; Wong, K. Effects of Ortho-Phenyl Substitution on the RISC Rate of D−A Type TADF Molecules. *J. Phys. Chem. C* **2018**, *122*, 7627–7634. https://doi.org/10.1021/acs.jpcc.8b01579.

(6)   Zhang, Q.; Li, B.; Huang, S.; Nomura, H.; Tanaka, H.; Adachi, C. Efficient Blue Organic Light-Emitting Diodes Employing Thermally Activated Delayed Fluorescence. *Nat. Photonics* **2014**, *8* (March), 1–7. https://doi.org/10.1038/nphoton.2014.12.

(7)   Dias, F. B.; Bourdakos, K. N.; Jankus, V.; Moss, K. C.; Kamtekar, K. T.; Bhalla, V.; Santos, J.; Bryce, M. R.; Monkman, A. P. Triplet Harvesting with 100% Efficiency by Way of Thermally Activated Delayed Fluorescence in Charge Transfer OLED Emitters. *Adv. Mater.* **2013**, *25* (27), 3707–3714. https://doi.org/10.1002/adma.201300753.

(8)   Wei, Q.; Voit, B. Thermally Activated Delayed Fluorescent Polymers: Structures, Properties, and Applications in OLED Devices. *Macromol. Rapid Commun.* **2018**, *40*, 1800570. https://doi.org/10.1002/marc.201800570.

(9)   Liang, J.; Zhong, Z.; Li, S.; Jiang, X.-F.; Ying, L.; Yang, W.; Peng, J.; Cao, Y. Efficient White Polymer Light-Emitting Diodes from Single Polymer Exciplex

Electroluminescence. *J. Mater. Chem. C* **2017**, *5* (9), 2397–2403. https://doi.org/10.1039/C6TC05264A.

(10)   Lin, X.; Zhu, Y.; Zhang, B.; Zhao, X.; Yao, B.; Cheng, Y.; Li, Z.; Qu, Y.; Xie, Z. Highly Efficient TADF Polymer Electroluminescence with Reduced Efficiency Roll-off via Interfacial Exciplex Host Strategy. *ACS Appl. Mater. Interfaces* **2018**, *10* (1), 47–52. https://doi.org/10.1021/acsami.7b16887.

(11)   Kim, K.-H.; Yoo, S.-J.; Kim, J.-J. Boosting Triplet Harvest by Reducing Nonradiative Transition of Exciplex toward Fluorescent Organic Light-Emitting Diodes with 100% Internal Quantum Efficiency. *Chem. Mater.* **2016**, *28*, 1936–1941. https://doi.org/10.1021/acs.chemmater.6b00478.

(12)   Moon, C.-K.; Huh, J.-S.; Kim, J.-M.; Kim, J.-J. Electronic Structure and Emission Process of Excited Charge Transfer States in Solids. *Chem. Mater.* **2018**, *30* (16), 5648–5654. https://doi.org/10.1021/acs.chemmater.8b02011.

(13)   Nakanotani, H.; Furukawa, T.; Morimoto, K.; Adachi, C. Long-Range Coupling of Electron-Hole Pairs in Spatially Separated Organic Donor-Acceptor Layers. *Sci. Adv.* **2016**, *2* (2), e1501470–e1501470. https://doi.org/10.1126/sciadv.1501470.

(14)   Graves, D.; Jankus, V.; Dias, F. B.; Monkman, A. Photophysical Investigation of the Thermally Activated Delayed Emission from Films of M-MTDATA:PBD Exciplex. *Adv. Funct. Mater.* **2014**, *24* (16), 2343–2351. https://doi.org/10.1002/adfm.201303389.

(15)   Al Attar, H. A.; Monkman, A. P. Electric Field Induce Blue Shift and Intensity Enhancement in 2D Exciplex Organic Light Emitting Diodes; Controlling Electron-Hole Separation. *Adv. Mater.* **2016**, *28*, 8014–8020. https://doi.org/10.1002/adma.201600965.

(16)   Chapran, M.; Pander, P.; Vasylieva, M.; Wiosna-Salyga, G.; Ulanski, J.; Dias, F. B.; Data, P. Realizing 20% External Quantum Efficiency in Electroluminescence with Efficient Thermally Activated Delayed Fluorescence from an Exciplex. *ACS Appl. Mater. Interfaces* **2019**, *11* (14), 13460–13471. https://doi.org/10.1021/acsami.8b18284.

(17)   Yuan, P.; Guo, X.; Qiao, X.; Yan, D.; Ma, D. Improvement of the Electroluminescence Performance of Exciplex-Based OLEDs by Effective Utilization of Long-Range

Coupled Electron–Hole Pairs. *Adv. Opt. Mater.* **2019**, *0* (0), 1801648. https://doi.org/10.1002/adom.201801648.

(18) Dias, F. B.; Santos, J.; Graves, D. R.; Data, P.; Nobuyasu, R. S.; Fox, M. A.; Batsanov, A. S.; Palmeira, T.; Berberan-Santos, M. N.; Bryce, M. R.; et al. The Role of Local Triplet Excited States and D-A Relative Orientation in Thermally Activated Delayed Fluorescence: Photophysics and Devices. *Adv. Sci. (Weinheim, Baden-Wurttemberg, Ger.* **2016**, *3* (12), 1600080. https://doi.org/10.1002/advs.201600080.

(19) Aesar, A. Density of Tetraphenylsilane.

(20) Davis, N. J. L. K.; MacQueen, R. W.; Roberts, D. A.; Danos, A.; Dehn, S.; Perrier, S.; Schmidt, T. W. Energy Transfer in Pendant Perylene Diimide Copolymers. *J. Mater. Chem. C* **2016**, *4*, 8270. https://doi.org/10.1039/c6tc02555b.

(21) Reed, L. H.; Allen, L. C. Bond Polarity Index : Application to Group Electronegativity. *J. Phys. Chem.* **1992**, *96*, 157–164. https://doi.org/10.1021/j100180a032.

(22) Hoang, H. M.; Pham, T. B. Van; Grampp, G.; Kattnig, D. R. Exciplexes versus Loose Ion Pairs: How Does the Driving Force Impact the Initial Product Ratio of Photoinduced Charge Separation Reactions? *J. Phys. Chem. Lett.* **2014**, *5*, 3188–3194.

(23) Lin, T.-C.; Sarma, M.; Chen, Y.-T.; Liu, S.-H.; Lin, K.-T.; Chiang, P.-Y.; Chuang, W.-T.; Liu, Y.-C.; Hsu, H.-F.; Hung, W.-Y.; et al. Probe Exciplex Structure of Highly Efficient Thermally Activated Delayed Fluorescence Organic Light Emitting Diodes. *Nat. Commun.* **2018**, *9* (1), 3111. https://doi.org/10.1038/s41467-018-05527-4.

(24) Yook, K. S.; Lee, J. Y. Organic Materials for Deep Blue Phosphorescent Organic Light-Emitting Diodes. *Adv. Mater.* **2012**, *24* (24), 3169–3190. https://doi.org/10.1002/adma.201200627.

(25) Lee, C. W.; Lee, J. Y. Low Driving Voltage and High Power Efficiency in Blue Phosphorescent Organic Light-Emitting Diodes Using Aromatic Amine Derivatives with Diphenylsilyl Linkage. *Synth. Met.* **2013**, *167*, 1–4. https://doi.org/10.1016/j.synthmet.2013.02.001.

(26) Liu, W.; Chen, J.; Zheng, C.; Wang, K.; Chen, D.; Li, F. Novel Strategy to Develop Exciplex Emitters for High- Performance OLEDs by Employing Thermally Activated Delayed Fluorescence Materials. *Adv. Funct. Mater.* **2016**, *26*, 2002–2008.

https://doi.org/10.1002/adfm.201505014.

(27) Natali, M.; Campagna, S.; Scandola, F. Photoinduced Electron Transfer across Molecular Bridges: Electron- and Hole-Transfer Superexchange Pathways. *Chem. Soc. Rev.* **2014**, *43* (12), 4005–4018. https://doi.org/10.1039/C3CS60463B.

(28) Wenger, O. S. Photoinduced Electron Tunneling between Randomly Dispersed Donors and Acceptors in Frozen Glasses and Other Rigid Matrices. *Phys. Chem. Chem. Phys.* **2013**, *15* (26), 10673–10685. https://doi.org/10.1039/C3CP00011G.

(29) Dinnocenzo, J. P.; Feinberg, A. M.; Farid, S. Multiple Intermolecular Exciplexes in Highly Polar Solvents. *J. Phys. Chem. A* **2017**, *121*, 3662–3670. https://doi.org/10.1021/acs.jpca.7b01461.

Chapter 5:

Identifying the factors that lead to PLQY enhancement in diluted TADF exciplexes based on carbazole donors

This chapter compares the effects of dilution on the photophysical and electrical performance of three TADF exciplexes based on CBP, CDBP and mCP donors with PO-T2T. Intrinsically different photophysical behaviour between CDBP and mCP exciplexes is observed when compared to CBP, which is explained by a heterogeneous distribution of triplet energies in the CBP molecules arising from a distribution of the biphenyl bridge twist angle. This study of different donors demonstrates that the PLQY enhancement of diluted exciplexes is independent of the separation associated spectral blueshift, with the latter being universal while the former is speculated to arise for donors with low structural rigidity. OLEDs produced from these carbazole based exciplexes show decreased EQEs likely due to the relatively low conductivity of donors and host, suggesting that functional conductive hosts may assist in translating PLQY enhancements in diluted exciplexes into improved electrical performance.

5.1 <u>Introduction</u>

The previous chapter demonstrated that diluting the TSBPA:PO-T2T exciplex in an inert host (UGH-3) leads to increasingly blueshifted emission and a considerable increase in the PLQY that translates into improved device EQEs[1,2]. This approach provides a promising new strategy to produce high efficiency blue OLEDs based on exciplexes. Although the observed blueshift of the exciplex emission can be rationalised in terms of the decreasing coulombic interaction between the donor and the acceptor, the origin of the PLQY increment is not as well understood.

This chapter compares the optical and electrical properties of three TADF exciplexes formed between carbazole based donors (mCP, CBP and CDBP) with PO-T2T as acceptor (Figure 5.1). These materials are diluted in UGH-3 as it was demonstrated in the previous chapter this host material provided the best results in both optical experiments and in OLED devices. Films were prepared at different host vol% keeping the D:A relative ratio always 1:1 by volume. The molecular structures of CDBP and CBP differ only by the two central methyl groups (Figure 5.1) which sterically induce a twist across the biphenyl bridge, locking its conformation. This twist reduces the conjugation across the molecule and leads to different triplet energies in CDBP (T_1 = 2.92 eV) compared to CBP (T_1 = 2.70 eV).[3] The mCP also possesses a twisted geometry, this time due to meta nitrogen linkages and the close packing of the carbazoles around the central benzene ring. These structural effects also lead to a high triplet level[4,5] (T_1 = 2.94 eV), similar to CDBP.
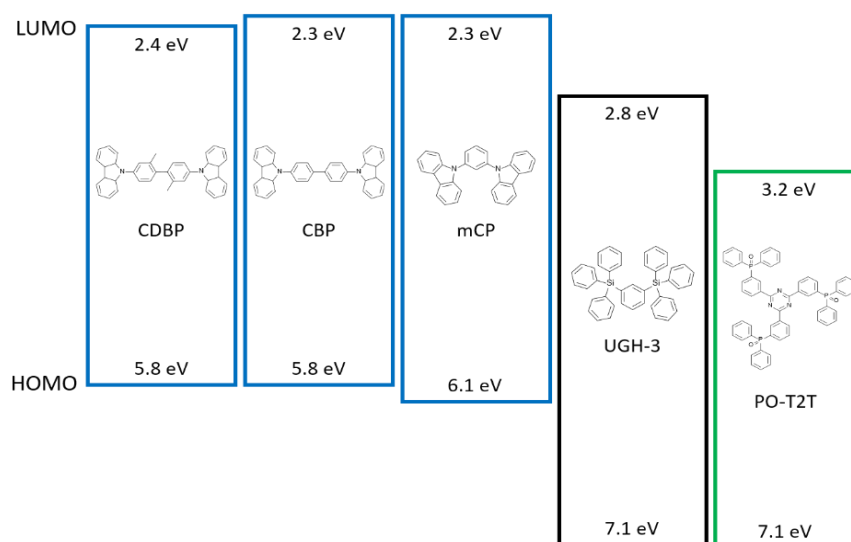
Figure 5.1 Molecular structures and HOMO/LUMO levels of the exciplex forming donors (CDBP, CBP and mCP), acceptor (PO-T2T) and the host used to dilute the exciplexes (UGH-3).

5.2 <u>Results and Discussion</u>

5.2.1 Photophysical characterization

In Figure 5.2a-c the absorption spectra of the three dilution series are presented, showing that no ground state interaction is present (i.e. no direct CT absorption band)[6] and that the absorption intensity is directly proportional to the donor and acceptor content of the films. Furthermore, to ensure that there is no interaction between the host and the three donors (exciplex formation or otherwise) the PL of the three donors in UGH-3 was also measured (Figure 5.2d). Only the emission from the donor molecules is observed, confirming the inert nature of the host.
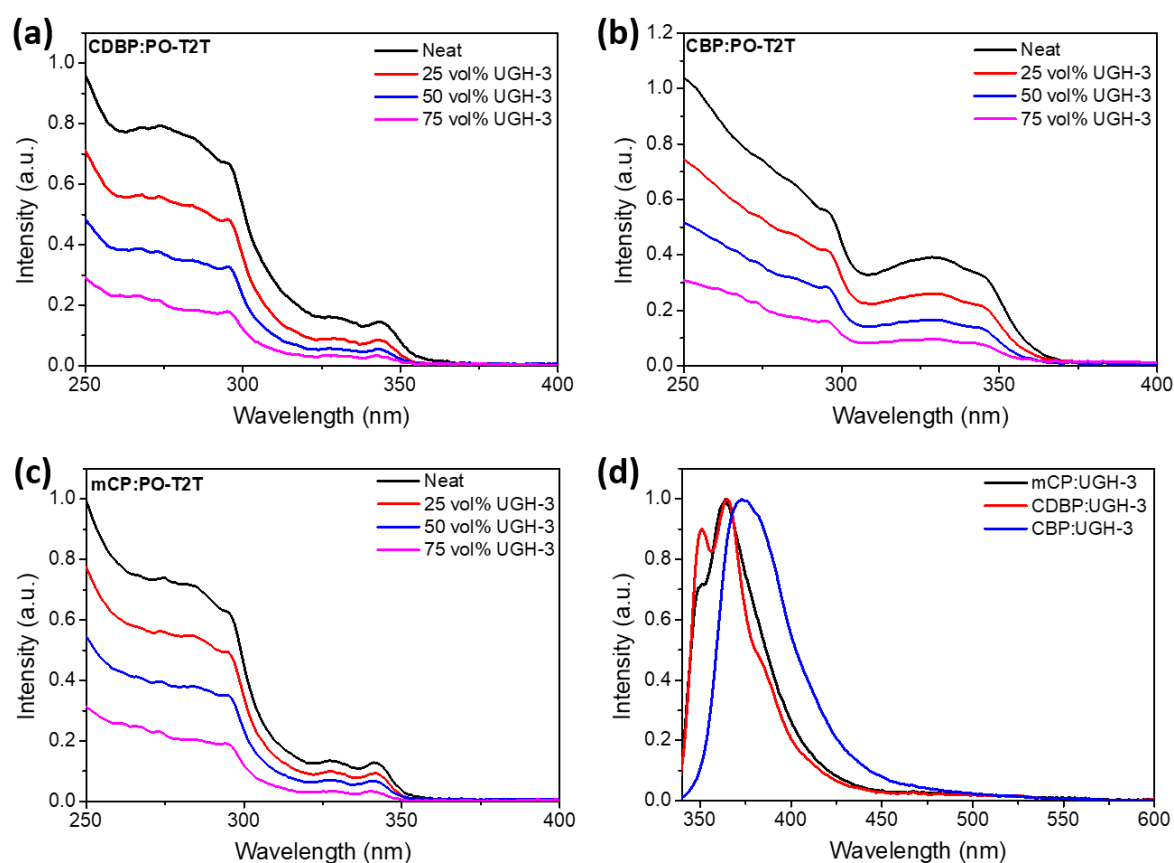
Figure 5.2 Absorption spectra for (a) CDBP:PO-T2T, (b) CBP:PO-T2T and (c) mCP:PO-T2T 1:1 vol% in different vol% of UGH-3, from Neat exciplex (0 vol% UGH-3) to 75 vol% of UGH-3. (d) Photoluminescence spectra of drop casted CBP, CDBP and mCP 10 vol% in UGH-3

All three exciplexes exhibit a blue shift of their PL with increasing dilution (Figure 5.3), consistent with results presented in the previous chapter for the TSBPA:POT2T exciplex.[1] This blueshift is rationalised in terms of a reduced coulombic energy term for the exciplex as the

electron-hole separation of the CT excited state increases. No donor emission is observed up to 25 vol% of UGH-3 in any film (Figure 5.3), while upon further dilution in the CDBP:PO-T2T and mCP:PO-T2T exciplexes only a small donor peak (365 nm) is observed at 50 vol% and 75 vol% of the host respectively. Stronger donor emission (360-380 nm) is observed in the CBP:PO-T2T films for the same dilutions, which suggests a stronger interaction of CDBP and mCP with PO-T2T compared to CBP assuming that the electron transfer (ET) mediated through the host remains similar for all exciplexes and that the PLQYs of the donor emissions are not greatly different. The former assumption is justified by the fact that the LUMO levels of the three donors CDBP (2.4 eV[7]), CBP (2.3 eV[8]) and mCP (2.3 eV[7]) all are above the LUMO of UGH-3 (2.8 eV[9]), thus allowing thermodynamically favourable electron hopping towards the deeper PO-T2T LUMO level (3.2 eV[1]), as schematically shown in Figure 5.1.

The stronger interaction of CDBP and mCP with PO-T2T (compared to CBP) is believed to be due to the molecular structure of the donors. Two methyl groups on the CDBP bridging benzene rings and the steric hinderance of the two closely connected carbazole units in the mCP both impart highly twisted structures. This twisted molecular structure leads to reduced conjugation across the molecules resulting in similarly high triplet levels in both. Furthermore, CDBP and mCP have natural transition orbitals (NTOs) localised on the carbazole units,[4,10] in contrast to CBP where the NTOs are spread across the biphenyl bridge[10]. This localised donor electron density may result in the increased capacity of CDBP and mCP to form exciplexes at large separation distances.
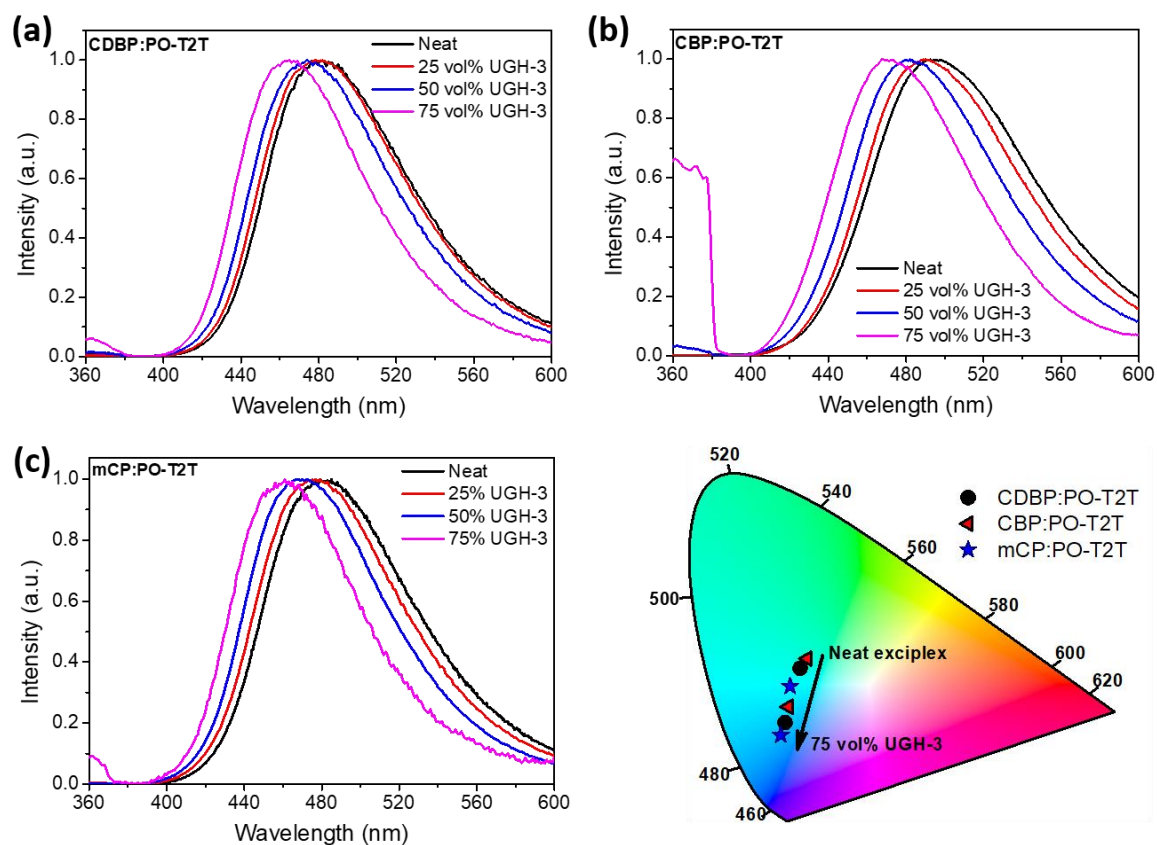
Figure 5.3 Photoluminescence spectra of (a) CDBP:PO-T2T 1:1 vol% ratio, (b) CBP:PO-T2T 1:1 vol% and (c) mCP:PO-T2T in different vol% of UGH-3 from Neat exciplex (0 vol% UGH-3) to 75 vol% of UGH-3. (d) 1931 CIE chromaticity diagram schematically showing the blueshift of the electroluminescence emission coordinates with increasing % vol% UGH-3 in all exciplexes studied.

Time resolved PL decays at room temperature (RT) (Figure 5.4) reveal quite different behaviour with dilution for CDBP:PO-T2T and mCP:PO-T2T compared to CBP:PO-T2T. The CDBP:PO-T2T and mCP:PO-T2T exciplexes possess delayed fluorescence (DF) with single exponential decay kinetics at all dilutions, and in both cases the DF lifetime (τ_{DF}) increases slightly with increasing dilution (Table 5.2). For the CDBP:PO-T2T exciplex an increase of τ_{DF} from 2.4 µs to 4.1 µs is observed (neat to 75% exciplex), while for mCP:PO-T2T there is a much smaller change, 2.1 to 2.6 µs.
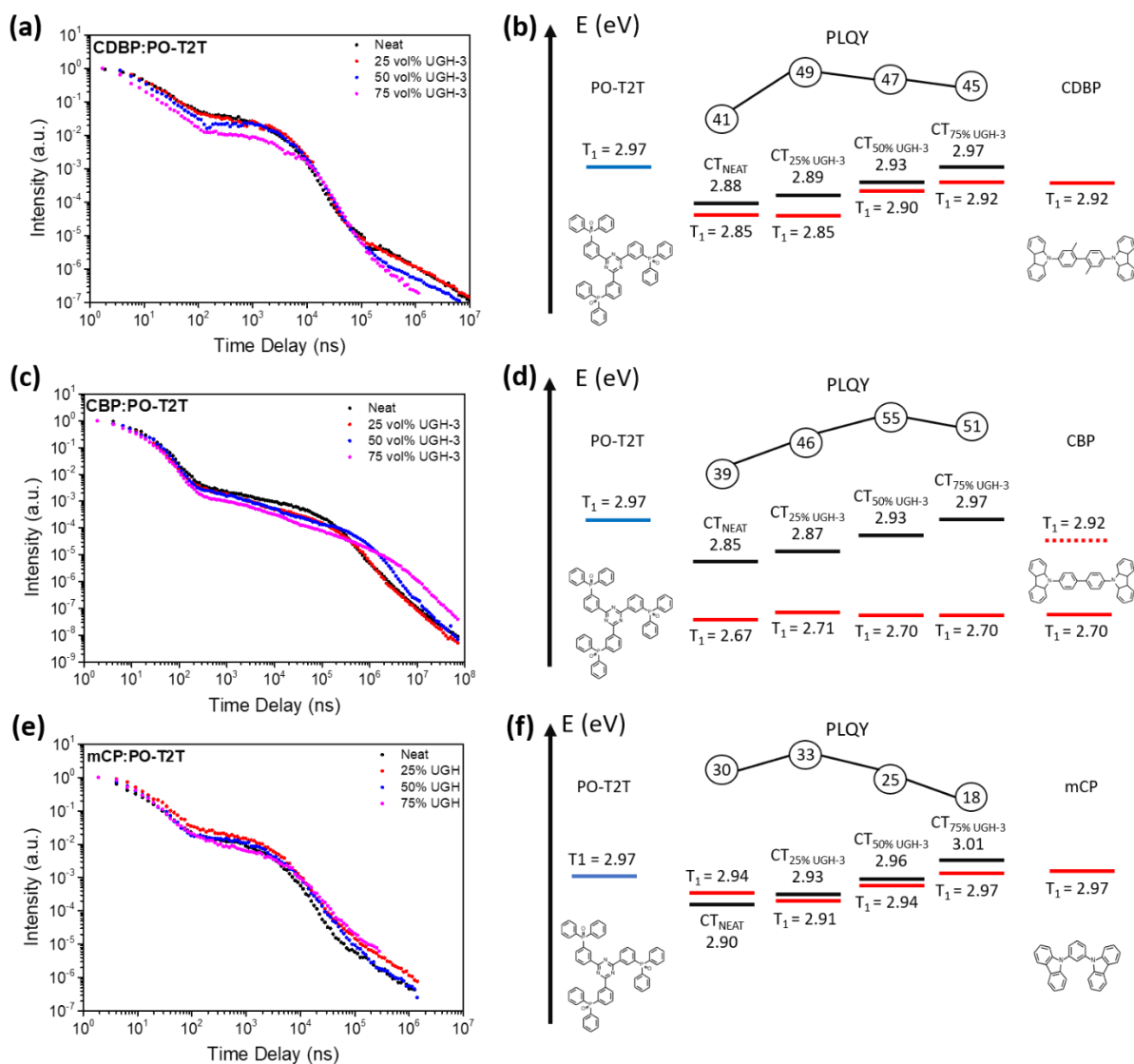
Figure 5.4 Left: Time resolved photoluminescence decays collected at room temperature of (a) CDBP:PO-T2T (c) CBP:PO-T2T and (e) mCP:PO-T2T exciplexes in different vol% of UGH-3. Right: Energy diagrams showing the lowest lying measured local triplets (solid red lines) of the exciplex forming molecules and the blue shifted CT energy (black lines) with increasing dilution for (b) CDBP:PO-T2T (d) CBP:PO-T2T and (f) mCP:PO-T2T. The blue lines indicate the local triplet of PO-T2T, while the dashed red line in d shows the level of the inferred triplet energy upon dilution, the same as in CDBP and discussed in the text below.

In contrast the CBP decays are predominantly bi-exponential. The first component was fitted using the same time constant as that obtained from the CDBP:PO-T2T decays at the corresponding dilution (as shown in Figure 5.5) with a longer lived component also required to fit the fully DF region. An additional third exponential was necessary to fully characterise the 75 vol% diluted film, with all fitting parameters reported in Table 5.1. The behaviour of the CBP films is interpreted as arising from the presence of a distribution of CBP conformations, characterised by different dihedral angles of the phenyl units across the biphenyl bridge. This distribution of CBP geometries (each with different levels of conjugation

between the two carbazole moieties) implies the presence of a distribution of triplet levels and associated ΔE_{ST} gaps within the films, leading to the multiexponential DF observed. As it is possible to fit the fast component of the CBP decays using the corresponding CDBP films this indicates that a proportion of the CBP molecules are in the same conformation as CDBP, i.e. highly twisted bridging phenyls and so low conjugation across the biphenyl bridge. This twisting confers a similar high triplet level (2.92 eV) to some of the CBP molecules and therefore a small ΔE_{ST} gap and fast rISC rate according to Equation 5.1.[11]

Equation 5.1

$$k_{rISC} \propto e^{-\Delta E_{ST}/k_B T}$$

However, in the PH measurements only the lowest energy population of CBP triplets can be observed (with onset energy 2.7 eV) because of energy transfer during the very long triplet lifetime. The slow DF decay component is given by that population of CBP molecules that retain a higher degree of conjugation across the biphenyl bridge, i.e. less twisting, (where the CBP triplet is 2.70 eV), bigger ΔE_{ST}, and a much slower rISC rate.
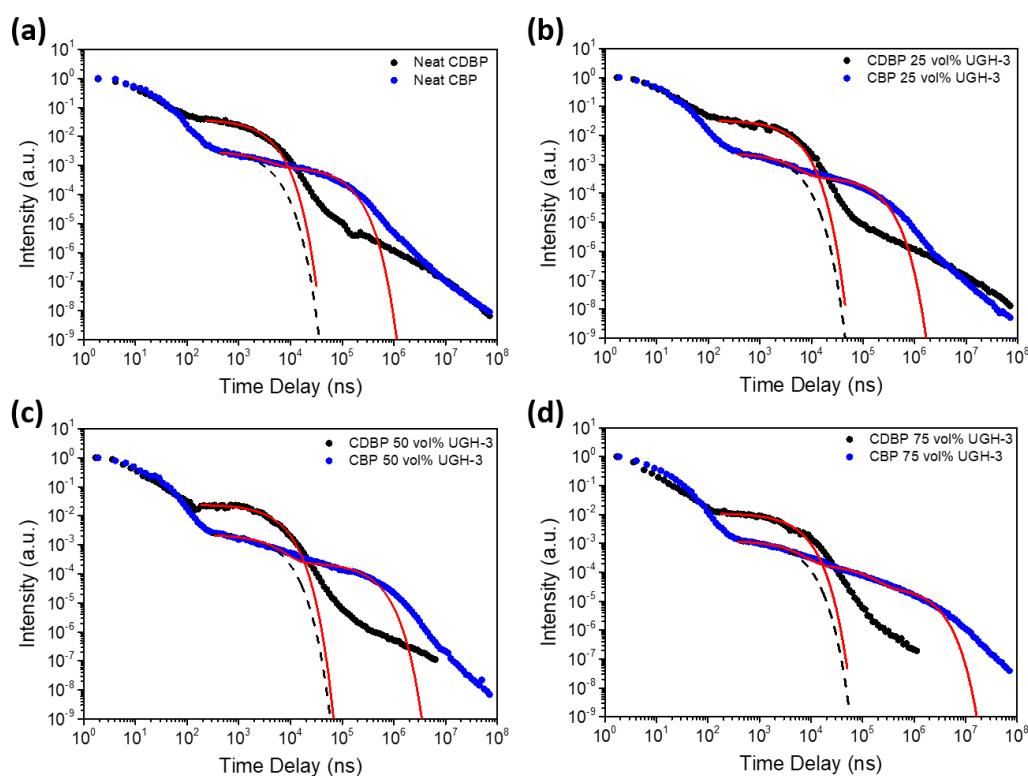
Figure 5.5 Time resolved photoluminescence decays collected at room temperature of CDBP:PO-T2T and CBP:PO-T2T at different dilution (a) neat exciplexes (b) 25 vol% UGH-3 (c) 50 vol% UGH-3 (d) 75 vol% UGH-3. The first component of the biexponential fitting (a,b and c) and the triexponential fitting (d) of the CBP:PO-T2T films is obtained from the fitted decay lifetime of the CDBP:PO-T2T film at the same dilution vol%, and is extended to guide the eye (black dashed line).

For CDBP, the ^{3}LE is always in close resonance with the exciplex ^{1}CT level due to its sterically locked twisted conformation, so the triplet level distribution is effectively homogeneous in the films. The resulting ΔE_{ST} gaps between the ^{1}CT and the T_1 of either the donor and the acceptor are always small, with values $0.03 < \Delta E_{ST} < 0.05$ eV (Table 5.3).

CBP:PO-T2T forms an exciplex with very similar energy to CDBP:PO-T2T (Table 5.3) due to the very similar HOMO levels. Upon dilution in UGH-3 the distribution of CBP linkage angles is changed, leading to a different distribution of triplet energies, ΔE_{ST} gaps, and rISC rates. Any concentration quenching mechanisms common to both CBP and CDBP must also be suppressed similarly in both systems, leading to their PLQYs converging to values of roughly 50% (+- 5% error). Decreases in the PLQY at 75% dilution are due to the increased D-A distances hindering the electron transfer from D to A that forms the exciplex, leading to the observed increase in donor emission.

The behaviour of the mCP dilution series further supports this interpretation since this material possesses CT and triplet energy levels very similar to CDBP, as schematically shown in Figure 5.4b and f. The mCP triplet is always in close resonance with the exciplex energy, and this does not change upon dilution due its rigid molecular structure. For mCP:PO-T2T the PLQY barely increases upon dilution (within error) but drops quickly as optically excited exciplex formation is again hindered at higher dilutions.

Table 5.1 Time constants obtained from the exponential fittings of DF component of the decays in Figure 5.5.

	τ_1 (μs)	τ_2 (μs)	τ_3 (ms)
CDBP:PO-T2T			
Neat	2.4	-	-
25 vol% UGH-3	3.1	-	-
50 vol% UGH-3	4.0	-	-
75 vol% UGH-3	4.1	-	-
CBP:PO-T2T			
Neat	2.4	83	-
25 vol% UGH-3	3.1	130	-
50 vol% UGH-3	4.0	280	-
75 vol% UGH-3	4.1	96	1.56

Figure 5.6-Figure 5.8 show spectra obtained at different delay times for the CDBP, CBP and mCP exciplexes. Consistent with what was observed in the previous chapter,[1] increasing host vol% causes a reduction in the time dependant shift observed for the onsets of the prompt (1.9 ns delay) and the most redshifted spectrum of the delayed PL component for all exciplexes

(Table 5.2). In all cases the initial spectrum recorded at 1.9 ns is found at higher energies at higher dilutions. The onset of the spectra redshifts over time, but by decreasing amounts at higher dilutions. This red shift is due to the presence of a heterogeneous distribution of CT lifetimes, where the highest energy CT states decay fastest (with blue emission) as they have more local LE character and stronger coupling to the ground state. The lower energy CT states decay more slowly as they are more weakly coupled to the ground state, leading to redder emission at longer times[12]. The reduced size of the onset shift at higher dilutions suggests that there are fewer low energy D-A "orientations" present in the film when the host vol% increases, which is intuitive as these low energy (short D-A distance) exciplexes will be the first to be disrupted as the host is incorporated[12–14]. As shown in Table 5.2, both prompt and delayed emission onsets blueshift with increasing host vol%, similar to the steady state PL discussed above. The fact that the onset of the prompt fluorescence blueshifts indicates that new higher energy exciplexes are formed which are not present in the undiluted films. This indicates that the average D-A separation increases with increasing dilution, creating more isolated D and A that can only form pairs at distances otherwise prevented by a closer nearest neighbour in an undiluted film. This change in the D-A distance distribution, substantially blueshifting the "centre of mass" of the CT band in the diluted films, which asymptotes at CT energies that correspond to separation distances at which the ET that forms the exciplex can no longer proceed.
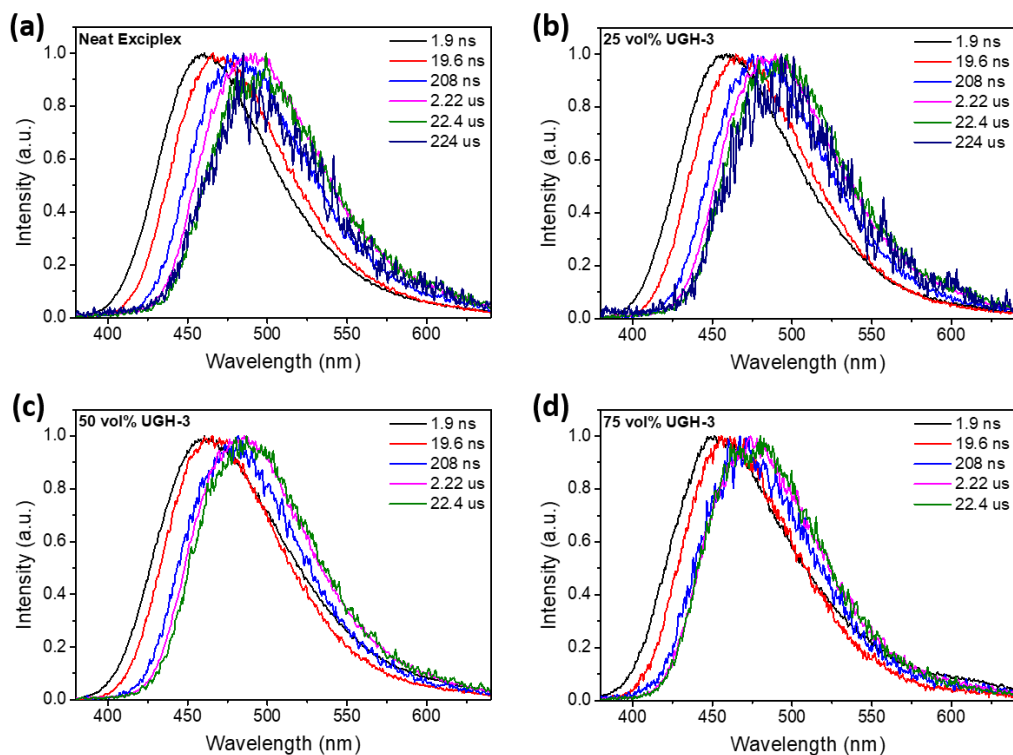
Figure 5.6 CDBP:PO-T2T spectra measured at different delay times at room temperature. (a) Neat CDBP:PO-T2T 1:1 exciplex film. (b) CDBP:PO-T2T 1:1 exciplex film diluted in 25 vol% UGH-3. (c) CDBP:PO-T2T 1:1 exciplex film diluted in 50 vol% UGH-3. (d) CDBP:PO-T2T 1:1 exciplex film diluted in 75 vol% UGH-3.
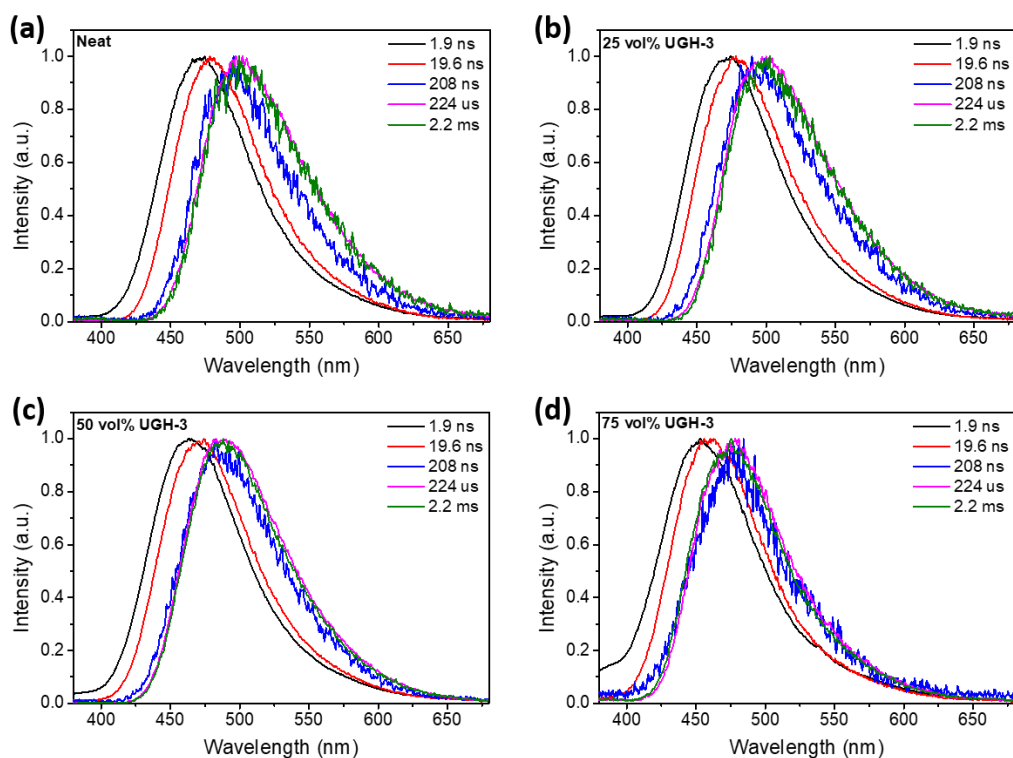
Figure 5.7 CBP:PO-T2T spectra measured at different delay times at room temperature. (a) Neat CBP:PO-T2T 1:1 exciplex film. (b) CBP:PO-T2T 1:1 exciplex film diluted in 25 vol% UGH-3. (c) CBP:PO-T2T 1:1 exciplex film diluted in 50 vol% UGH-3. (d) CBP:PO-T2T 1:1 exciplex film diluted in 75 vol% UGH-3.
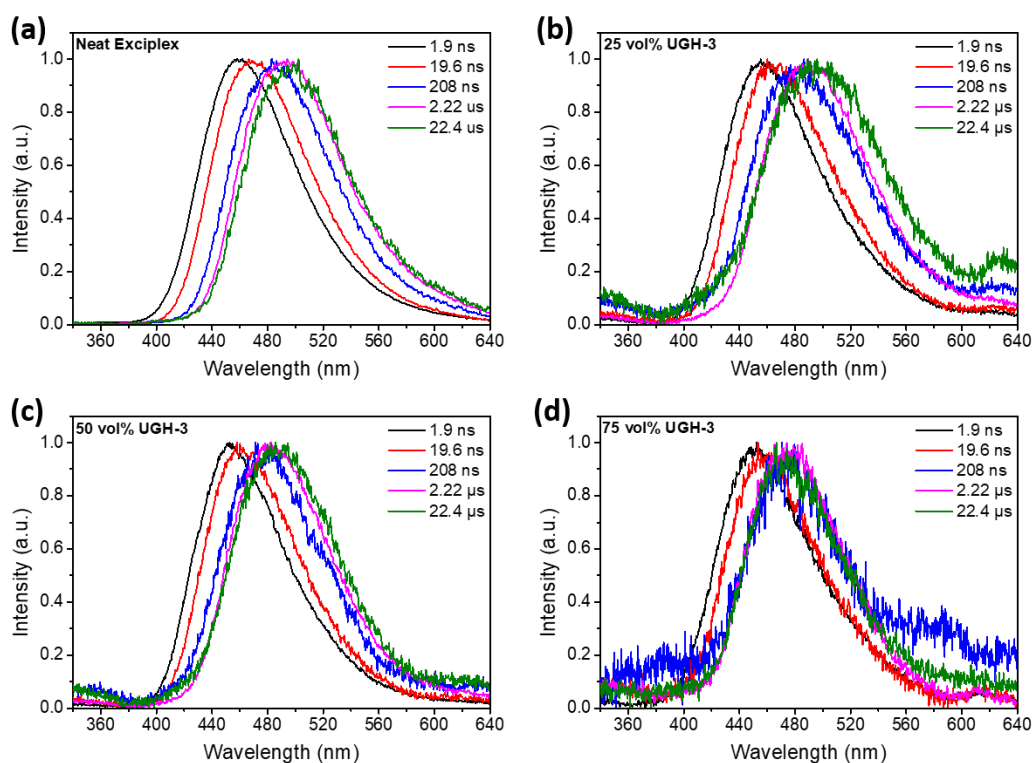
Figure 5.8 mCP:PO-T2T spectra measured at different delay times at room temperature. (a) Neat mCP:PO-T2T 1:1 exciplex film. (b) mCP:PO-T2T 1:1 exciplex film diluted in 25 vol% UGH-3. (c) mCP:PO-T2T 1:1 exciplex film diluted in 50 vol% UGH-3. (d) mCP:PO-T2T 1:1 exciplex film diluted in 75 vol% UGH-3.

Table 5.2 Lifetimes and spectral onsets of PL decays of the CDBP, CBP and mCP based exciplex series. Slope of the linear fit of the log-log plot of the PL integrated intensity vs laser power

	τ_{DF} (μs)	LF slope	CT prompt / delayed onset (eV)	CT prompt / delayed shift (eV)
CDBP:PO-T2T				
Neat	2.4	0.87	3.03 / 2.83	0.20
25 vol% UGH-3	3.1	0.95	3.07 / 2.85	0.22
50 vol% UGH-3	4.0	0.95	3.06 / 2.87	0.19
75 vol% UGH-3	4.1	1.01	3.11 / 2.96	0.15
CBP:PO-T2T				
Neat	-	0.86	2.97 / 2.74	0.23
25 vol% UGH-3	-	0.86/1.32	2.96/ 2.76	0.20
50 vol% UGH-3	-	0.90	3.02 / 2.84	0.18
75 vol% UGH-3	-	0.95	3.13 / 2.92	0.21
mCP:PO-T2T				
Neat	2.1	0.96	3.05 / 2.84	0.21
25 vol% UGH-3	2.1	0.96	3.07 / 2.89	0.18
50 vol% UGH-3	2.5	0.99	3.07 / 2.89	0.18
75 vol% UGH-3	2.6	0.96	2.11 / 2.96	0.15

To exclude the contribution of other DF processes such as TTA, laser fluences (LF) were measured for different excitation doses in each exciplex at each dilution. For the CDBP exciplex the LFs (Figure 5.9) were measured at a delay time and integration times of 0.25 µs and 1.5 µs respectively, to ensure that only the behaviour of the delayed part of the decay was assessed. The LFs measured were fitted with two linear regions. The high power region (laser power $> 10µJ$) showed sublinear dependence of the measured emission intensity with excitation dose, indicating that singlet-singlet quenching is likely active at high excitation powers. In the low power region (laser power $< 10µJ$) a behaviour closer to the ideal slope of 1 is observed. As phosphorescence is unlikely at room temperature in these systems, the observed DF is attributed to a pure TADF mechanism in the CDBP:PO-T2T exciplexes across all dilutions.

Since the CBP exciplexes showed such a long DF, the LFs were measured both in the early and in a later region of the DF to assess if different triplet harvesting processes were present at later delay times (Figure 5.10). In both the early DF (0.5 µs delay time/1.5 µs integration time) and longer DF (80 µs delay time/420 µs integration time) two regimes of laser power dependence were observed, similarly to the CDBP exciplex. In the high power region, a more severe sublinearity is observed, and for the neat film gradients are as low as 0.51 and 0.32 for the early and late high power LFs are observed. These results indicate stronger singlet-singlet quenching processes in the CBP exciplex, which is unsurprising based on the much slower triplet harvesting (and longer exciton lifetimes) in this exciplex series. Indeed, when comparing the early DF and later DF LFs in the high power region, a stronger quenching of the LF measured at longer delay time is always observed – indicating that the longest lived excitons (those least able to be rapidly harvested for emission) are the most likely to suffer from multi-exciton deactivation processes (possibly through non-emissive triplet fusion that is hindered by reduced triplet mobility at higher dilution). The same trend is observed in the low power regions of the LFs, with the early time LFs always showing slightly higher gradients than the LFs measured at later time. Nonetheless these gradients are all close to 1, indicating that the CBP:PO-T2T exciplex is also dominated by the TADF mechanisms despite the CBP T_1 being substantially lower than the exciplex energy at all dilutions.

The mCP:PO-T2T LFs were also measured in the DF region from 0.25 to 1.5 µs (Figure 5.11) showing trends similar to what discussed for the CDBP exciplex. In this exciplex again excited state quenching in the high power region is observed. This effect disappears for the exciplex diluted with 75vol% UGH-3. As for the other two exciplexes, the low power region is

characterised by a slope very close to 1 thus indicating the dominating TADF character of the DF at all dilutions. Another trend also observed in the LFs of all three exciplexes is that the sublinearity of the high power region becomes less severe with increasing dilution. This can be explained by considering that with increasing dilution vol% in the films, the exciton density will be become lower at all times (fewer exciplexes per volume unit) making the exciton concentration dependant quenching pathways less efficient[15]. The quenching mechanisms may include singlet-singlet annihilation in the early PF region (depleting the exciton population available for DF emission later on), as well as non-emission triplet-triplet annihilation in the DF region itself.
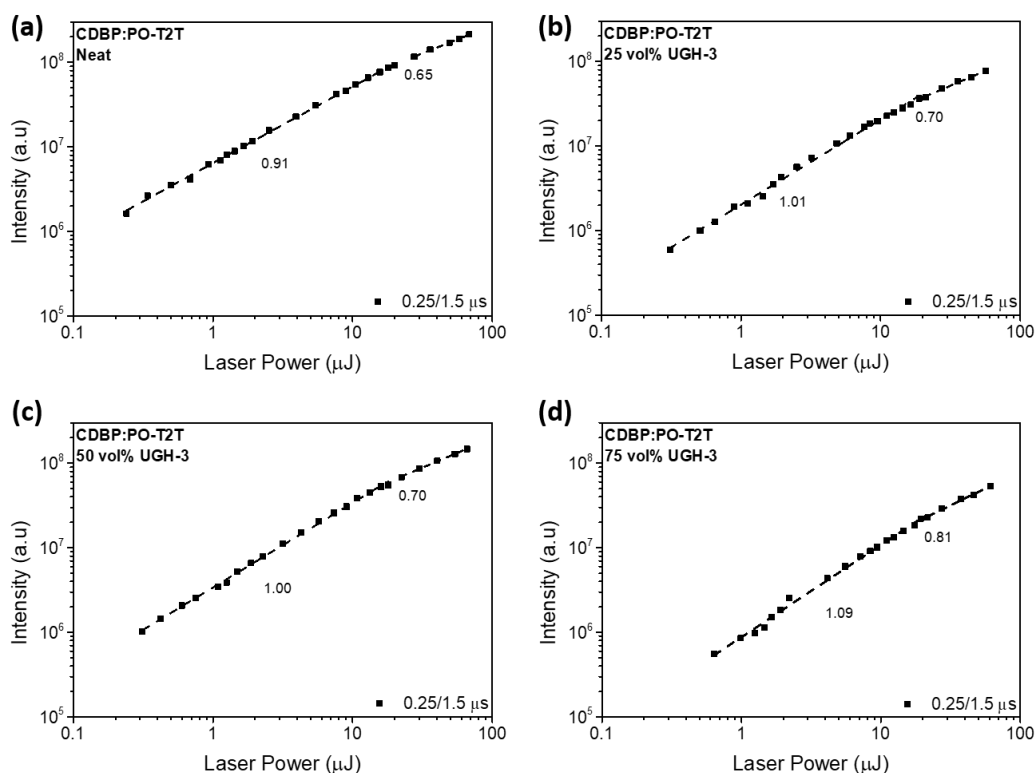
Figure 5.9 Linear fit of the of the integrated photoluminescence intensity vs the laser power measured at 0.25μs delay and 1.5 μs integration time of CDBP:PO-T2T 1:1 ratio evaporated films, (a) neat exciplex, (b) diluted in 25vol% UGH-3, (c) diluted in 50vol% UGH-3, (d) diluted in 75vol% UGH-3.
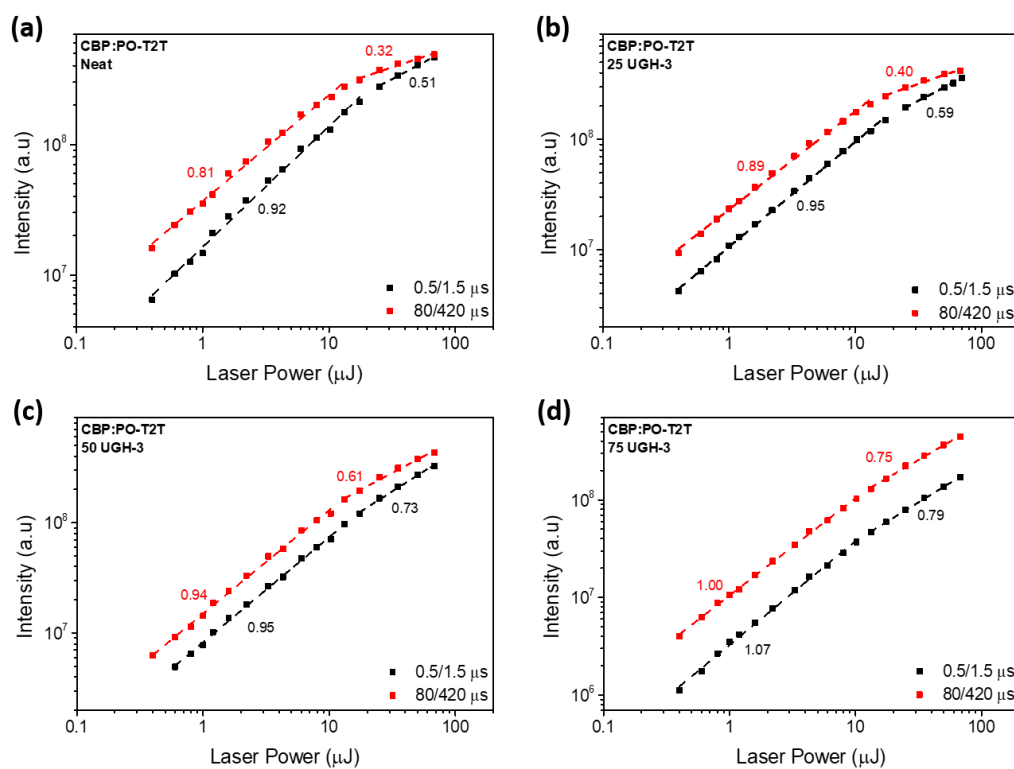
Figure 5.10 Linear fit of the of the integrated photoluminescence intensity vs the laser power measured at 0.25μs delay and 1.5 μs integration time of CBP:PO-T2T 1:1 ratio evaporated films, (a) neat exciplex, (b) diluted in 25vol% UGH-3, (c) diluted in 50vol% UGH-3, (d) diluted in 75vol% UGH-3.
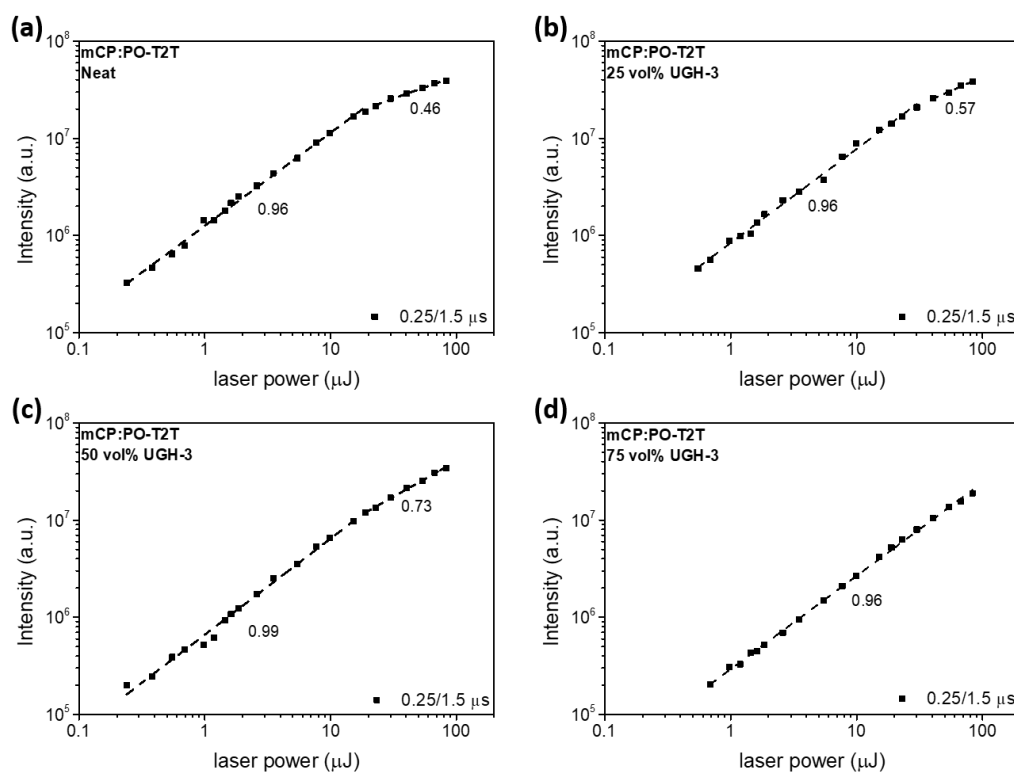
Figure 5.11 Linear fit of the of the integrated photoluminescence intensity vs the laser power measured at 0.25μs delay and 1.5 μs integration time of mCP:PO-T2T 1:1 ratio evaporated films, (a) neat exciplex, (b) diluted in 25vol% UGH-3, (c) diluted in 50vol% UGH-3, (d) diluted in 75vol% UGH-3.

PL decays were also measured at low temperatures for both dilution series (Figure 5.12 a,c and e). Even at 80K the CDBP and mCP exciplexes retain a strong DF component (in contrast to the CBP films) as a result of the smaller ΔE_{ST} and faster rISC rate in the these exciplexes. Spectra were also measured at 80K with 80 ms delay (Figure 5.12b, d and f) in order to capture the phosphorescence of the exciplex films. For the CDBP series (Figure 5.12b) this failed to unambiguously resolve the phosphorescence of the films to obtain the T_1 energies. The spectra collected are instead still DF from the exciplex state and are clearly blueshifted with dilution, similarly to the steady state spectra (Figure 5.3a). This kind of concerted blueshift upon dilution is not expected for phosphorescence. In order to obtain a better estimation of the ΔE_{ST} of the CDBP exciplex series, the phosphorescence of evaporated films of CDBP in UGH-3 were measured at concentrations of 10, 25 and 50 vol% without PO-T2T (Figure 5.13). The 10% CDBP films shows a phosphorescence onset of 2.92 eV, while the 25 and 50 vol% films possess a slightly lower phosphorescence onset of 2.90 eV and 2.85eV respectively. This redshift of the phosphorescence with the increasing concentration is likely due to excimer formation[10]. For the CBP series, structured emission is always obtained even in the presence of PO-T2T (Figure 5.12d) with onset energies between 2.67 and 2.71 eV, consistent with literature reports of the CBP triplet energy[3]. Similarly, the mCP series also showed a consistent phosphorescent spectra (Figure 5.12f) with onset energy between 2.91 eV and 2.97 eV from the exciplex films.

Table 5.3 Comparison between the PLQY values and the ΔE_{ST} of the CDBP, CBP and mCP based exciplex

	PLQY (%)	PL onset (eV)	PH onset (eV)	ΔE_{ST} (eV)
CDBP:PO-T2T				
Neat	41	2.88	2.85[a]	0.03
25 vol% UGH-3	49	2.89	2.85[a]	0.04
50 vol% UGH-3	47	2.93	2.90[a]	0.03
75 vol% UGH-3	45	2.97	2.92[a]	0.05
CBP:PO-T2T				
Neat	39	2.85	2.67	0.18
25 vol% UGH-3	46	2.87	2.71	0.16
50 vol% UGH-3	55	2.92	2.70	0.22
75 vol% UGH-3	51	2.97	2.71	0.26
mCP:PO-T2T				
Neat	30	2.90	2.94	-0.04
25 vol% UGH-3	33	2.93	2.91	0.02
50 vol% UGH-3	25	2.96	2.94	0.02
75 vol% UGH-3	18	3.01	2.97	0.03

[a] phosphorescence value measured for CDBP:UGH-3 evaporated films at 10-25 and 50 CDBP vol% (i.e. without PO-T2T)
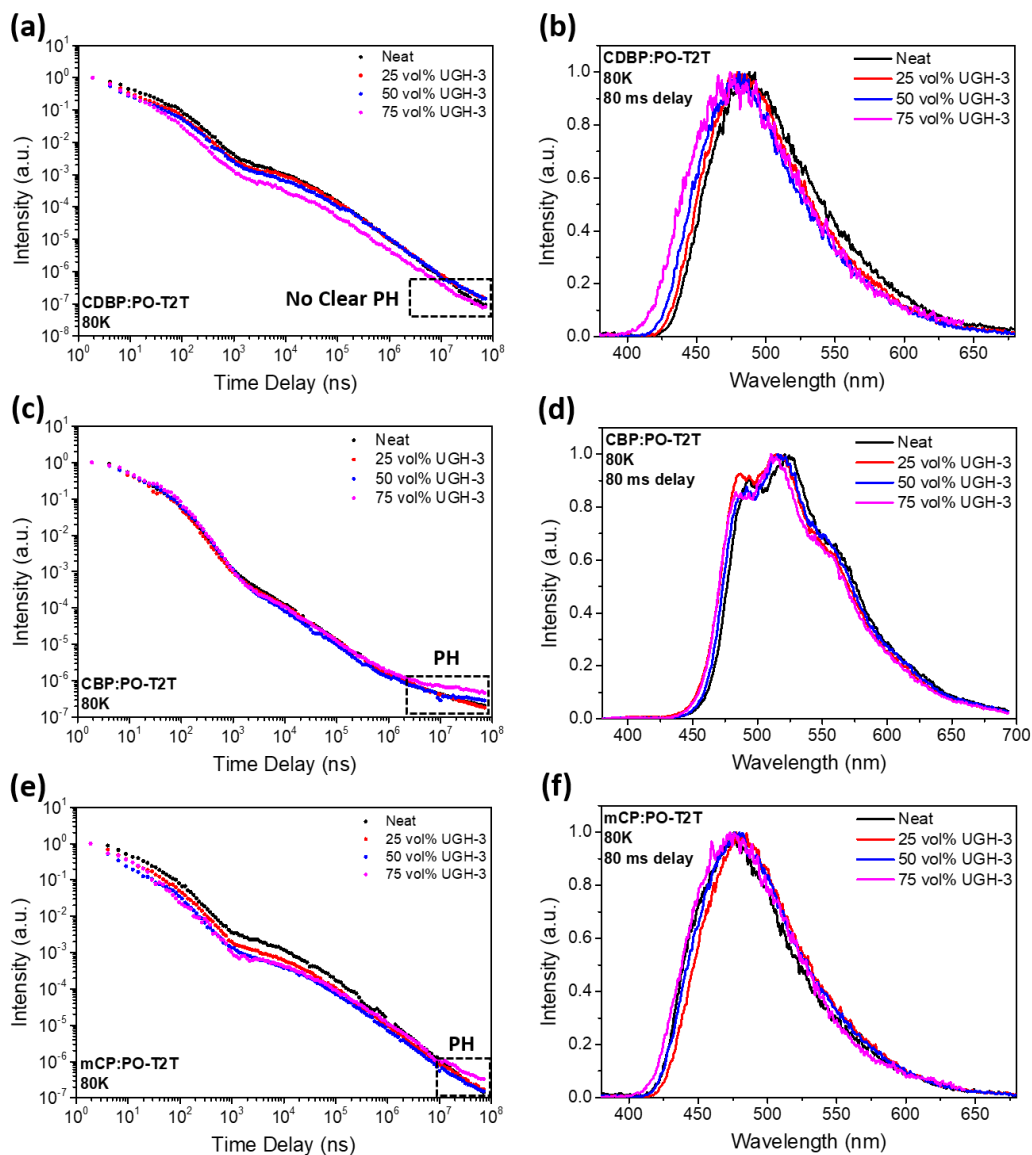
Figure 5.12 Left: Time resolved photoluminescence decays collected at 80K of (a) CDBP:PO-T2T (c) CBP:PO-T2T and (e) mCP:PO-T2T 1:1 vol% ratio and in different vol% of UGH-3. Right: PL spectra measured at 80K and 80 ms delay time and 10 ms integration time of (b) CDBP:PO-T2T (d) CBP:PO-T2T and (f) mCP:PO-T2T 1:1 vol% ratio and in different vol% of UGH-3
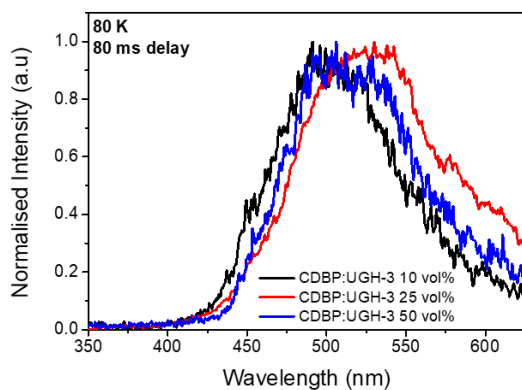
Figure 5.13 Phosphorescence spectra of vacuum deposited films of CDBP:UGH-3 at different CDBP vol%.

Photoluminescence Quantum Yields (PLQYs) were measured for all exciplex films (Table 5.3) in anticipation of a significant efficiency enhancement with dilution as observed for TSBPA:PO-T2T in the previous chapter.[1] Instead, the CDBP series shows only a small PLQY increment, from 41% for the neat exciplex to 49% for the 25 % UGH-3 film. At 50 vol% UGH-3 the PLQY remains essentially unchanged while it deceases at 75% dilution to 45%. The mCP series shows only a decrease of the PLQY with dilution. For CBP the PLQY instead increases from the 39% measured for the neat film to 55% obtained for the sample diluted with 50 vol% of UGH-3, then decreases slightly at 51% at 75% dilution. The general decrease of PLQY at 75 vol% dilution can be explained by observing the steady state PL spectra (Figure 5.3a), as at this level of dilution all three exciplexes show donor emission under optical excitation, inevitably lowering the PLQY.

The differences in PLQY behaviour for the different exciplex series is unexpected, and hints towards the mechanism of the efficiency enhancement, as seen in the previous chapter, which is correlated to the different rigidities of the donor molecules. Rigid CDBP and mCP possess NTOs localised on the carbazole moieties and higher local triplet energies as a result of their reduced (phenyl bridge) conjugation, yielding a small ΔE_{ST} for the resulting exciplex. It is reasonable to suggest that this rigidity may also reduce excited state quenching processes (eg, vibrationally driven IC) that are conversely active in CBP. As the inclusion of the UGH-3 host does not change the structure (and hence the triplet energy) or reduce any quenching mechanisms in these rigid materials, dilution cannot improve the PLQY from its starting value for mCP and CDBP. Instead, the PLQY can only decrease as exciplex formation becomes more and more hindered and donor emission becomes a competing emission channel. A blueshift in the emission is nonetheless observed, as the coulombic energy always changes with increasing separation independently of any efficiency increase.

Conversely dilution is able to enhance CBP by providing a rigid host, which increases the proportion of the twisted CBP molecules having higher triplet energy and thus more efficient rISC (similar to CDBP). Dilution will also spatially isolate any low triplet CBP molecule that would otherwise act as a low efficiency triplet trap, likely populated by short range Dexter transfer. Therefore the PLQY can be enhanced on dilution because of the flexible CBP, similarly to what observed in the previous chapter with the flexible TSBPA based exciplex[1], whilst PLQY remains largely unchanged in the rigid CDBP because there is no scope for the host to change the photophysics. It is also therefore no coincidence that the CBP PLQY rises to meet that of the CDBP, while the radically different molecular structure of mCP means that

no additional insight can be gleaned from comparing its absolute PLQY values to the other two.

5.2.2 Device Performance

The OLED devices were then prepared using these diluted exciplexes to test the performance as emitters of the films analysed in the previous sections of the chapter (Figure 5.14 Figure 5.16). The OLED stack used for all the devices was NPB 40 nm|Donor 10 nm|Donor:PO-T2T in x vol% UGH-3 30 nm|PO-T2T 50 nm where Donor represents CBP, CDBP or mCP and x vol% values were 0 (neat exciplex), 25, 50 and 75. In all three dilution series studied, the electroluminescence (EL) blueshifts in line with the PL. The maximum brightness monotonically decreases with increasing host vol% due to the decreased concentration and total loading of exciplex emitter in the emissive layer (EML). The only exception to this trend is the device with CBP diluted at 50 vol%, where the maximum brightness is higher than in the neat undiluted exciplex. This can be explained by considering that at this dilution the CBP exciplex show the maximum PLQY value (55 %) which is able to offset other factors common to all three series that would otherwise decrease its brightness. The overall resistivity of the OLED devices increases, requiring higher driving voltage to reach similar currents due to the presence of the resistive UGH-3. In all exciplexes the EQE decreases with increasing dilution, despite the increased PLQY values for CBP.[1] This unexpected result is assigned to the low conductivity of the chosen donors and host and suggests that, when exciplexes are formed by donors with relatively low conductivity are diluted (eg carbazole), the hole injection capability in the EML drops critically, making it impossible to achieve the full performance of the exciplex as an emitter as indicated by the PLQY. This may be remedied in future by using diluting hosts with ambipolar transport properties, although finding such a host that does not also form a competing exciplex with PO-T2T will likely prove challenging. For TSBPA the greater conductivity of the diphenyl amine (DPA) unit means that hole injection is not a limiting factor even at high dilution so that the EQE can improve in line with the PLQY.
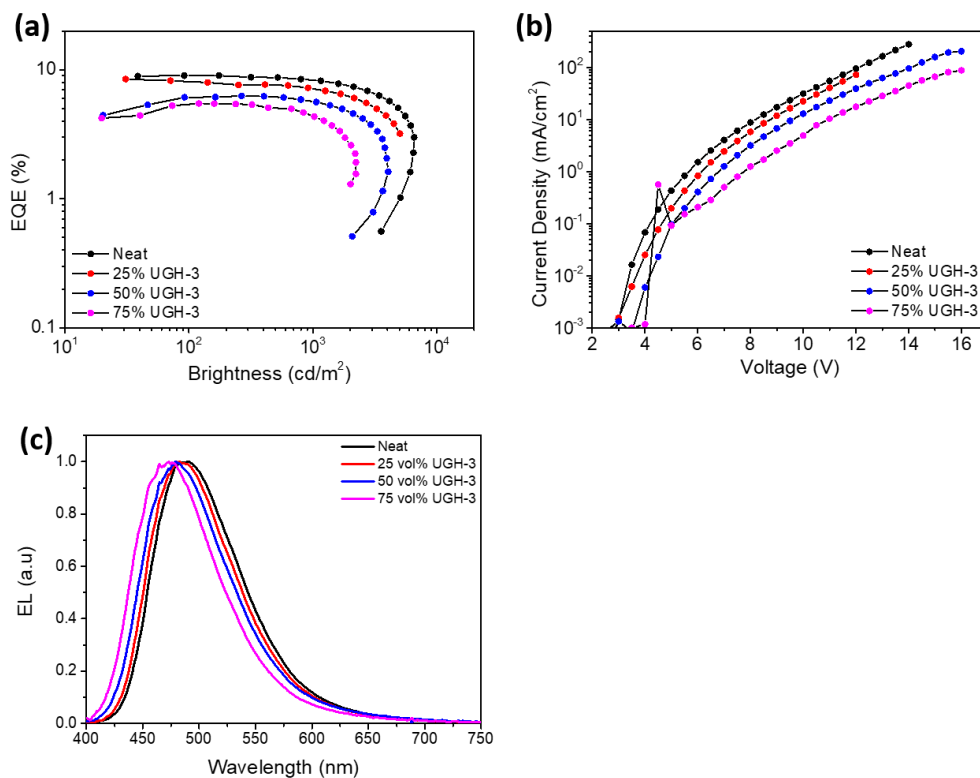
Figure 5.14 CDBP:PO-T2T 1:1 vol% ratio OLEDs characteristics for different vol% of UGH-3 in the emissive layer blend. From Neat exciplex (0 vol% UGH-3) to 75 vol% of UGH-3. (a) EQE vs Brightness. (b) Current density vs voltage. (c) Normalised electroluminescence spectra
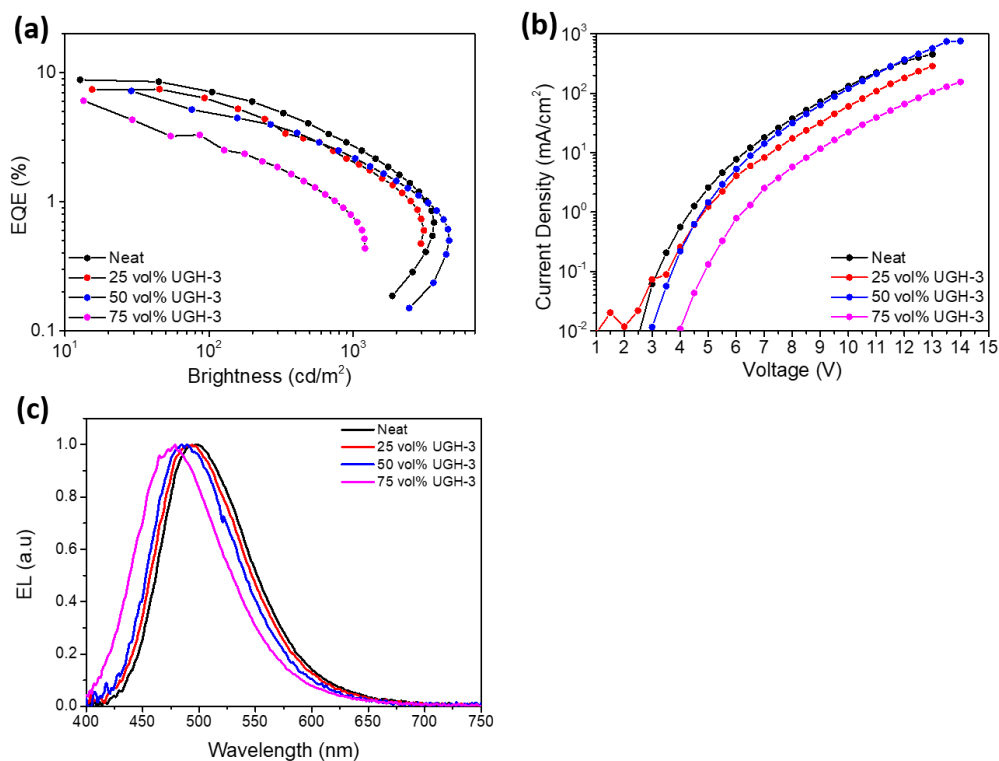
Figure 5.15 CBP:PO-T2T 1:1 vol% ratio OLEDs characteristics for different vol% of UGH-3 in the emissive layer blend. From Neat exciplex (0 vol% UGH-3) to 75 vol% of UGH-3. (a) EQE vs Brightness. (b) Current density vs voltage. (c) Normalised electroluminescence spectra.
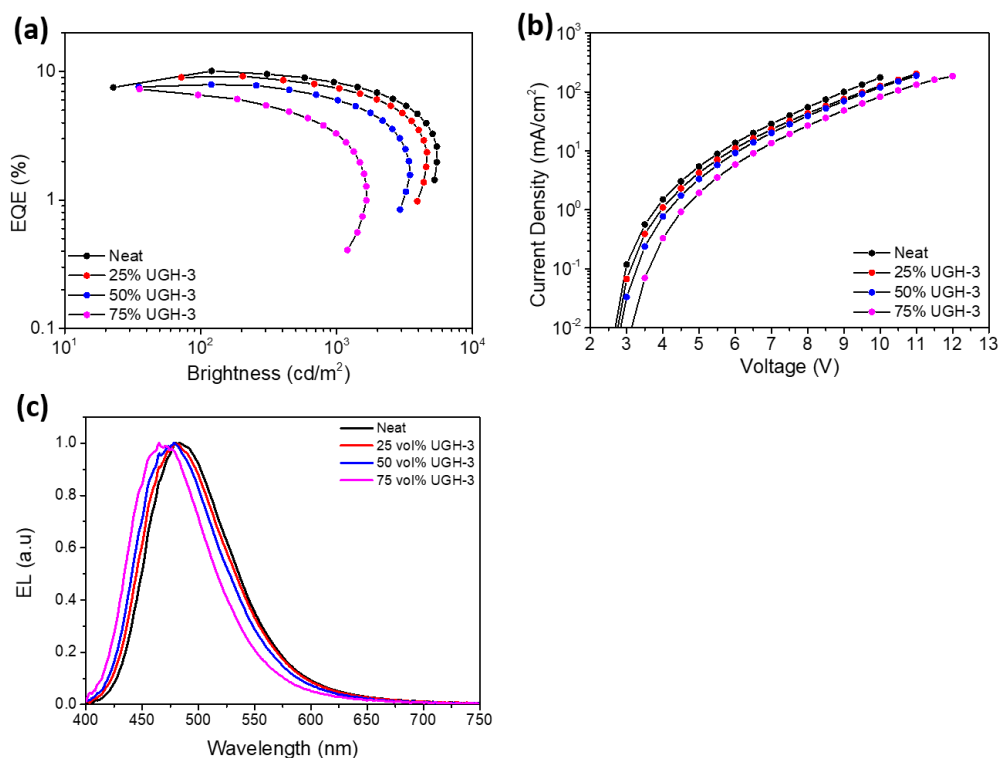
Figure 5.16 mCP:PO-T2T 1:1 vol% ratio OLEDs characteristics for different vol% of UGH-3 in the emissive layer blend. From Neat exciplex (0 vol% UGH-3) to 75 vol% of UGH-3. (a) EQE vs Brightness. (b) Current density vs voltage. (c) Normalised electroluminescence spectra.

5.3 Conclusion

In conclusion, the effect of dilution on the photophysical and electrical performances of three TADF exciplexes based on CBP, CDBP and mCP donors with PO-T2T is compared. CDBP and mCP exciplexes show intrinsically different photophysical behaviour when compared to CBP despite the similarities in the structures of CBP and CDBP. This has been assigned to a heterogeneous distribution of triplet energies in the CBP molecules arising from a distribution of conformations of the CBP molecule -between planar and highly twisted biphenyl bridges- which introduces a distribution of ΔE_{ST} gaps, as evidences by a highly multiexponential time resolved PL decay.

Furthermore, this result show that the PLQY enhancement of the diluted exciplexes is independent of the D-A separation associated with the spectral blueshift, and suggest that only donor molecules with low structural rigidity are able to enhance exciplexes PLQY through

dilution. Finally, OLEDs produced from these carbazole based exciplexes show decreased EQEs with increasing dilution, which it is assigned to the relatively low conductivity of the carbazole based donors. This limiting factor is only exacerbated by the inclusion of the resistive UGH-3, which outcompetes the modest increase in PLQY observed for CBP in determining the overall device performance. This problem might be addressed in future studies by employing functional hosts that can assist the charge injection and conduction across the EML, in contrast to resistive UGH-3.

5.4 References

(1)   Colella, M.; Danos, A.; Monkman, A. P. Less Is More: Dilution Enhances Optical and Electrical Performance of a TADF Exciplex. *J. Phys. Chem. Lett.* **2019**, 793–798. https://doi.org/10.1021/acs.jpclett.8b03646.

(2)   Yuan, P.; Guo, X.; Qiao, X.; Yan, D.; Ma, D. Improvement of the Electroluminescence Performance of Exciplex-Based OLEDs by Effective Utilization of Long-Range Coupled Electron–Hole Pairs. *Adv. Opt. Mater.* **2019**, *0* (0), 1801648. https://doi.org/10.1002/adom.201801648.

(3)   Bagnich, S. A.; Rudnick, A.; Schroegel, P.; Strohriegl, P.; Köhler, A. Triplet Energies and Excimer Formation in Meta- and Para-Linked Carbazolebiphenyl Matrix Materials. *Philos. Trans. A. Math. Phys. Eng. Sci.* **2015**, *373* (2044), 20140446. https://doi.org/10.1098/rsta.2014.0446.

(4)   Dong, S. C.; Zhang, L.; Liang, J.; Cui, L. S.; Li, Q.; Jiang, Z. Q.; Liao, L. S. Rational Design of Dibenzothiophene-Based Host Materials for PHOLEDs. *J. Phys. Chem. C* **2014**, *118* (5), 2375–2384. https://doi.org/10.1021/jp412107g.

(5)   Zhang, D.; Cai, M.; Bin, Z.; Zhang, Y.; Zhang, D.; Duan, L. Highly Efficient Blue Thermally Activated Delayed Fluorescent OLEDs with Record-Low Driving Voltages Utilizing High Triplet Energy Hosts with Small Singlet–triplet Splittings. *Chem. Sci.* **2016**, *7* (5), 3355–3363. https://doi.org/10.1039/C5SC04755B.

(6)   Dias, F. B.; Penfold, T. J.; Monkman, A. P. Photophysics of Thermally Activated Delayed Fluorescence Molecules. *Methods Appl. Fluoresc.* **2017**, *5* (1), 012001. https://doi.org/10.1088/2050-6120/aa537e.

(7)   Wu, Z.; Yu, L.; Zhao, F.; Qiao, X.; Chen, J.; Ni, F.; Yang, C.; Ahamad, T.; Alshehri, S. M.; Ma, D. Precise Exciton Allocation for Highly Efficient White Organic Light-Emitting Diodes with Low Efficiency Roll-Off Based on Blue Thermally Activated Delayed Fluorescent Exciplex Emission. *Adv. Opt. Mater.* **2017**, *5* (20), 1700415. https://doi.org/10.1002/adom.201700415.

(8)   Zhang, T.; Liang, Y.; Cheng, J.; Li, J. A CBP Derivative as Bipolar Host for Performance Enhancement in Phosphorescent Organic Light-Emitting Diodes. *J. Mater. Chem. C* **2013**, *1* (4), 757–764. https://doi.org/10.1039/C2TC00305H.

(9) Ren, X.; Li, J.; Holmes, R. J.; Djurovich, P. I.; Forrest, S. R.; Thompson, M. E. Ultrahigh Energy Gap Hosts in Deep Blue Organic Electrophosphorescent Devices. *Chem. Mater.* **2004**, *16* (23), 4743–4747. https://doi.org/10.1021/cm049402m.

(10) Bagnich, S. A.; Athanasopoulos, S.; Rudnick, A.; Schroegel, P.; Bauer, I.; Greenham, N. C.; Strohriegl, P.; Köhler, A. Excimer Formation by Steric Twisting in Carbazole and Triphenylamine-Based Host Materials. *J. Phys. Chem. C* **2015**, *119* (5), 2380–2387. https://doi.org/10.1021/jp512772j.

(11) Dias, F. B.; Penfold, T. J.; Berberan-Santos, M. N.; Monkman, A. P. Photophysics of Thermally Activated Delayed Fluorescence in Organic Molecules. *Methods Appl. Fluoresc.* **2017**, *5*, 012001. https://doi.org/10.1142/9789813230194_0006.

(12) Graves, D.; Jankus, V.; Dias, F. B.; Monkman, A. Photophysical Investigation of the Thermally Activated Delayed Emission from Films of M-MTDATA:PBD Exciplex. *Adv. Funct. Mater.* **2014**, *24* (16), 2343–2351. https://doi.org/10.1002/adfm.201303389.

(13) Moon, C.-K.; Huh, J.-S.; Kim, J.-M.; Kim, J.-J. Electronic Structure and Emission Process of Excited Charge Transfer States in Solids. *Chem. Mater.* **2018**, *30*, 5648–5654. https://doi.org/10.1021/acs.chemmater.8b02011.

(14) Serevičius, T.; Skaisgiris, R.; Dodonova, J.; Jagintavičius, L.; Bucevičius, J.; Kazlauskas, K.; Juršėnas, S.; Tumkevičius, S. Emission Wavelength Dependence on the RISC Rate in TADF Compounds with Large Conformational Disorder. *Chem. Commun.* **2019**, *55* (13), 1975–1978. https://doi.org/10.1039/C8CC08906J.

(15) Fujitsuka, M.; Satyanarayana, K.; Luh, T.-Y.; Majima, T. Singlet–singlet and Singlet–triplet Annihilations in Structure-Regulated Porphyrin Polymers. *J. Photochem. Photobiol. A Chem.* **2016**, *331*, 56–59. https://doi.org/https://doi.org/10.1016/j.jphotochem.2015.10.011.

Chapter 6:

Solution Processable TADF OLED Based on Small Molecule Exciplex

This chapter presents the optimisation of a solution processable TADF exciplex emitter in OLED devices formed by the small molecules DCz-DBTO2 and TAPC. This exciplex was previously reported by Jankus et al.[1] to give vacuum deposited devices current efficiency, power efficiency and EQE of 32.3 cd/A, 26.7 lm/W and 10.3 % obtained with DCz-DBTO2:TAPC vol% ratio of 30:70. The thickness and ratio of the exciplex layer was optimised for solution processing using two different solvents, chlorobenzene and chloroform. The best results were achieved when the two solvents were mixed (5 vol% of chlorobenzene in chloroform). With this solvent mixture comparable results to evaporated devices were achieved; 27.5 ± 3.5 cd/A, 16.5 ± 2.0 lm/W and EQE of 8.9 ± 0.6 % at DCz-DBTO2:TAPC wt% ratio of 30:70. This result demonstrates the suitability of small molecule TADF exciplexes as solution processable emissive layer for OLEDs.

6.1 <u>Introduction</u>

Currently, there are two approaches commercially viable to fabricate OLEDs - vacuum deposition and solution processing. The first offers great control over the deposition process and has been the main deposition technique for work presented in the previous chapters. Indeed, thermal vacuum deposition is also the main fabrication method used for commercial OLEDs. This technique allows to build complex multilayer stacks that often results in more efficient and stable devices, which has led to evaporated OLEDs dominating the present markets. On the other hand, this technique needs to be performed under costly high vacuum conditions, and the usage of material can be far greater than in solution processing – both of which are very important costs considerations for mass production.

For this reason, efficient solution processable OLEDs are still of great interest in order to be integrated in solution based roll-to-roll deposition systems to lower the production costs[2]. An important task is therefore to determine fabrication procedures that produces comparable devices from solution processing to those obtained via thermal evaporation. Good results have already been achieved with solution processed PhOLEDs[3,4], while in recent years good results have been obtained also via solution processing TADF small molecules and TADF exciplex hosts doped with fluorescent or phosphorescent emitters[5–10]. However they do not quite match the performance of evaporated devices yet.

In this chapter, a TADF exciplex formed by the D-A-D molecule 9-[2,8]-9-carbazole-[dibenzothiophene-*S,S*-dioxide]-carbazole (DCz-DBTO2) and 4,4′-cyclohexylidenebis[*N,N*-bis(4-methylphenyl)benzenamine] (TAPC) (Figure 6.1d) has been solution processed, with molecular structures shown in Figure 6.1b. This exciplex was selected because it has already been demonstrated to harvest nearly 100% of the triplets via TADF, with a PLQY of 53 $\pm$ 4 % in a co-evaporated film consisting of 30%wt of DCz-DBTO2 in TAPC. [1]

To develop a suitable solution process it is noted that both molecules have good solubility in chlorinated solvents (>20 mg mL^{-1}) such as Chlorobenzene (CB) and Chloroform (CF). The deposition parameters were optimised to maximise OLED performance, obtaining a maximum current efficiency of 27.5 $\pm$ 3.5 cd/A, a maximum power efficiency of 16.5 $\pm$ 2.0 lm/W, a maximum EQE of 8.9 $\pm$ 0.6 and luminances > 4000 cd/m^2. These are comparable results to the evaporated devices published by Jankus et al. of 32.3 cd/A, 26.7 lm/W and 10.3 % for a device with the same DCz-DBTO2:TAPC wt% of 30:70.[1] The effect of the thickness and DCz-

DBTO2:TAPC ratio was also explored in both solvents, and find that the two solvent mixed together (ratio of CB:CF 5:95 vol%) gives the best wettability offered by the CF with an improved surface tension provided by the CB. [11,12]
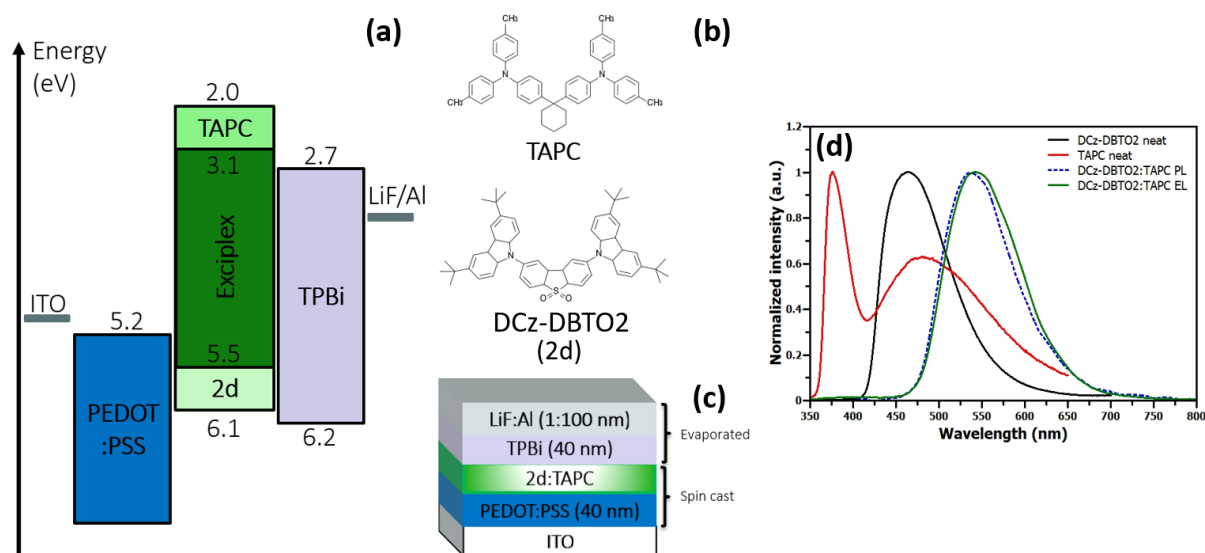
Figure 6.1 (a)The energy diagram of the devices produced in this study. (b) The molecular structures of TAPC and DCz-DBTO2. (c) the device structure of the devices used in this work. The PEDOT:PSS and the DCz-DBTO2:TAPC layer have been deposited via spin coating while TPBi and the cathode via thermal evaporation. (d) Normalised photoluminescence of DCz-DBTO2, TAPC, DCz-DBTO2:TAPC thin films and electroluminescence spectrum of the DCz-DBTO2:TAPC used as EML in the OLED devices. The red-shifted peak in the TAPC fluorescence spectrum is assigned to excimers formed in solid state.

6.2 Results and Discussion

6.2.1 EML processed from Chlorobenzene

6.2.1.1 Thickness

Figure 6.2 shows the results obtained for devices with the structure ITO|PEDOT:PSS 40 nm| DCz-DBTO2:TAPC (30:70 x nm)|TPBi 40 nm|LiF 1nm|Al 100 nm. The schematic representation of the device structure and the energy levels of the OLEDs produced are shown in Figure 6.1a and c. This ratio between DCz-DBTO2 and TAPC was chosen as a starting point for the study because it had already been shown to give the highest values of current and power

efficiency in the evaporated devices[1]. The thickness of the EML was varied from 15 to 48 nm with results summarised in Table 6.1. It is clear from Figure 6.2a that increasing the EML thickness from 15 to 20 nm does not substantially affect the performance of the devices in terms of resistivity, efficiency and turn on voltage (V_{ON} all ~3.5 V). When the EML thickness is further increased from 24 to 34 nm, the resistivity and V_{ON} of the devices increases. In terms of efficiency, the greater EML thickness does not substantially vary the maximum efficiency, which is reached around 100 cd/m^2. Surprisingly the maximum CE is not affected by the thickness variation, showing values within 10 ± 2 cd/A. The EQE can also be interpreted as constant within the standard deviation (3 ± 0.9 %).

The efficiency of the device with the EML of 48 nm is the lowest at low luminance which is interpreted as a result of current leakage (visible in Figure 6.2a). This leakage is probably caused by the low spin speed used to deposit the DCz-DBTO2:TAPC layer (500 rpm)[13–15] leading to an increased roughness of the film that can affect the conduction of the device.[16]
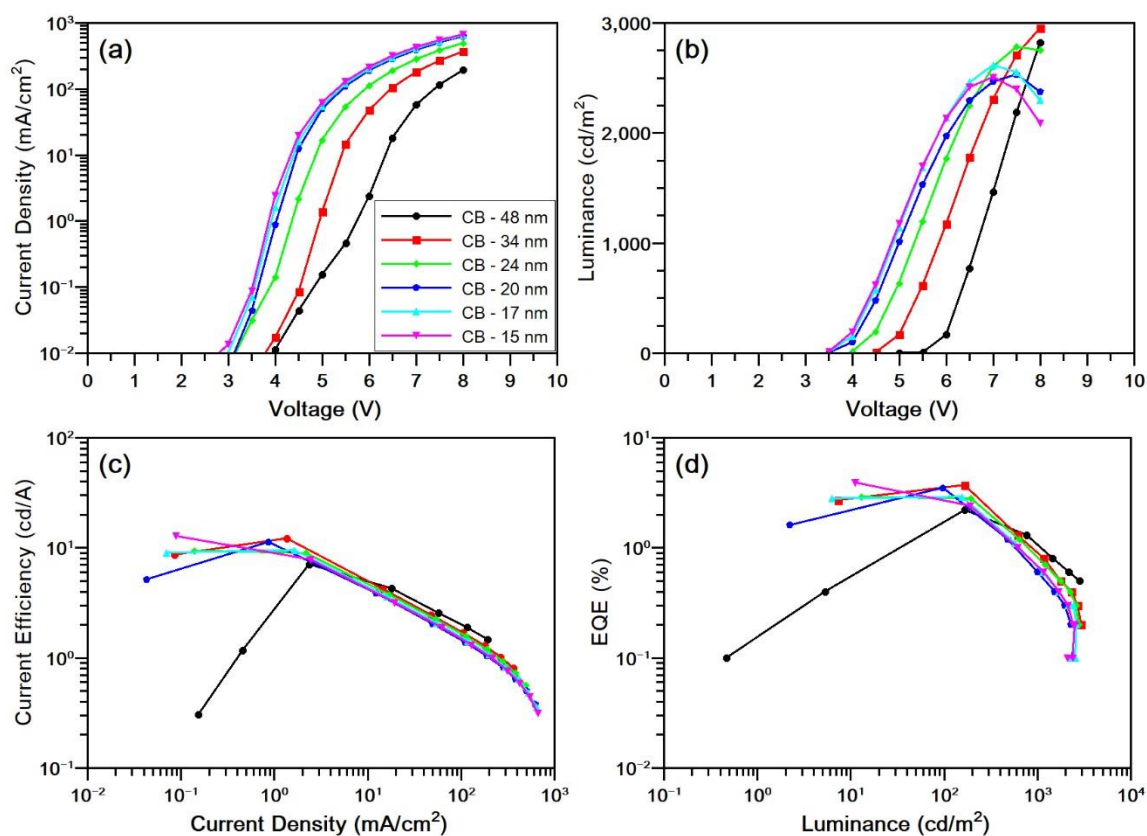
Figure 6.2 Device characteristics for ITO|PEDOT:PSS (40 nm)| DCz-DBTO2:TAPC 30:70 (15-17-20-24-34-48 nm)|TPBi (40 nm)|LiF (1 nm)|Al (100 nm) deposited from chlorobenzene. (a) Current density vs driving voltage. (b) Luminance vs driving voltage. (c) Current efficiency vs current density. (d) Power efficiency vs Luminance.

Table 6.1 Performance summary of OLEDs produced with the structure ITO|PEDOT:PSS (40 nm)| DCz-DBTO2:TAPC 30:70 (15-17-20-24-34-48 nm)|TPBi (40 nm)|LiF (1 nm)|Al (100 nm) deposited from chlorobenzene.

	48 nm	34 nm	24 nm	20 nm	17 nm	15 nm
Max CE (cd/A)	6.5 ± 2.2	11.1 ± 2.2	7.8 ± 2.0	11.5 ± 0.8	9.3 ± 0.7	12.3 ± 1.9
Max PE (lm/W)	3.4 ± 1.2	7.1 ± 1.4	6.0 ± 1.5	9.1 ± 0.6	7.4 ± 0.6	11.0 ± 1.7
Max EQE (%)	2.1 ± 0.5	3.4 ± 0.7	2.4 ± 0.6	3.5 ± 0.2	2.8 ± 0.2	3.7 ± 0.6
Max Luminance (cd/m^2)	3033 ± 105	3296 ± 240	2787 ± 192	2436 ± 214	2566 ± 157	2254 ± 250
V$_{ON}$ @ 1cd/m^2 (V)	5 ± 0.5	4 ± 0.5	4 ± 0.5	3.5 ± 0.5	3.5 ± 0.5	3.5 ± 0.5

6.2.1.2 DCz-DBTO2:TAPC Ratio

The same device structure was used to optimise the ratio between the two exciplex forming molecules. To ensure consistency in the processing the EML layer was fixed at 20 nm since this thickness gave the second highest CE and EQE value with the smallest standard deviation (Table 6.1). The ratio between DCz-DBTO2 and TAPC has then been variated from 10:90 to 50:50 wt%, with the results summarised in Table 6.2.

Figure 6.3a shows that the DCz-DBTO2:TAPC ratio has no effect on the J-V characteristics of the devices passing from 20:80 wt% to 50:50 wt% ratio. Only the 10:90 wt% ratio shows a slightly lower current, likely due to the reduced ability of DCz-DBTO2 to conduct electrons from the TPBi into the EML and is in agreement with what was shown by Jankus et al[1]. However, Figure 6.3b shows that the 10:90 ratio achieves the highest maximum brightness having only 10 wt% of DCz-DBTO2. It is interesting also that the maximum brightness monotonically diminishes with the increasing concentration of DCz-DBTO2 in the EML. This is attributed to an increased leakage of electrons through the DCz-DBTO2, since no electron blocking layer (EBL) is present between the PEDOT:PSS layer and the EML in the OLED stack (Figure 6.1a).

In terms of efficiency the highest values are surprisingly achieved for the two extreme ratios, 10:90 and 50:50 (Table 6.2). On the other hand, as shown in Figure 6.3c and d, the devices with 50:50 wt% showed their efficiency peak at very low current density and luminance and the worst roll-off. The other ratios instead show the maximum efficiency at values around 100 cd/m^2, which represents the nominal value for display application. This behaviour can be

explained by considering that increasing the DCz-DBTO2 loading moves the recombination zone towards the HIL, balancing the charges at lower current density values than for the ratios where less DCz-DBTO2 is present.
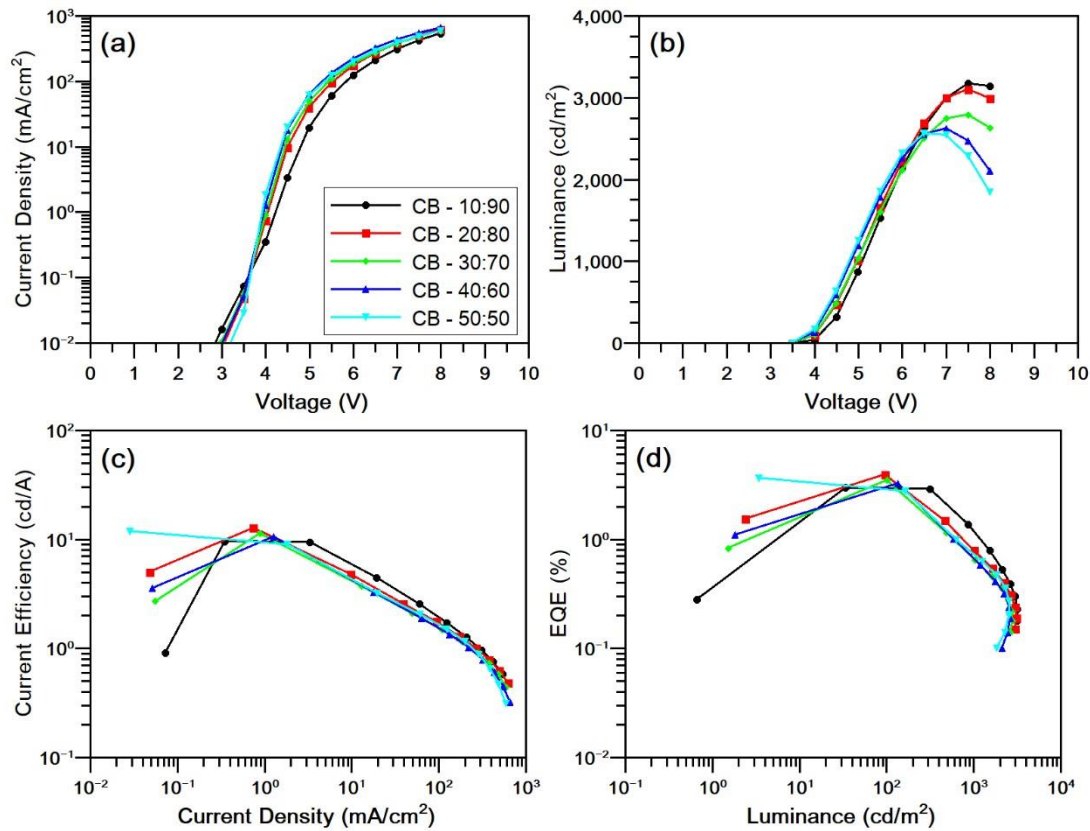
Figure 6.3 Device characteristics for structure ITO|PEDOT:PSS (40 nm)| DCz-DBTO2:TAPC 10:90-20:80-30:70-40:60-50:50 (20 nm)|TPBi (40 nm)|LiF (1 nm)|Al (100 nm) deposited from chlorobenzene. (a) Current density vs driving voltage. (b) Luminance vs driving voltage. (c) Current efficiency vs current density. (d) Power efficiency vs Luminance.

Table 6.2 Summary of results obtained for OLEDs produced with the structure ITO|PEDOT:PSS (40 nm)|DCz-DBTO2:TAPC 10:90-20:80-30:70-40:60-50:50 (60 nm)|TPBi (40 nm)|LiF (1 nm)|Al (100 nm) deposited from chlorobenzene.

	10:90	20:80	30:70	40:60	50:50
Max CE (cd/A)	14.2 ± 3.4	11.6 ± 1.2	13.0 ± 2.6	11.7 ± 1.0	14.1 ± 2.5
Max PE (lm/W)	11.2 ± 2.7	9.1 ± 0.9	10.2 ± 2.0	9.2 ± 0.8	12.7 ± 2.2
Max EQE (%)	4.3 ± 1.0	3.5 ± 0.4	3.9 ± 0.8	3.5 ± 0.3	4.2 ± 0.8
Max Luminance (cd/m^2)	3200 ± 165	2876 ± 200	2786 ± 146	2583 ± 126	2449 ± 139
V_{ON} @ 1cd/m^2 (V)	3.5 ± 0.5	3.5 ± 0.5	3.5 ± 0.5	3.5 ± 0.5	3.5 ± 0.5

6.2.2 EML processed from Chloroform

Since the efficiency was not comparable to vacuum deposited devices (EQE > 10%) when processing from CB (EQE < 5%) CF was exploited for its better wettability and very low surface tension (32.2 mN/m for CB and 26.0 mN/m for for CF). This solvent properties allow the film to solidify onto the substrate much faster than CB leading to better film quality. [17]

6.2.2.1 Thickness

As previously shown for the CB devices, the influence of the EML thickness has been studied for EMLs spin cast from CF. Figure 6.4 shows that increasing the EML thickness increases monotonically the resistivity of the device. The devices with a 50 nm EML showed the highest CE, PE and EQE maximum values, 17.3 ± 2.7 cd/A, 10.9 ± 1.7 lm/W and 5.2 ± 0.8 % respectively. The highest average maximum brightness is 3,982 ± 312 cd/m^2 and was achieved for the devices with the EML 60 nm thickness. When comparing devices produced with similar EML, (Table 6.1 and Table 6.3) higher maximum brightness and efficiencies are consistently obtained from devices where CF was used to deposit the EML. This discrepancy can be explained considering the reduced drying time achieved when spin casting the devices using the more volatile CF solutions. The solution dries on the substrate in less than 1 second, minimising the π-π stacking of the carbazoles on the DCz-DBTO2 molecules[18,19].
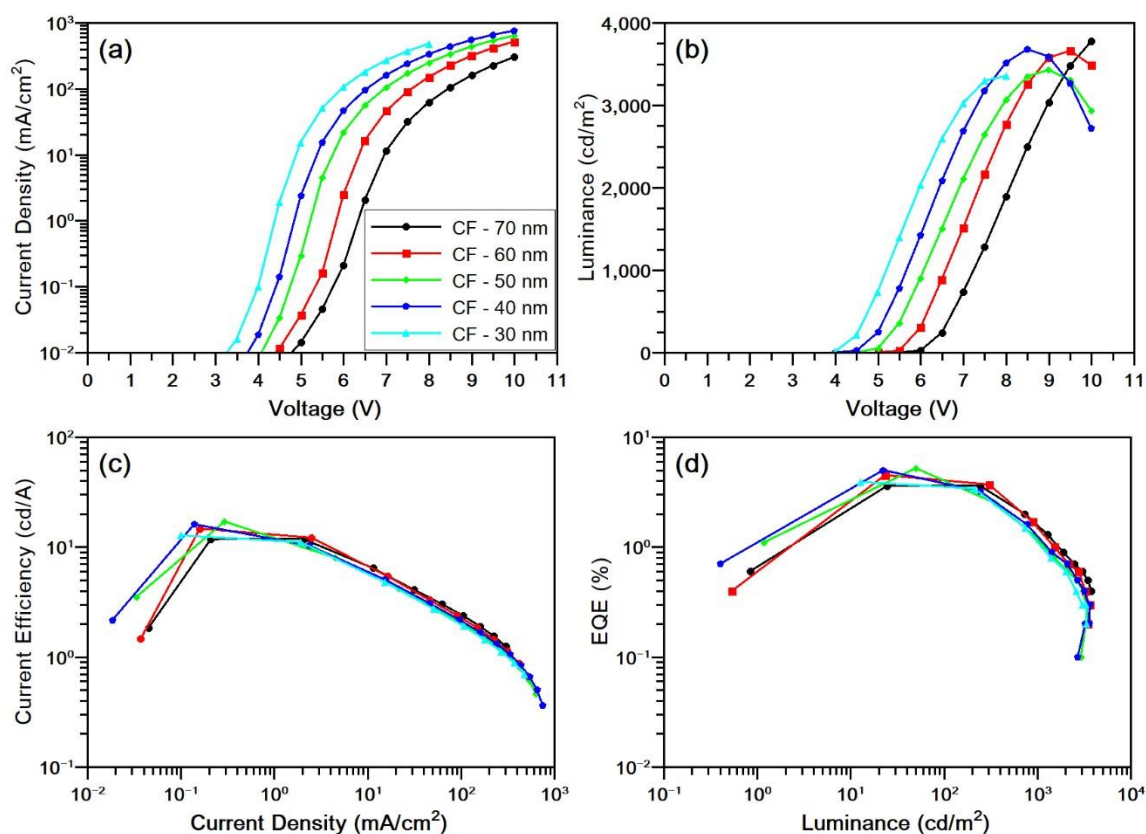
Figure 6.4 Device characteristics for ITO|PEDOT:PSS (40 nm)|DCz-DBTO2:TAPC 30:70 (30-40-50-60-70 nm)|TPBi (40 nm)|LiF (1 nm)|Al (100 nm) deposited from chloroform. (a) Current density vs driving voltage. (b) Luminance vs driving voltage. (c) Current efficiency vs current density. (d) Power efficiency vs Luminance.

Table 6.3 Summary of results obtained for OLEDs produced with the structure ITO|PEDOT:PSS (40 nm)|DCz-DBTO2:TAPC 30:70 (30-70 nm)|TPBi (40 nm)|LiF (1 nm)|Al (100 nm) deposited from chloroform.

	70 nm	**60 nm**	**50 nm**	**40 nm**	**30 nm**
Max CE (cd/A)	12.9 ± 2.1	14.1 ± 2.3	17.3 ± 2.7	14.7 ± 3.2	13.0 ± 2.7
Max PE (lm/W)	6.6 ± 1.2	7.6 ± 1.4	10.9 ± 1.7	10.2 ± 2.2	9.8 ± 2.4
Max EQE (%)	3.9 ± 0.6	4.2 ± 0.7	5.2 ± 0.8	5.1 ± 0.8	4.0 ± 0.8
Max Luminance (cd/m^2)	$3{,}533 \pm 593$	$3{,}982 \pm 312$	$3{,}816 \pm 315$	$3{,}454 \pm 280$	$3{,}272 \pm 216$
V$_{ON}$ @ 1cd/m^2 (V)	5.5 ± 0.5	5.5 ± 0.5	4.5 ± 0.5	4.0 ± 0.5	4.0 ± 0.5

6.2.2.2 DCz-DBTO2:TAPC Ratio

In order to get the highest possible film quality for a second ratio study the spin speed was set at 6000 rpm and use 20 mg/ml CF solution which deposited a 60 nm DCz-DBTO2:TAPC layer. The ratio between DCz-DBTO2 and TAPC was again varied between 10:90 and 50:50 wt%.

The results show that similar results are obtained across a range of DCz-DBTO2:TAPC ratios from 20:80 to 40:60 as shown in Table 6.4.

There is no large difference in the maximum EQE values for the devices with DCz-DBTO2 content between 20-40 wt%. Even the devices with a lower DCz-DBTO2 content (10 and 20 wt%) show a mean value of the maximum EQE of 5.6 % and 6.4 %, respectively, that peaks at 10 cd/ m^2. The devices with DCz-DBTO2 content of 30 and 40 wt% show similar maximum EQEs of 6.2 % and 6.1 % respectively, obtained at 100 cd/m^2 which represents the brightness reference value for OLED display devices.

Figure 6.5a shows that the current increases with increasing DCz-DBTO2 concentration in the blend, saturating above 30 wt% DCz-DBTO2. This can be explained by considering that increasing the DCz-DBTO2 content in the device increases the contribution of the electron current. The luminance also follows a similar trend, with the maximum brightness increasing with the increasing current reaching a maximum value for the 30:70 ratio of 3061 cd/m^2. The maximum brightness decreases at 50:50 ratio, probably due to DCz-DBTO2 π-π stacking that reduces the probability of exciplex formation and thus the brightness of the device.

The slightly different behaviour observed between the ratio studies (in CF and CB) can be attributed to the different EML thicknesses deposited, which is 3 times higher for CF than in the films deposited from CB. This leads to a different optimal position of the recombination zone inside the EML.

These results can be compared to those of reported previously by Jankus et al.[1]. The optimum donor acceptor ratio found for more complex devices (featuring exciton blocking layers) was found to be 38:62, yielding devices having respectively current efficiency, power efficiency and EQE of 32.3 cd/A, 26.7 lm/W and 14%. Such EBLs are not straightforward to deposit by solution processing, as subsequent solvent depositions can dissolve previous ones. Nonetheless, for the simpler solution processed devices, without blocking layers, the performance of evaporated devices was approached when optimum charge balance is achieved. With the inclusion of blocking layers in more complex device structures, this performance can likely be improved further. However, the result clearly suggests that by achieving optimal charge balance in solution cast devices, performance levels matching evaporated devices can be achieved in exciplex based TADF devices.
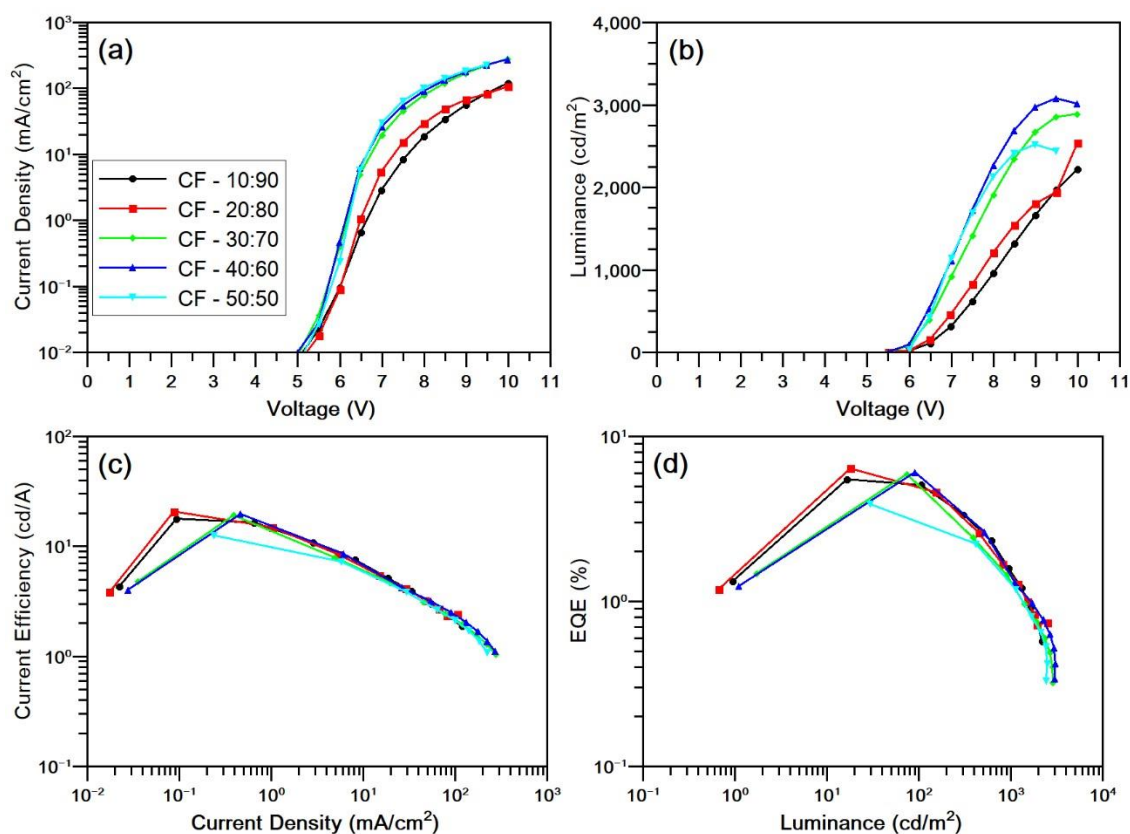
Figure 6.5 Device characteristics for structure ITO|PEDOT:PSS (40 nm)| DCz-DBTO2:TAPC 10:90-20:80-30:70-40:60-50:50 (60 nm)|TPBi (40 nm)|LiF (1 nm)|Al (100 nm) deposited from chloroform. (a) Current density vs driving voltage. (b) Luminance vs driving voltage. (c) Current efficiency vs current density. (d) Power efficiency vs Luminance.

Table 6.4 Summary of results obtained for OLEDs produced with the structure ITO|PEDOT:PSS (40 nm)|DCz-DBTO2:TAPC 10:90-20:80-30:70-40:60-50:50 (60 nm)|TPBi (40 nm)|LiF (1 nm)|Al (100 nm) deposited from chloroform.

	10:90	20:80	30:70	40:60	50:50
Max CE (cd/A)	18.5 ± 2.6	21.1 ± 7.3	20.7 ± 3.8	19.5 ± 4.0	15.4 ± 4.4
Max PE (lm/W)	9.5 ± 1.2	11.0 ± 3.9	10.9 ± 2	10.2 ± 2.1	7.2 ± 2.7
Max EQE (%)	5.6 ± 0.8	6.4 ± 1.9	6.2 ± 1.4	6.1 ± 1.1	4.1 ± 1.4
Max Luminance (cd/m^2)	2210 ± 104	2821 ± 332	3061 ± 131	2998 ± 350	2528 ± 207
V_{ON} @ 1cd/m^2 (V)	6.0 ± 0.5	5.5 ± 0.5	5.5 ± 0.5	5.5 ± 0.5	5.5 ± 0.5

6.2.3 EML processed from Chlorobenzene:Chloroform solvent blend

Both optimization studies have shown that the optimal exciplex D:A ratio lies between 20:80 and 30:70, and the CF thickness optimization identified 60 nm EML as optimal as long as it

can be deposited uniformly. To further improve the deposition procedure a final study using 5 vol% of CB in CF was performed, as it has been shown in the literature that improves the film quality while still limiting the π-π stacking of the carbazoles on the DCz-DBTO2. [11,12] With this solvent blend, the thickness of the EML was once again optimised, maintaining constant the ratio between DCz-DBTO2 and TAPC at 30:70 wt%.

The results are summarised in Table 6.5 Summary of results obtained for OLEDs produced with the structure   ITO|PEDOT:PSS (40 nm)| DCz-DBTO2:TAPC 30:70 (15-21-30-60 nm)|TPBi (40 nm)|LiF (1 nm)|Al (100 nm) deposited from a 5:95 chlorobenzene:chloroform solution. These results show that the best results are obtained for an EML thickness of 60 nm as expected from the results of the CF study and since the solvent blend is formed by 95% of CF. Maximum CE and EQE of 27.5 ± 3.3 cd/A and 8.9 ± 0.6 % are achieved as well as a maximum brightness close to 5000 cd/m^2. As seen in Figure 6.6a, the devices with the EML 15 nm thick have current leakage even at low voltage probably because of pin holes formed due to the low thickness of the layer. A similar problem was also observed for the devices deposited from CB with the same EML thickness.

The resistivity of the OLEDs increases with increase of the EML thickness as expected. Curiously, the devices with the 15 nm thick EML show higher brightness than those of 21 nm. This behaviour is attributed to the current leakage present in the latter devices. In the devices with 30 and 60 nm thick EML the brightness increases monotonically with thickness, again as expected as they contain more exciplex forming material.
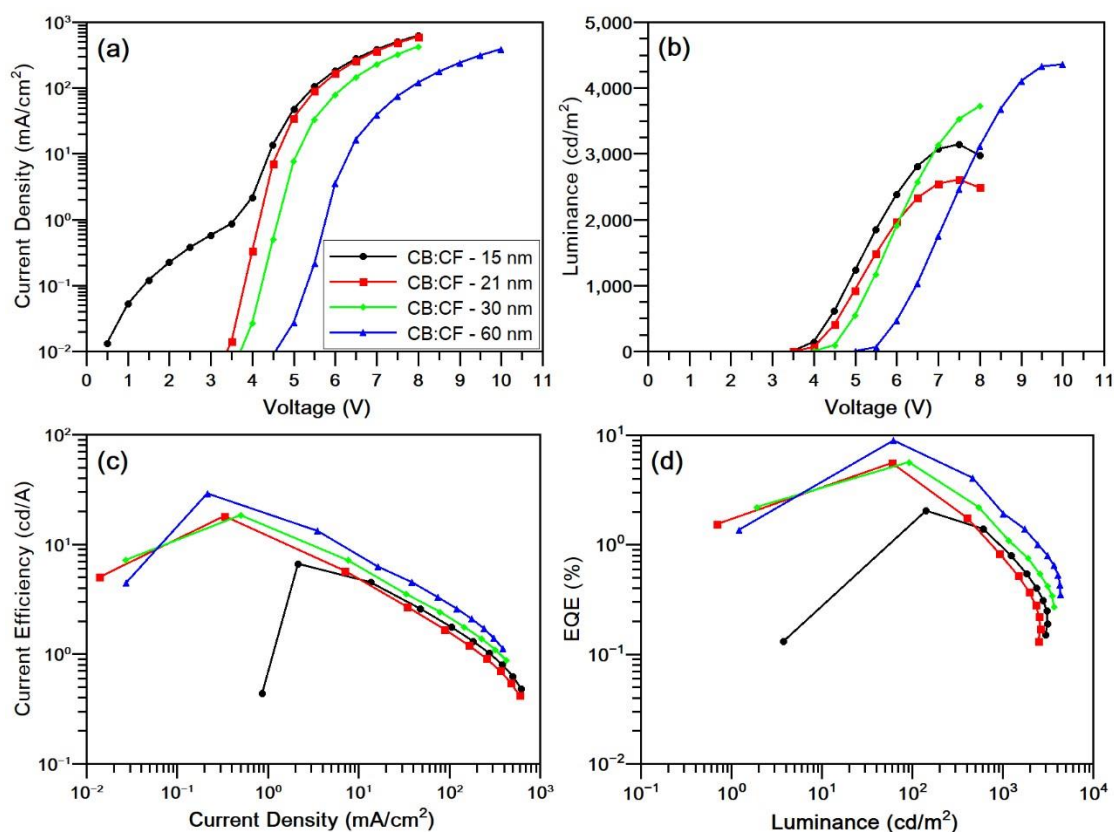
Figure 6.6 Device characteristics for ITO|PEDOT:PSS (40 nm)| DCz-DBTO2:TAPC 30:70 (15-21-30-60 nm)|TPBi (40 nm)|LiF (1 nm)|Al (100 nm) deposited from a 5:95 chlorobenzene:chloroform solution. (a) Current density vs driving voltage. (b) Luminance vs driving voltage. (c) Current efficiency vs current density. (d) Power efficiency vs Luminance.

Table 6.5 Summary of results obtained for OLEDs produced with the structure ITO|PEDOT:PSS (40 nm)| DCz-DBTO2:TAPC 30:70 (15-21-30-60 nm)|TPBi (40 nm)|LiF (1 nm)|Al (100 nm) deposited from a 5:95 chlorobenzene:chloroform solution.

	60 nm	**30 nm**	**21 nm**	**15 nm**
Max CE (cd/A)	27.5 ± 3.3	18.0 ± 1.0	20.2 ± 2.0	5.9 ± 2.8
Max PE (lm/W)	15.0 ± 1.9	12.6 ± 0.7	15.9 ± 1.2	4.6 ± 2.3
Max EQE (%)	8.9 ± 0.6	5.4 ± 0.4	6.1 ± 0.6	2.7 ± 0.7
Max Luminance (cd/m^2)	4679 ± 304	3657 ± 187	2992 ± 280	3020 ± 142
V_{ON} @ 1cd/m^2 (V)	5.5 ± 0.5	4.0 ± 0.5	3.5 ± 0.5	3.5 ± 0.5

6.3 <u>Conclusion</u>

This chapter successfully demonstrates the feasibility of solution processing of TADF exciplexes as emissive layers in OLEDs using the DCz-DBTO2:TAPC TADF exciplex as EML. The effect on the performance of the devices with the variation of the EML thickness and DCz-DBTO2:TAPC ratio has been systematically studied for devices prepared from CB, CF and 5:95 vol% blend of CB:CF. With the solvent blend, comparable results to those obtained by evaporation deposition by Jankus et al [1] has been achieved in terms of brightness, current efficiency, power efficiency and EQE. The best result obtained in this work is 27.5 ± 3.3 cd/A with a maximum brightness if 4679 ± 304 cd/m^2 and EQE of $8.9 \pm 0.6\%$, at the same DCz-DBTO2:TAPC ratio of 30:70. This result can confidently be improved through further optimization of the device stack by introducing electron and hole blocking layers for better confinement of carriers within the exciplex for example. Moreover, an in-depth morphological study is needed on these films to understand if the increasing in performance is really due to a better homogeneity of the film or if the surface roughness is playing an important role as well. These results nonetheless are of fundamental importance because they demonstrate the suitability of TADF exciplexes for high throughput roll to roll fabrication techniques that may dramatically lower the industrial fabrication costs.

6.4 <u>References</u>

(1)   Jankus, V.; Data, P.; Graves, D.; McGuinness, C.; Santos, J.; Bryce, M. R.; Dias, F. B.; Monkman, A. P. Highly Efficient TADF OLEDs: How the Emitter-Host Interaction Controls Both the Excited State Species and Electrical Properties of the Devices to Achieve near 100% Triplet Harvesting and High Efficiency. *Adv. Funct. Mater.* **2014**, *24* (39), 6178–6186. https://doi.org/10.1002/adfm.201400948.

(2)   Krebs, F. C.; Søndergaard, R. R.; Markus, H. Roll-to-Roll Fabrication of Large Area Functional Organic Materials. **2013**, 16–34. https://doi.org/10.1002/polb.23192.

(3)   Lee, C. W.; Lee, J. Y. High Quantum Efficiency in Solution and Vacuum Processed Blue Phosphorescent Organic Light Emitting Diodes Using a Novel Benzofuropyridine-Based Bipolar Host Material. *Adv. Mater.* **2013**, *25*, 596–600. https://doi.org/10.1002/adma.201203180.

(4)   Lin, W.; Huang, W.; Huang, M.; Fan, C.; Lin, H.-W.; Chen, L.-Y.; Liu, J.-S.; Chao, T.-C.; Tseng, M.-R. A Bipolar Host Containing Carbazole/Dibenzothiophene for Efficient Solution-Processed Blue and White Phosphorescent OLEDs. *J. Mater. Chem. C* **2013**, *1*, 6835–6841. https://doi.org/10.1039/c3tc31357c.

(5)   Kim, Y. H.; Wolf, C.; Cho, H.; Jeong, S. H.; Lee, T. W. Highly Efficient, Simplified, Solution-Processed Thermally Activated Delayed-Fluorescence Organic Light-Emitting Diodes. *Adv. Mater.* **2016**, *28* (4), 734–741. https://doi.org/10.1002/adma.201504490.

(6)   Li, Y.; Xie, G.; Gong, S.; Wu, K.; Yang, C. Dendronized Delayed Fluorescence Emitters for Non-Doped, Solution-Processed Organic Light-Emitting Diodes with High Efficiency and Low Efficiency Roll-off Simultaneously: Two Parallel Emissive Channels. *Chem. Sci.* **2016**, *7* (8), 5441–5447. https://doi.org/10.1039/C6SC00943C.

(7)   Zhang, Y.; Wang, B.; Yuan, Y.; Hu, Y.; Jiang, Z.; Liao, L. Solution-Processed Thermally Activated Delayed Fluorescence Exciplex Hosts for Highly Efficient Blue Organic Light-Emitting Diodes. *Adv. Opt. Mater.* **2017**, *5*, 1700012. https://doi.org/10.1002/adom.201700012.

(8)   Han, T.-H.; Choi, M.; Jeon, C.; Kim, Y.; Kwon, S.; Lee, T. Ultrahigh-Efficiency Solution-Processed Simplified Small-Molecule Organic Light-Emitting Diodes Using Universal Host Materials. *Sci. Adv.* **2016**, *2* (October), e1601428.

(9)   Duan, L.; Hou, L.; Lee, T.-W.; Qiao, J.; Zhang, D.; Dong, G.; Wang, L.; Qiu, Y. Solution Processable Small Molecules for Organic Light-Emitting Diodes. *J. Mater. Chem.* **2010**, *20* (31), 6392–6407. https://doi.org/10.1039/b926348a.

(10)   Huang, T.; Jiang, W.; Duan, L. Recent Progress in Solution Processable TADF Materials for Organic Light-Emitting Diodes. *J. Mater. Chem. C* **2018**, *6*, 5577. https://doi.org/10.1039/c8tc01139g.

(11)   Zhang, B. F.; Jespersen, K. G.; Björström, C.; Svensson, M.; Andersson, M. R.; Sundström, V.; Magnusson, K.; Moons, E.; Yartsev, A.; Inganäs, O. Influence of Solvent Mixing on the Morphology and Performance of Solar Cells Based on Polyfluorene Copolymer / Fullerene Blends. *Adv. Funct. Mater.* **2006**, *16*, 667–674. https://doi.org/10.1002/adfm.200500339.

(12)   Ye, T.; Shao, S.; Chen, J.; Wang, L.; Ma, D. Efficient Phosphorescent Polymer Yellow-Light-Emitting Diodes Based on Solution-Processed Small Molecular Electron Transporting Layer. *ACS Appl. Mater. Interfaces* **2011**, *3*, 410–416. https://doi.org/10.1021/am1010018.

(13)   Norrman, K.; Ghanbari-Siahkali, A.; Larsen, N. B. Studies of Spin-Coated Polymer Films. *Annu. Reports Sect. "C"* **2005**, *101*, 174–201. https://doi.org/10.1039/b408857n.

(14)   Choi, D.; Ahn, B.; Kim, S. H.; Hong, K.; Ree, M.; Park, C. E. High-Performance Triisopropylsilylethynyl Pentacene Transistors via Spin Coating with a Crystallization-Assisting Layer. *ACS Appl. Mater. Interfaces* **2011**, *4*, 117–122. https://doi.org/10.1021/am201074n.

(15)   Lee, B. T.; Noh, T.; Shin, H.; Kwon, O.; Park, J.; Choi, B.; Kim, M.; Shin, D. W.; Kim, Y. Characteristics of Solution-Processed Small-Molecule Organic Films and Light-Emitting Diodes Compared with Their Vacuum-Deposited Counterparts. *Adv. Funct. Mater.* **2009**, *19*, 1625–1630. https://doi.org/10.1002/adfm.200801045.

(16)   Kumar, Sanat, K.; Strawhecker, K. E.; Douglas, J. F.; Karim, A. The Critical Role of Solvent Evaporation on the Roughness of Spin-Cast Polymer Films. *Macromolecules* **2001**, *34*, 4669–4672. https://doi.org/10.1021/ma001440d.

(17)   Chen, B. T. Investigation of the Solvent-Evaporation Effect on Spin Coating of Thin Films. *Polym. Eng. Sci.* **1983**, *23*, 399–403.

(18)   Xue, P.; Wang, P.; Chen, P.; Yao, B.; Gong, P.; Sun, J.; Zhang, Z.; Lu, R. Chemical Science Bright Persistent Luminescence from Pure Organic Molecules through a Moderate Intermolecular Heavy Atom e Ff Ect †. *Chem. Sci.* **2017**, *8*, 6060–6065. https://doi.org/10.1039/C5SC03739E.

(19)   Yin, C.; Ye, S.; Zhao, J.; Yi, M.; Xie, L.; Lin, Z.; Chang, Y.; Liu, F.; Xu, H.; Shi, N.; et al. Hindrance-Functionalized π-Stacked Polymer Host Materials of the Cardo-Type Carbazole-Fluorene Hybrid for Solution-Processable Blue Electrophosphorescent Devices. *Macromolecules* **2011**, *44*, 4589–4595. https://doi.org/10.1021/ma200624u.

Chapter 7:

The Effects of Exciton Localisation Induced by an Interfacial TADF Exciplex on PhOLED Efficiency and Stability

In this chapter, a TADF exciplex formed between the EML host 26DCzPPy and the ETL PO-T2T is employed at the interface between the EML and the ETL to improve the stability and efficiency of a phosphorescence OLED based on Ir(dmpq)$_2$acac. We show that the presence of the TADF exciplex at the EML-ETL interface induces an efficient localisation of the recombination zone which is confined within the 5 nm thick EML. Furthermore, the TADF exciplex allows harvesting of the holes and electrons that accumulate at the EML-ETL interface, transferring the resultant excited state energy to the phosphorescent emitter through Förster and/or Dexter energy transfer. This approach effectively improves the LT90 of devices from <1 min to 6 h by limiting recombination processes outside of the 5 nm EML.

7.1 <u>Introduction</u>

Since 2008 Kondakova et al started combining exciplexes and phosphorescent emitters showing performance enhancement[1] Later, Fukagawa et al.[2] demonstrated performance enhancement of PhOLEDs when a TADF host was used, many other groups also have published similar results using either TADF small molecules or exciplexes as hosts. These improvements in performance are explained by the effective Förster resonant energy transfer (FRET) to the emitter that these systems can provide, jointly with the 100% triplet harvesting via the TADF host[3–11]. Furthermore, Duan et al. [8] demonstrated that by inserting a TADF exciplex at the interface between the host and the hole transport layer (HTL) of a PhOLED, it is possible to enhance the stability and the performance of the device exploiting the energy transfer from the interfacial exciplex and the guest material.

This chapter shows the effect of using a TADF exciplex on the electron side of a PhOLED device to improve the charge balance and control the localisation of the recombination zone in the EML. In fact, the electron mobility in OLED devices is indeed commonly lower than the hole mobility, causing the holes to pile-up at the interface between emissive layer (EML) and electron transport layer (ETL). This imbalance could well be a source of device degradation thus lead to low operational lifetime. To address this problem, a TADF exciplex formed by the well-known bipolar EML host 2,6-bis[3-(9H-carbazol-9-yl)phenyl]pyridine (26DCzPPy) and the donor 2,4,6-tris[3-(diphenylphosphinyl)phenyl]-1,3,5-triazine (PO-T2T) used as ETL, was introduced to avoid the pile-up problem. All the devices were doped with bis(2-(3,5-dimethylphenyl)quinoline-C2,N')(acetylacetonato)iridium(III) (Ir(dmpq)$_2$acac) to obtain efficient FRET from the interfacial exciplex due to the extensive overlap of the absorption spectrum of the dopant with the exciplex emission as well as yielding 100% phosphorescent emission. The molecular structure of the molecules involved in the FRET process are shown in Figure 7.1a. Furthermore, we have employed a device architecture with an unusually thin 5 nm EML, that allows us to assess the localization of the recombination zone and obtain more information about the energy transfer mechanisms between the exciplex and the dopant. We were indeed able to observe when exciton localisation was lost simply by observing the changes in the electroluminescence spectrum, and by relating those changes to the variations in the stability of the device with the different device structures.

A maximum EQE of 28.6% at 100 cd/m^2 as well as a very low roll-off with an efficiency of 25.2 % at 1000 cd/m^2 was achieved using this architecture. Further device structures were used

introducing a 1nm spacer layer between the EML and the exciplex, and by substituting PO-T2T alternatively with 2,2',2''-(1,3,5-benzinetriyl)-tris(1-phenyl-1-H-benzimidazole) (TPBi) and 2,9-dimethyl-4,7-diphenyl-1,10-phenanthroline (BCP) to assess the role of energy transfer to the Ir(dmpq)$_2$acac. All the results highlight the importance of the energy transfer process from the interfacial exciplex to the phosphorescent guest in the enhancement of both performances and stability of the devices.

7.2 <u>Results and Discussion</u>

7.2.1 Photophysical characterization

Although the 26DCzPPy:PO-T2T exciplex has been previously reported [12] there has been little explanation to its photophysics. First of all, the exciplex time resolved PL decay at room temperature (Figure 7.1c) shows a biexponential characteristic with PF decay time ($\tau_{PF} = 14.4 \pm 0.4$ ns) and DF decay time ($\tau_{DF} = 3.0 \pm 0.2$ μs). From the integral of the PF and DF regions of the PL decay, the ratio between the DF and PF contribution to the emission has been calculated (DF/PF ≈ 2.5) while the rISC rate is 1.1 x 10^6 s^{-1} calculated accordingly to the procedure reported by Dias et al.[13]. The singlet-triplet gap is estimated to be $\Delta E_{ST} = 0.09$ eV.
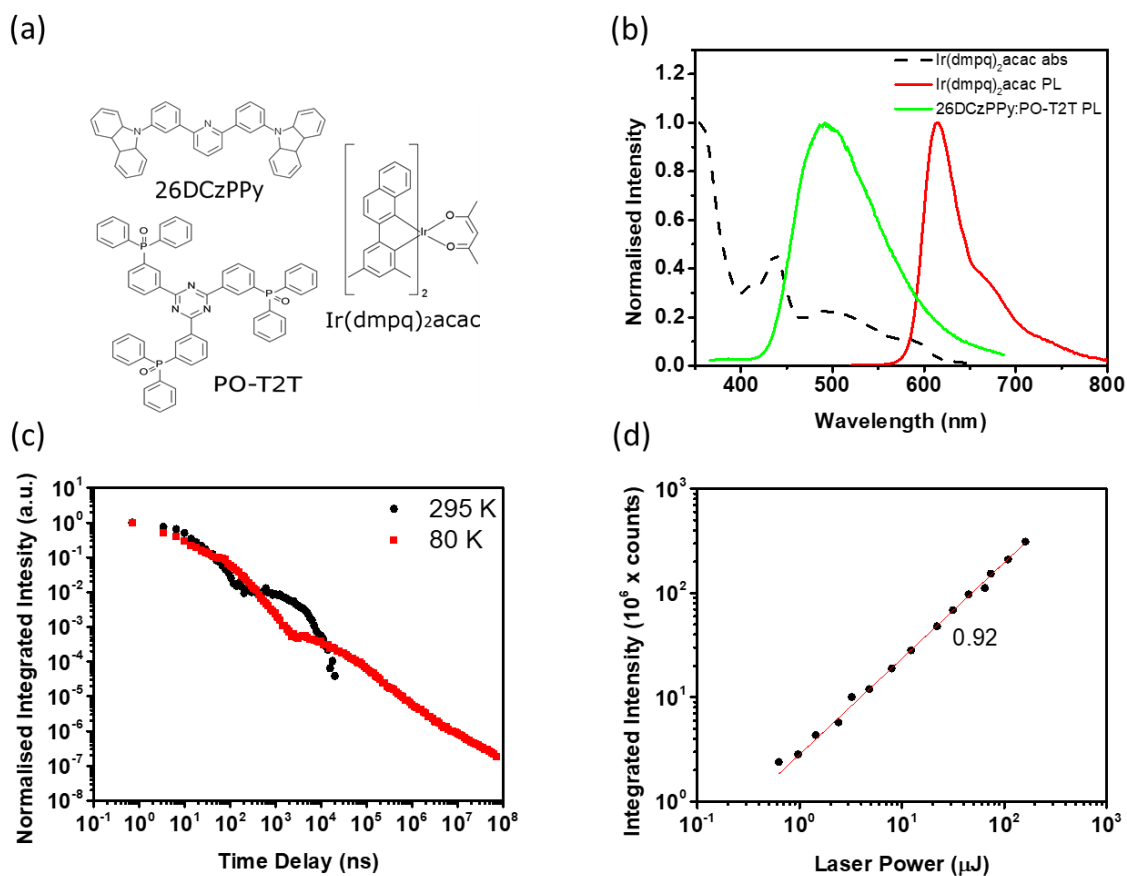
Figure 7.1 (a) Molecular structure of the exciplex forming donor (26DCzPPy), acceptor (PO-T2T) and phosphorescent emitter (Ir(dmpq)$_2$acac) used in this study. **(b)** The normalised absorption and PL spectra of Ir(dmpq)$_2$acac and 26DCzPPy:PO-T2T exciplex. **(c)** Time resolved fluorescence decay curves of the exciplex blend at 80 K and 295 K. **(d)** Integrated area as a function of the laser excitation (355 nm) of 26DCzPPy:PO-T2T exciplex blend.

The delayed fluorescence changes its intensity and kinetics with temperature as depicted in the exciplex photoluminescence decays between 295 and 80 K (Figure 7.1c) which confirms the thermally-activated nature of the DF. Furthermore, the delayed fluorescence component shows a laser fluence dependency with 0.92 exponent (Figure 7.1d). This being close to 1, indicates a single exciton process which, along with the strongly temperature dependent delayed fluorescence (Figure 7.1c) indicates that the TADF mechanism is the main triplet harvesting mechanism involved (i.e. excluding TTA).

Interestingly, the prompt and delayed fluorescence spectra of the exciplex blend are distinct (Figure 7.2). The early emission spectrum at 0.7 ns delay shows emission maximum at ≈ 460 nm while at later time delays there is a gradual redshift observed and the delayed fluorescence shows a maximum at ≈ 490 nm the same as the steady state PL spectrum in Figure 7.1b. This behaviour is consistent with a distribution of D-A orientations and distances with different

energies[14]. The TADF emission clearly dominates at 295 K, but at 80 K the weak delayed fluorescence (1-100 μs delay), is accompanied by phosphorescence emission (> 10 ms delay) of 26DCzPPy (Figure 7.2)[15]. This observation suggests that the local triplet state of 26DCzPPy is coupled with the exciplex CT state and the coupling of ^{1}CT and ^{3}CT with the ^{3}LE gives rise to TADF in this system. Figure 7.1b shows the extensive overlap between the absorption of Ir(dmpq)$_2$acac and the 26DCzPPy:PO-T2T PL, which is necessary to provide efficient FRET between the exciplex and the phosphorescent emitter.
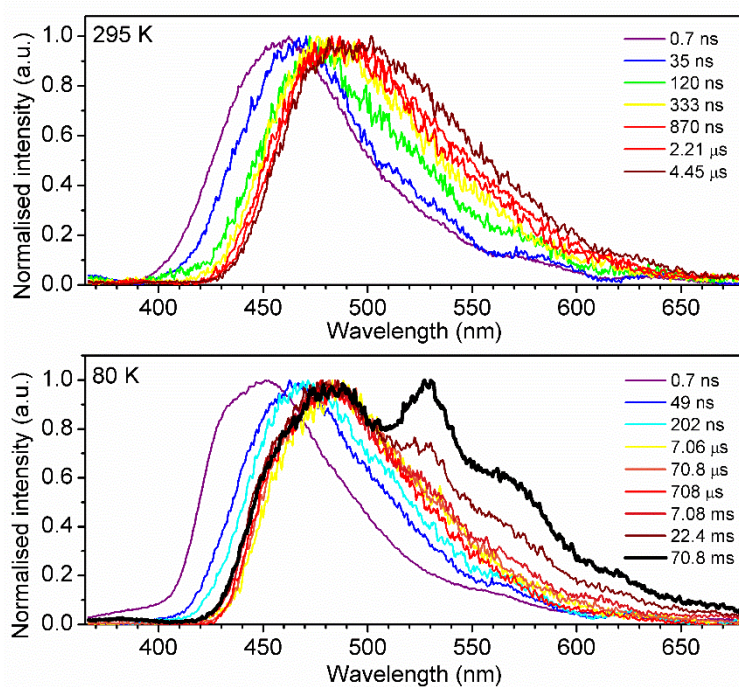
Figure 7.2 Time-resolved photoluminescence spectra of the 26DCzPPy:PO-T2T exciplex blend at 295 K and 80 K. The double peak arising at 22.4 and 70.8 ms delay time at 80 K are assigned to the phosphorescence of 26DCzPPy.

7.2.2 Device Performance

Initially, we optimised the concentration of the dopant by implementing a device structure of NPB (40nm)|TCTA (10 nm)|26DCzPPy (5 nm)|1-4-10 wt% of Ir(dmpq)$_2$acac in 26DCzPPy (5 nm)|PO-T2T (50 nm)|LiF (1nm)|Al (100 nm) which are respectively labelled as Dev1, Dev2 and Dev3. The 5 nm buffer layer of 26DCzPPy was used to avoid direct injection of holes from the TCTA layer into Ir(dmpq)$_2$acac, This choice maximises the charge recombination at the

exciplex interface and therefore assists the energy transfer process from the interfacial exciplex to the guest phosphor, allowing this process to dominate the device physics. The slight redshift observed with the increased doping concentration in Figure 7.3c is due to reabsorption of the emitter emission. In fact, the emission and the absorption spectrum overlap in the region between 550 and 650 nm showing a rather small Stokes shift as visible in Figure 7.1b.

In Figure 7.3a it can be seen that the current density of the devices increases with the concentration of Ir(dmpq)$_2$acac in the EML. This is a typical behavior in PhOLEDs due to charge trapping on the Iridium complexes since they act as deep traps for both holes and electrons[16]. The energy difference between the HOMO and LUMO levels of 26DCzPPy and Ir(dmpq)$_2$acac is 0.61 eV and 0.74 eV respectively[5,17,18]. In terms of efficiency, we find the device loaded with 4 wt% Ir(dmpq)$_2$acac (Dev2) to exhibit the highest EQE at both reference brightness (100 cd/m^2 and 1000 cd/m^2) of 28.6 % and 25.2 % respectively. We attribute this small roll-off to triplet-polaron quenching[19]. In general, all three devices show an efficiency roll-off of only 10 % between 100 cd/m^2 and 1000 cd/m^2. Interestingly the device with 1 wt% Ir(dmpq)$_2$acac (Dev1) shows similar performances to the device with 10 wt% Ir(dmpq)$_2$acac (Dev3) up to the brightness of 2000 cd/m^2. Afterwards the efficiency drops significantly faster compared to the more heavily doped devices. This can be explained comparing the electroluminescence (EL) spectra shown in Figure 7.3c and Figure 7.3d. The figures show the EL spectra at the same brightness of 1,000 cd/m^2 and 10,000 cd/m^2 respectively. No exciplex emission is visible in any of the devices at 1,000 cd/m^2. However, in the spectra collected at brightness of 10,000 cd/m^2 (Figure 7.3d) Dev1 shows a strong exciplex emission at 471 nm (inset of Figure 7.3d) which is not visible in either Dev2 or Dev3. This observation confirms that the exciplex is indeed populated and that, even with a doping concentration as low as 1%, it can be fully harvested via FRET at moderately low current density. The abrupt EQE roll off observed for Dev1 at high current density is therefore assigned as a consequence of saturating the energy transfer process, which leads to the exciplex peak to arise in the EL spectrum. The exciplex emission observed in the EL spectrum is blue shifted by $\approx$ 20 nm from the PL spectrum of Figure 7.2b due to the interfacial geometry of the exciplex under the influence of the electric field in the OLED structure[20]. It should also be considered that the EML thickness is only 5 nm which is within the typical triplet exciton diffusion length, making Dexter energy transfer (DET) from the 26DCzPPy-PO-T2T interface a non-negligible effect in this particular device structure especially with the increment of doping concertation [21].
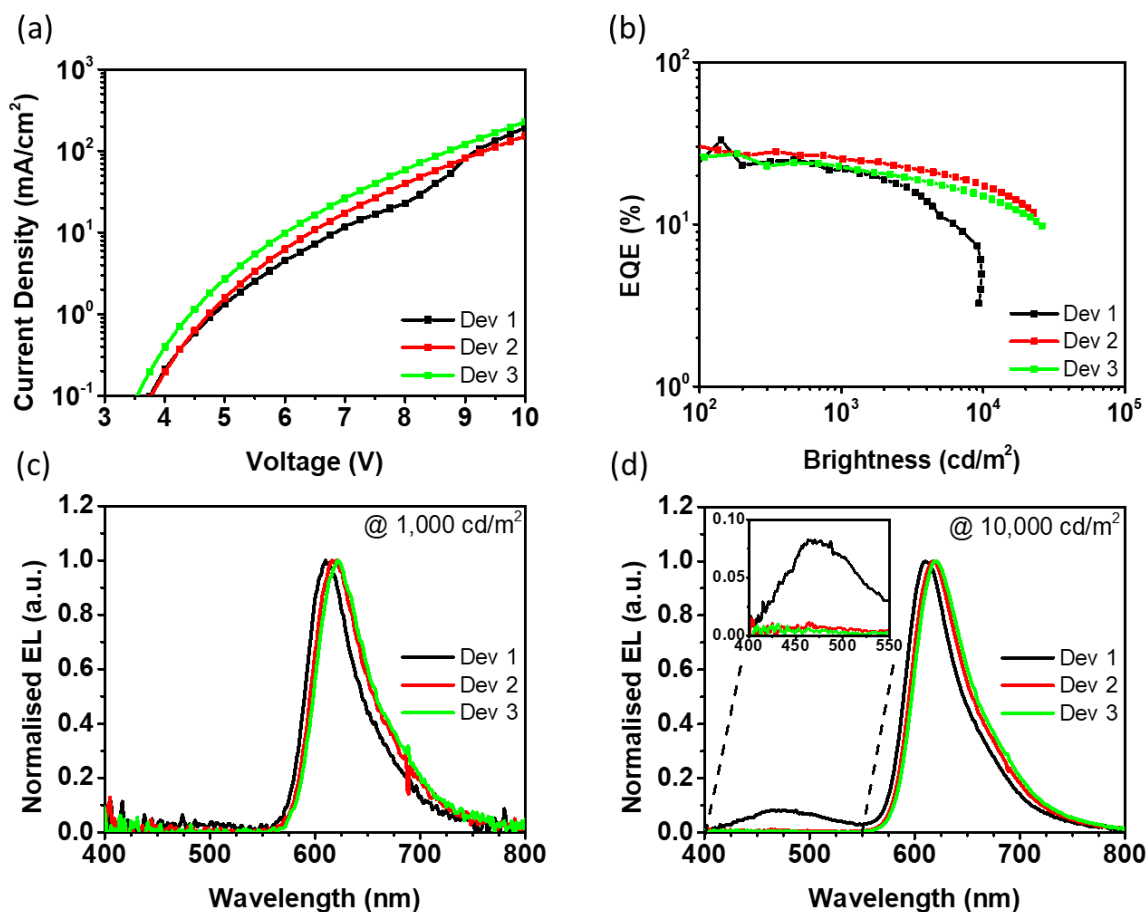
Figure 7.3 (a) JV and (b) EQE curves of the PhOLEDs with different doping level of Ir(dmpq)2acac. Normalised EL spectra of the PhOLEDs at constant brightness of (c) 1000 cd/m^2 and (d) 10000 cd/m^2.

Table 7.1 Exciplex photophysical properties at different dilutions in UGH-3 or DPEPO

wt% Ir(dmpq)2acac	@ 100 cd/m2			@ 1000 cd/m2			
	V	cd/A	EQE	V	cd/A	EQE	LT90 (h)
Dev1 - 1 wt%	4.3	29.8 ± 9.1	24.5 ± 1.2	5.8	31.5 ± 0.9	21.9 ± 1.1	0.02
Dev2 - 4 wt%	4.3	36.6 ± 6.6	28.6 ± 1.4	5.5	30.7 ± 0.8	25.2 ± 1.3	1
Dev3 - 10 wt%	4.0	27.3 ± 4.5	26.0 ± 1.3	5.3	24.6 ± 0.5	22.7 ± 1.1	6
Dev4 - 4 wt% 1 nm spacer	4.3	26.0 ± 2.7	18.4 ± 0.9	5.3	23.4 ± 0.4	18.6 ± 0.9	1
Dev5 - 4 wt% TPBi	4.3	26.1 ± 3.9	15.6 ± 0.8	5.0	26.4 ± 0.5	21.3 ± 1.1	0.13
Dev6 - 7 wt% BCP	5.5	21.4 ± 2.9	31.5 ± 1.6	7.0	15.3 ± 0.4	15.3 ± 0.8	> 0.01

To separate the contributions of DET and FRET to total energy transfer devices were produced with a 1 nm spacer layer introduced between the EML and the PO-T2T. The device structure used is NPB (40nm)|TCTA (10 nm)|26DCzPPy (5 nm)|4 wt% of Ir(dmpq)$_2$acac in 26DCzPPy (5 nm)|26DCzPPy (1 nm)|PO-T2T (50 nm)|LiF (1nm)|Al (100 nm) labelled Dev4. In Figure 7.4b the performance of Dev4 is compared to Dev2 since both possess the same structure, differentiated only by the 1 nm spacer present in Dev4. At 100 cd/m^2 the EQE drops from 28.6 % for Dev2 to 18.4 % with the spacer, as summarised in Table 7.1. Dev4 maintains a constant EQE of 18.6 up to 1000 cd/m^2 showing that the device still possesses a good charge balance with the turn-on voltage unaffected by the 1 nm 26DCzPPy layer. Figure 7.4c shows that at 1000 cd/m^2 no exciplex emission is visible in the EL spectrum, indicating that, all the exciplexes produced at the 26DCzPPy:PO-T2T interface are transferred via FRET to the dopant, since the DET has been greatly reduced by the spacer layer separation. On the other hand, in the inset of Figure 7.4d at a brightness of 10,000 cd/m^2, the exciplex emission is again clearly visible, at the same spectral position as observed for Dev1. The exciplex emission peaks at 471 nm indicates the incomplete energy transfer from the interfacial exciplex to the dopant, assuming that the 1 nm spacer layer does not affect the FRET efficacy but that DET must have been substantially eliminated[22]. The difference in efficiency between the devices with and without the spacer is attributed to the effective suppression of the DET contribution. Thus, the exciplex emission appears at high brightness even at 4 wt% doped EML. This indicates that the process of energy transfer from the interfacial exciplex to the dopant must be maximised to optimise the device efficiency.
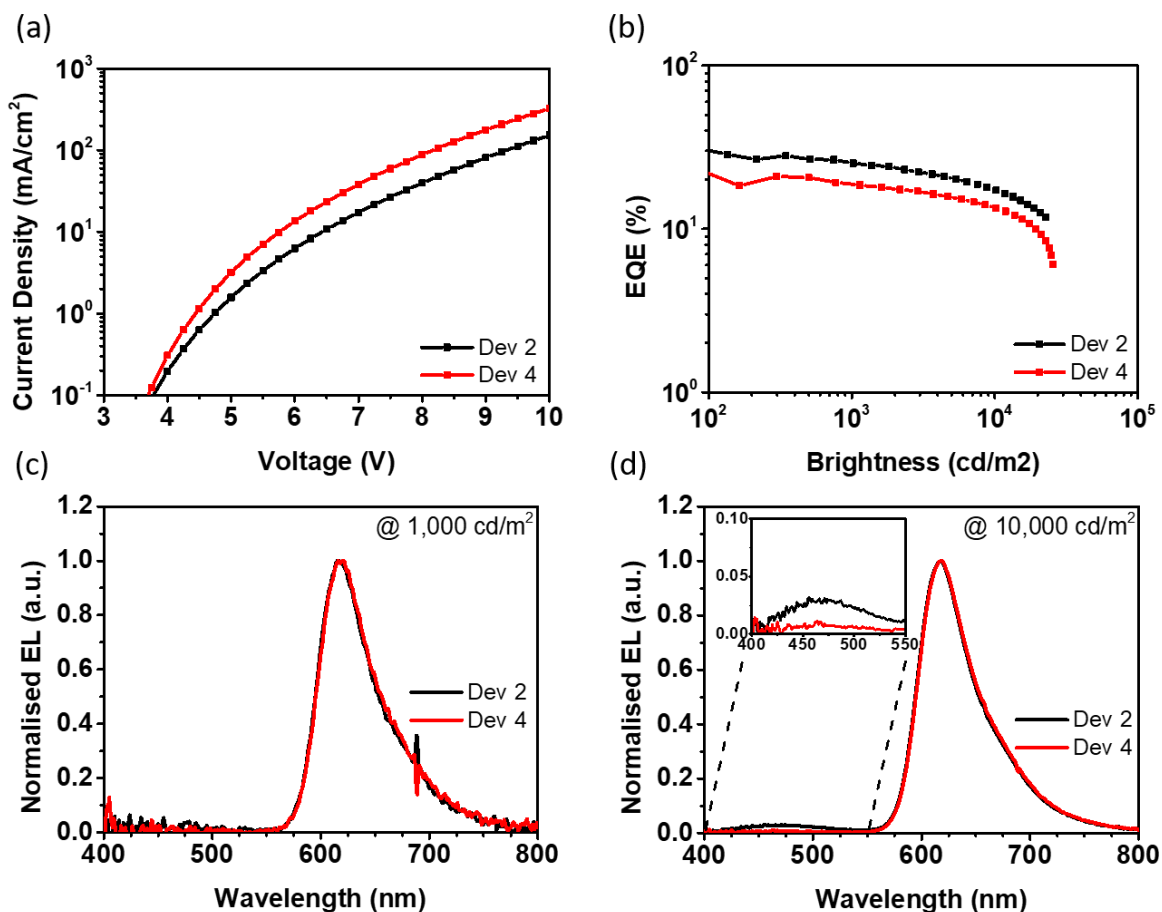
Figure 7.4 (a) JV and (b) EQE curves of the PhOLEDs with and without the 1 nm 26DCzPPy spacer layer at the EML|ETL interface. EL spectra of the PhOLEDs at constant brightness of (c) 1000 cd/m^2 and (d) 10000 cd/m^2.

PO-T2T was then replaced with two standard electron transport materials, TPBi and BCP. TPBi was chosen due to the very good LUMO alignment with 26DCzPPy, with a $\Delta E_{LUMO} = 0.14$ eV [23,24]. BCP, on the other hand, was chosen because it has the very similar LUMO energy to PO-T2T [25,26]. Despite having the same LUMO level as PO-T2T, BCP does not produce exciplex emission when blended with 26DCzPPy and neither does TPBi, Figure 7.5a and Figure 7.5b.
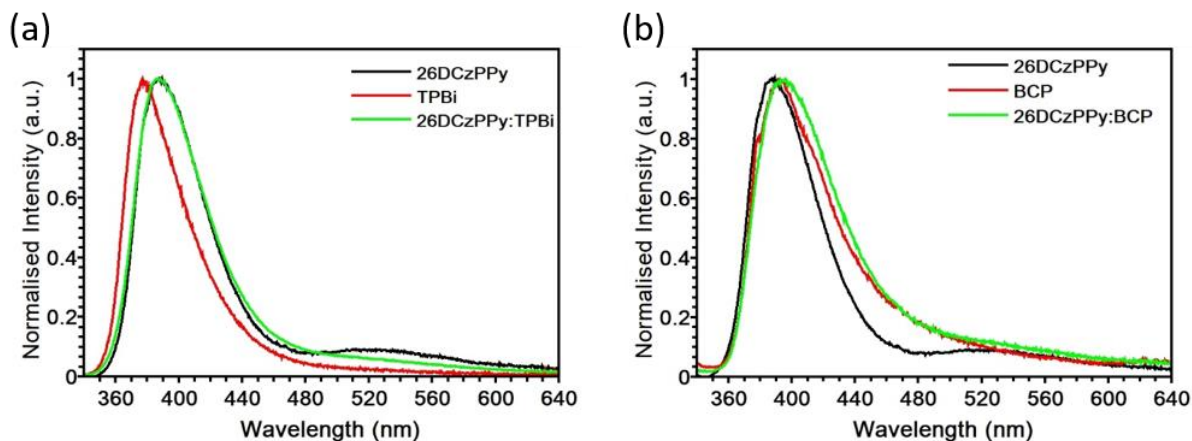
Figure 7.5 (a) Photoluminescence spectra of 26DCzPPy, TPBi and 26DCzPPy:TPBi blend. (b) Photoluminescence spectra of 26DCzPPy, BCP and 26DCzPPy:BCP blend.

Figure 7.6 shows the results for the PhOLEDs with the structures; NPB (40nm)|TCTA (10 nm)|26DCzPPy (5 nm)|4 wt% of Ir(dmpq)$_2$acac in 26DCzPPy (5 nm)|TPBi (50 nm)|LiF (1nm)|Al (100 nm) and NPB (40nm)|TCTA (10 nm)|26DCzPPy (5 nm)| 7 wt% of Ir(dmpq)$_2$acac in 26DCzPPy (5 nm)| BCP (50 nm)|LiF (1nm)|Al (100 nm) respectively labelled as Dev5 and Dev6. Dev5 shows lower performance in respect to the exciplex enhanced devices, with good roll off and EQE of 21.3 % at 1000 cd/m^2, Table 7.1. The most interesting aspect is the substantial difference between the EQE obtained for the same doping level of 4 wt%, at 100 cd/m^2. The device where TPBi is used (Dev5) shows a build-in of efficiency with the EQE at 100 cd/m^2 of only 15.6 % compared to 28.6 % for Dev2. The good resistance to roll-off is provided by the good energy level alignment with the bipolar host 26DCzPPy that guarantees the balance of the charges in the EML. On the other hand, the resulting performance is lower due to the absence of the energy transfer as well as a recombination zone localization effect arising from the TADF exciplex. Evidence of this is provided by comparing the EL spectra of the devices in Figure 7.6c and Figure 7.6d. At 1,000 cd/m^2 only the emission from the Ir(dmpq)$_2$acac is observable whereas at 10,000 cd/m^2 the emission from the adjacent layer of 26DCzPPy is clearly visible, demonstrating the broadening of the recombination zone with the increasing voltage in the absence of the TADF exciplex at the host-ETL interface.

The same mechanism occurs when BCP is used to replace PO-T2T. In this last case, due to the large electron injection barrier alongside the low conductivity of BCP itself [27] the operational voltage increases substantially, as visible in Figure 7.6a, increasing from 4.3 V with the

exciplex to 5.5 V without, at 100 cd/m^2. The difference becomes even bigger at brightness of 1000 cd/m^2 passing from 5.5 V with the exciplex to 7 V with the BCP layer.

On the other hand, when BCP is used, very high efficiency of 31.5% is found at 100 cd/m^2, out performing all the other devices assessed in this work (Figure 7.6b). This is considered to be the effect of the device structure used. At low voltage the electrons pile up at the ETL-EML interface as they cannot easily overcome the injection barrier between the BCP and 26DCzPPy (0.34 eV) and are more likely to be directly injected into the Ir(dmpq)$_2$acac. Once injected into the dopant the electrons are well confined by the 5 nm 26DCzPPy undoped layer. The only possibility for recombination is then with the holes trapped by the dopant, giving rise at a very sharp emission onset at very low current and thus resulting in extremely high efficiency thanks to the high PLQY of excitons localized on the Ir(dmpq)$_2$acac[28]. At higher voltage the electrons possess enough potential energy to inject into the EML host, bypassing this initially very efficient mechanism and causing the efficiency to reduce, with the EQE halving at 1000 cd/m^2.
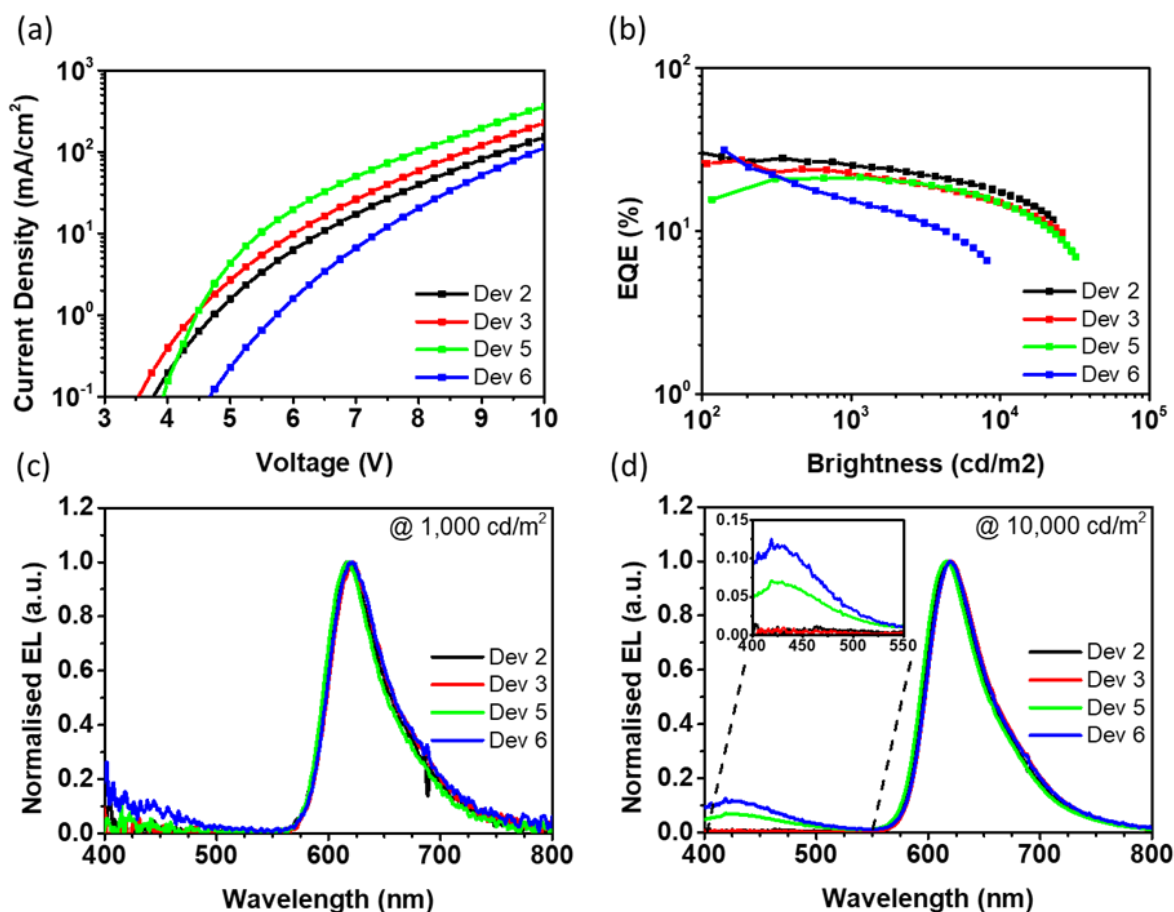
Figure 7.6 (a) JV and (b) EQE curves of the PhOLEDs with BCP and TPBi as ETL and a 1 nm spacer between the EML and PO-T2T. Normalised EL spectra of the PhOLEDs at constant brightness of (c) 1000 cd/m^2 and (d) 10000 cd/m^2.

Among the devices produced in this study, the only one showing a detectable secondary emission in the EL spectrum at 1000 cd/m^2 (Figure 7.6c) is the device with BCP as ETL (Dev6), confirming the earlier suggestion that, for this device, the electrons have enough potential energy to overcome the injection barrier into the host which moves the recombination zone towards the undoped 26DCzPPy layer. This effect is seen to increase at 10,000 cd/m^2 where both TPBi and BCP show emission from the host at ≈ 425 nm. The host emission in the EL spectrum is redshifted of 33 nm from the PL (Figure 7.5) again due to partial reabsorption by the Ir complex. The secondary emission from the host is a clear sign of the loss of confinement of charge recombination in the EML.

Finally, in Figure 7.7 the stability of the devices is compared by operating the OLEDs at constant current with an initial brightness (L$_0$) of 1000 cd/m^2. When the exciplex interface is present in the device structure, the lifetime increases monotonically with the concentration of dopant. The devices show LT90 of < 1 min for 1 wt% increasing to ≈ 1 hour at 4 wt% and ≈ 6 hours for 10 wt%. We attribute this increment to the increase of efficacy of the energy transfer process due to the presence of a greater number of dopant molecules, thus avoiding charge build up and quenching at the interface and degradation of the exciplex itself. Interestingly, the initial behaviour of the device with the 1nm spacer layer (Dev 4) shows the same LT90 as the one without the spacer layer (Dev 2). Its decay rate accelerates with LT50 of 13.5 h with the 1 nm spacer layer whereas the device without the spacers has an LT50 of 24 h. This difference highlights the role of DET in reducing charge pile-up and thus degradation at the interface. Moreover, PhOLEDs where BCP (Dev 6) and TPBi (Dev 5) were used showed LT90 of < 1 min and 8 minutes respectively. We attribute the longer LT90 of the TPBi device over the BCP one to the better confinement of the recombination zone, as shown from the EL spectra (Figure 7.6) and discussed above. The interfacial exciplex turns the piled-up charges into useful exciplexes that are transferred to the Ir(dmpq)$_2$acac through FRET and DET, reducing the degradation mechanisms associated with it. The BCP device exhibits lower stability than TPBi due to the loss of exciton confinement in the 5 nm thick EML, spreading the recombination zone to non-efficient areas of the device more prone to degradation than the high PLQY Ir doped layer, i.e. the undoped host.
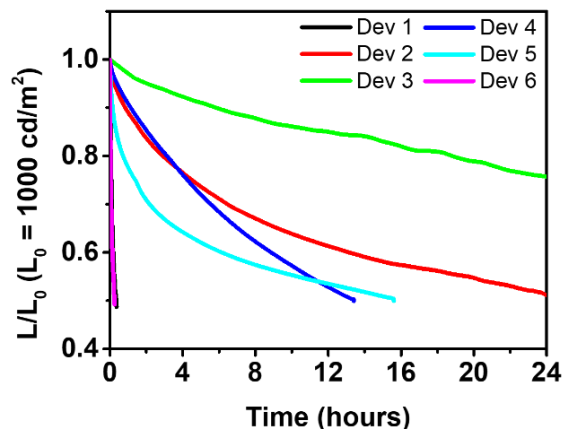
Figure 7.7 Luminance decay of the OLEDs measured at constant current. All the devices kept at the current value that corresponds to the initial luminance of $L_0 = 1000$ cd/m^2.

7.3 Conclusion

This chapter demonstrates that utilising a TADF exciplex at the interface between EML and ETL can improve the efficiency and stability of PhOLEDs. We highlight this improvement as a consequence of an extremely effective localisation of the excitons into the 5 nm EML. The interfacial exciplex not only localises the recombination zone onto the EML-ETL interface, but also harvests the holes and electrons piled-up at that interface and recycling them into useful light in the emitter. We show clearly that both DET and FRET mechanisms are responsible for the energy transfer process from the exciplex to the dopant, and that the DET process provides a very important contribution to the overall efficiency of the devices. Using the TADF exciplex interface layer on the electron side of the device greatly increases device lifetime LT90 from minutes to hours at 1000 cd/m^2. In the future, this strategy may be promising to apply to hyperfluorescent OLEDs to further improve the energy transfer mechanisms and boost the efficiency without the use of heavy metals.

7.4 <u>References</u>

(1)   Kondakova, M. E.; Pawlik, T. D.; Young, R. H.; Giesen, D. J.; Kondakov, D. Y.; Brown, C. T.; Deaton, J. C.; Lenhard, J. R.; Klubek, K. P. High-Efficiency, Low-Voltage Phosphorescent Organic Light-Emitting Diode Devices with Mixed Host. *J. Appl. Phys.* **2008**, *104*, 094501. https://doi.org/10.1063/1.3000046.

(2)   Fukagawa, H.; Shimizu, T.; Kamada, T.; Kiribayashi, Y.; Osada, Y.; Hasegawa, M.; Morii, K.; Yamamoto, T. Highly Efficient and Stable Phosphorescent Organic Light-Emitting Diodes Utilizing Reverse Intersystem Crossing of the Host Material. *Adv. Opt. Mater.* **2014**, *2*, 1070–1075. https://doi.org/10.1002/adom.201400242.

(3)   Fukagawa, H.; Shimizu, T.; Kamada, T.; Yui, S.; Hasegawa, M.; Morii, K.; Yamamoto, T. Highly Efficient and Stable Organic Light-Emitting Diodes with a Greatly Reduced Amount of Phosphorescent Emitter. *Sci. Rep.* **2015**, *5*, 9855. https://doi.org/10.1038/srep09855.

(4)   Fukagawa, H.; Shimizu, T.; Iwasaki, Y.; Yamamoto, T. Operational Lifetimes of Organic Light-Emitting Diodes Dominated by Förster Resonance Energy Transfer. *Sci. Rep.* **2017**, *7* (1), 1–8. https://doi.org/10.1038/s41598-017-02033-3.

(5)   Park, Y.-S.; Lee, S.; Kim, K.-H.; Kim, S.-Y.; Lee, J.-H.; Kim, J.-J. Exciplex-Forming Co-Host for Organic Light-Emitting Diodes with Ultimate Efficiency. *Adv. Funct. Mater.* **2013**, *23* (39), 4914–4920. https://doi.org/10.1002/adfm.201300547.

(6)   Lee, S.; Koo, H.; Kwon, O.; Jae Park, Y.; Choi, H.; Lee, K.; Ahn, B.; Min Park, Y. The Role of Charge Balance and Excited State Levels on Device Performance of Exciplex-Based Phosphorescent Organic Light Emitting Diodes. *Sci. Rep.* **2017**, *7* (1), 1–9. https://doi.org/10.1038/s41598-017-12059-2.

(7)   Duan, L.; Hou, L.; Lee, T.-W.; Qiao, J.; Zhang, D.; Dong, G.; Wang, L.; Qiu, Y. Solution Processable Small Molecules for Organic Light-Emitting Diodes. *J. Mater. Chem.* **2010**, *20* (31), 6392–6407. https://doi.org/10.1039/b926348a.

(8)   Zhang, D.; Cai, M.; Zhang, Y.; Bin, Z.; Zhang, D.; Duan, L. Simultaneous Enhancement of Efficiency and Stability of Phosphorescent OLEDs Based on Efficient Förster Energy Transfer from Interface Exciplex. *ACS Appl. Mater. Interfaces* **2016**, *8* (6), 3825–3832.

https://doi.org/10.1021/acsami.5b10561.

(9)   Zhao, B.; Zhang, T.; Chu, B.; Li, W.; Su, Z.; Wu, H.; Yan, X.; Fangming, J.; Gao, Y.; Chengyuan, L. Highly Efficient Red OLEDs Using DCJTB as the Dopant and Delayed Fluorescent Exciplex as the Host. *Sci. Rep.* **2015**, *5*, 10697. https://doi.org/10.1038/srep10697.

(10)   Sarma, M.; Wong, K.-T. Exciplex: An Intermolecular Charge-Transfer Approach for TADF. *ACS Appl. Mater. Interfaces* **2018**, *10* (23), 19279–19304. https://doi.org/10.1021/acsami.7b18318.

(11)   Zhang, D.; Duan, L.; Zhang, D.; Qiu, Y. Towards Ideal Electrophosphorescent Devices with Low Dopant Concentrations : The Key Role of Triplet up-Conversion. *J. Mater. Chem. C* **2014**, *2*, 8983–8989. https://doi.org/10.1039/C4TC01757A.

(12)   Liu, X.-K.; Chen, W.; Thachoth Chandran, H.; Qing, J.; Chen, Z.; Zhang, X.-H.; Lee, C.-S. High-Performance, Simplified Fluorescence and Phosphorescence Hybrid White Organic Light-Emitting Devices Allowing Complete Triplet Harvesting. *ACS Appl. Mater. Interfaces* **2016**, *8* (39), 26135–26142. https://doi.org/10.1021/acsami.6b07629.

(13)   Dias, F. B.; Penfold, T. J.; Monkman, A. P. Photophysics of Thermally Activated Delayed Fluorescence Molecules. *Methods Appl. Fluoresc.* **2017**, *5* (1), 012001. https://doi.org/10.1088/2050-6120/aa537e.

(14)   Moon, C.-K.; Huh, J.-S.; Kim, J.-M.; Kim, J.-J. Electronic Structure and Emission Process of Excited Charge Transfer States in Solids. *Chem. Mater.* **2018**, *30* (16), 5648–5654. https://doi.org/10.1021/acs.chemmater.8b02011.

(15)   Su, S.-J.; Sasabe, H.; Takeda, T.; Kido, J. Pyridine-Containing Bipolar Host Materials for Highly Efficient Blue Phosphorescent OLEDs. *Chem. Mater* **2008**, *20* (5), 1691–1693.

(16)   Gong, X.; Ostrowski, J. C.; Moses, D.; Bazan, G. C.; Heeger, A. J. Electrophosphorescence from a Polymer Guest-Host System with an Iridium Complex as Guest: Förster Energy Transfer and Charge Trapping. *Adv. Funct. Mater.* **2003**, *13* (6), 439–444. https://doi.org/10.1002/adfm.200304334.

(17)   Lin, W.; Huang, W.; Huang, M.; Fan, C.; Lin, H.-W.; Chen, L.-Y.; Liu, J.-S.; Chao, T.-C.; Tseng, M.-R. A Bipolar Host Containing Carbazole/Dibenzothiophene for Efficient

Solution-Processed Blue and White Phosphorescent OLEDs. *J. Mater. Chem. C* **2013**, *1*, 6835–6841. https://doi.org/10.1039/c3tc31357c.

(18)   Soon, B.; Jeon, O.; Yook, K. S.; Joo, C. W.; Lee, J. Y. Phenylcarbazole-Based Phosphine Oxide Host Materials For High Efficiency In Deep Blue Phosphorescent Organic LightEmitting Diodes. *Adv. Funct. Mater.* **2009**, *19*, 3644–3649. https://doi.org/10.1002/adfm.200901274.

(19)   Song, D.; Zhao, S.; Luo, Y.; Aziz, H. Causes of Efficiency Roll-off in Phosphorescent Organic Light Emitting Devices : Triplet-Triplet Annihilation versus Triplet-Polaron Quenching. *Appl. Phys. Lett.* **2010**, *97*, 243304. https://doi.org/10.1063/1.3527085.

(20)   Al Attar, H. A.; Monkman, A. P. Electric Field Induce Blue Shift and Intensity Enhancement in 2D Exciplex Organic Light Emitting Diodes; Controlling Electron-Hole Separation. *Adv. Mater.* **2016**, *28*, 8014–8020. https://doi.org/10.1002/adma.201600965.

(21)   O'Brien, D. F.; Baldo, M. A.; Thompson, M. E.; Forrest, S. R. Improved Energy Transfer in Electrophosphorescent Devices. *Appl. Phys. Lett.* **1999**, *74*, 442.

(22)   Luhman, W. A.; Holmes, R. J. Investigation of Energy Transfer in Organic Photovoltaic Cells and Impact on Exciton Diffusion Length Measurements. *Adv. Funct. Mater.* **2011**, *21*, 764–771. https://doi.org/10.1002/adfm.201001928.

(23)   Cai, C.; Su, S.; Chiba, T.; Sasabe, H.; Pu, Y.; Nakayama, K.; Kido, J. High-Efficiency Red , Green and Blue Phosphorescent Homojunction Organic Light-Emitting Diodes Based on Bipolar Host Materials. *Org. Electron.* **2011**, *12*, 843–850. https://doi.org/10.1016/j.orgel.2011.01.021.

(24)   Jankus, V.; Chiang, C.-J.; Dias, F.; Monkman, A. P. Deep Blue Exciplex Organic Light-Emitting Diodes with Enhanced Efficiency; P-Type or E-Type Triplet Conversion to Singlet Excitons? *Adv. Mater.* **2013**, *25* (10), 1455–1459. https://doi.org/10.1002/adma.201203615.

(25)   Adamovich, V.; Brooks, J.; Tamayo, A.; Alexander, A. M.; Djurovich, P. I.; Andrade, B. W. D.; Adachi, C.; Forrest, R.; Thompson, M. E. High Efficiency Single Dopant White Electrophosphorescent Light Emitting Diodes. *New J. Chem.* **2002**, *26*, 1171–1178. https://doi.org/10.1039/b204301g.

(26) Hung, W.-Y.; Fang, G.-C.; Lin, S.-W.; Cheng, S.-H.; Wong, K.-T.; Kuo, T.-Y.; Chou, P.-T. The First Tandem, All-Exciplex-Based WOLED. *Sci. Rep.* **2014**, *4*, 5161.

(27) Wu, I. W.; Wang, P. S.; Tseng, W. H.; Chang, J. H.; Wu, C. I. Correlations of Impedance-Voltage Characteristics and Carrier Mobility in Organic Light Emitting Diodes. *Org. Electron. physics, Mater. Appl.* **2012**, *13* (1), 13–17. https://doi.org/10.1016/j.orgel.2011.09.016.

(28) Kim, D. H.; Cho, N. S.; Oh, H. Y.; Yang, J. H.; Jeon, W. S.; Park, J. S.; Suh, M. C.; Kwon, J. H. Highly Efficient Red Phosphorescent Dopants in Organic Light-Emitting Devices. *Adv. Mater.* **2011**, *23* (24), 2721–2726. https://doi.org/10.1002/adma.201100405.

Chapter 8:

Concluding Remarks

This thesis has presented a multifaceted research program concerning TADF exciplexes; their intrinsic emission mechanisms and how to tune this through dilution, their suitability as solution processable emitters, and their applicability in OLED structures as a tool for achieving exciton confinement.

In Chapter 4 it is demonstrated, for the first time that exciplex colour and performance are not fixed and can be tuned and enhanced through solid state dilution. Before this study it was common belief that diluting an exciplex in a host would only hinder the exciplex formation and thus emission. Instead for the TSBPA:PO-T2T exciplex it is possible to controllably blueshift its emission and improve its PLQY (from 58% to 80%). This improvement can be directly translated into OLED's performance where the EQE passed from 14.8% to 19.2%. The blueshift is rationalised in terms of a reduced coulombic binding energy term in the expression for exciplex total energy. The chapter also highlights the importance of the choice of the host for photophysical experiments, since inappropriate energy level alignment (donor-host-acceptor) can hinder electron transfer from the excited donor to the acceptor that forms the exciplex. Level alignment is shown to not be as important in devices, where the exciplex formation happens through direct injection of holes and electrons (and the host does not play a role).

These dilution effects are further investigated in Chapter 5 where a family of three exciplex forming carbazole donors (mCP, CBDP and CBP) where studied with the PO-T2T acceptor. The three carbazole donors differed (only slightly) in their molecular structure, so that the different photophysical behaviour could be attributed to these differences. All three exciplexes showed a consistent blueshift with increasing dilution, in agreement with what observed for the TSBPA:PO-T2T exciplex, although the same cannot be said for the PLQY enhancement effect. Instead the two more rigid structures (mCP and CDBP) do not provide any substantial variations in PLQY, and at high dilutions the PLQY drops due to the increased number of

isolated donors that cannot contribute to the exciplex emission. The third more flexible donor (CBP), in contrast does show a PLQY enhancement from 39% to 55% the same value observed for the similarly structured (but rigid) CDBP. This suggests that a certain degree of molecular flexibility is necessary to provide room to observe a PLQY enhancement as quenching processes are deactivated. EQE values of the OLEDs produced with the diluted exciplexes as EMLs did not closely follow the PLQY values, probably due to the relatively low conductivity of the carbazole based donors. In contrast to highly conductive TSBPA, the carbazole devices are strongly affected by the introduction of the host, probably due to the disruption of the percolation pathways necessary for conduction. This problem might be addressed in future studies by employing functional hosts that can assist the charge injection and conduction across the EML, but without interfering with the exciplex formation process (i.e. forming other competing exciplexes).

Shifting focus, in Chapter 6 it is shown how OLEDs of a previously reported TADF exciplex formed between DCz-DBTO2 and TAPC can be effectively solution processed with little loss of the overall performance. The challenge of this work was to optimise the solvent system used to spin cast suitably smooth EMLs. Initially chlorobenzene was used due to its high boiling point, good film forming properties and high repeatability. The devices produced this way showed nonetheless poor performance, due to aggregation problems in the film nanostructure. This problem was addressed by using chloroform as solvent where the low boiling point results in extremely fast drying time and thus a much reduced propensity to form aggregates. However, chloroform is a challenging solvent to handle as it dries almost instantly during deposition leading to irregular films. For this reason, 5% of chlorobenzene was add to the chloroform solution and this approach demonstrated to provide the best results with an EQE of $8.9 \pm 0.6\%$ was achieved. The improvement is due to the 5% of chlorobenzene stabilizing the film while covering the substrate without substantially increasing the drying time, thus leading to a better nanostructure and performance.

Finally, Chapter 7 shows how the presence an interfacial TADF exciplex at the EML-ETL interface can improve both performance and stability of a PhOLED. The improvement arises from the extremely narrow charge confinement within the 5nm EML made possible by the presence of the exciplex. The exciplex not only confines the recombination zone but also prevents the piled up charges at the EML-ETL interface by rapidly depleting both singlets and triplets (through energy transfer mechanisms back to the phosphorescent emitter). This strategy

improves the LT90 of the PhOLED from a few minutes for a standard (without exciplex) device stack.

In conclusion, this thesis demonstrates the strong potential that TADF exciplexes possess for application in OLEDs. As emitters more investigation is surely needed, in particular on the role that the host plays in the performance enhancement effect (if any) when diluting the exciplex.

Furthermore Chapter 5 has highlighted the need for the development of functional conducting hosts in order to avoid the performance reduction due to problems related to the low conductivity of the diluted exciplex films. Further investigation on the mechanism that drives the PLQY enhancement of the exciplexes is also necessary to clarify the role of molecular flexibility highlighted in this thesis. These questions may be answered by investigating different families of exciplex forming donors and acceptors with the investigations focused on trying to separate the contributions between the donor and acceptor molecular conformations and the respective electron donating and electron accepting strength of the exciplex forming molecules. Moreover, very useful information could be extracted by an in depth morphological study on the effect of different degrees of dilution vs performance change using different hosts to try to understand if certain hosts induce or not a preferable donor-acceptor orientation that favourites the exciplex formation thus higher PLQY.

Concerning the photophysical investigation since the energy splitting between the CT singlet and CT triplet is effectively zero due to the fact that the CT state is formed between two different molecules, it would interesting to observe the change of the photophysical behaviour of different exciplexes at low temperature (below 80 K) to try to understand if coupling effects beyond the vibronic one (like hyperfine coupling) are providing a non-negligent contribution to the rISC process.

In Chapter 6 solution processing it has been shown which constitutes a viable approach and that the solvent system used to deposit the exciplex layer is critical to maximise the OLED performance. On the other hand, the development of dendrimers and polymers, containing exciplex forming moieties could further improve the development of such devices and reduce the issues related to the film quality being so closely dependant by the solvent system used.

Finally, the approach presented in Chapter 7 showed to be generally promising and it will be interesting to apply to enhance the efficiency and stability of small molecule based TADF OLEDs and hyperfluorescent devices to try to approach the holy grail of a stable and commercially viable blue emitter.